UNIVERSITY OF CALIFORNIA

Santa Barbara

Heterogeneous Monometallic and Bimetallic Catalysts for Deoxydehydration and Catalytic Transfer Hydrogenation: Valorization of Sugar Alcohols and Acids

A dissertation submitted in partial satisfaction of the

requirements for the degree Doctor of Philosophy

in Chemical Engineering

by

Jun Hee Jang

Committee in charge:

Professor Mahdi M. Abu-Omar, Chair

Professor Susannah L. Scott

Professor Michael J. Gordon

Professor Gabriel Ménard

December 2020

The dissertation of Jun Hee Jang is approved.

_____

Susannah L. Scott

_____

Michael J. Gordon

_____

Gabriel Ménard

_____

Mahdi M. Abu-Omar, Committee Chair

December 2020

Heterogeneous Monometallic and Bimetallic Catalysts for Deoxydehydration and Catalytic Transfer Hydrogenation: Valorization of Sugar Alcohols and Acids

ACKNOWLEDGEMENTS

First and foremost, praises and thanks to God, for his endless blessings and strengths that helped me to complete my studies.

I would like to express my deep and sincere gratitude to my advisor, Prof. Mahdi Abu-Omar. Under his exceptional guidance and support, I had opportunities to participate in cutting-edge research projects and to learn research and presentation skills. He was not only my advisor, but he was a trusted teacher, a great mentor, and an inspiring role model. Without him, this thesis would never be possible. I specially thank my committee, Profs. Susannah Scott, Michael Gordon, and Gabriel Ménard for their invaluable feedback and suggestions.

I am deeply grateful to my collaborators for their supports and insightful discussions. I want to thank Prof. Phillip Christopher, Prof. Insoo Ro, and Jordan Finzel for the wonderful collaborative work on the synthesis and characterization of bimetallic catalysts projects. I also want to express my appreciation to Dr. Massimiliano Delferro, Dr. Hyuntae Shon, Dr. Jeffrey Camacho-Bunquin, and Dr. Dali Yang for X-ray absorption spectroscopy results. Many thanks to the Crossroad Fellowship team, Prof. Sangwon Suh, Ali Chamas, Hyunjin Moon, Jiajia Zheng, Yang Qiu, and Tarnuma Tabassum for writing a valuable review paper and sharing diverse perspectives.

I would like to extend my thanks to my mentors, colleagues, and friends. Prof. Whasik Min provided opportunities to work in his lab as an undergraduate researcher and great advices on my career. Special thanks to Prof. Kyu-Soon Shin, my life mentor, for teaching research skills and perspectives and supporting my whole graduate career. I am also grateful to my master's advisor, Prof. Chung-Hak Lee, for giving me invaluable research experience

and guidance. I especially thank Dr. Chan Young Park who is more than colleague. He is my best friend, great mentor, inspiring researcher, and teacher of English. Many thanks to my coffee meeting members who were postdoctoral researchers at UCSB and are professors in Korea, Prof. Seung Joon Yoo, Prof. Jaewon Lee, and Prof. Insoo Ro, for endless discussion about research and lives. Thanks to all the Abu-Omar group members, especially Baoyuan Liu for training instruments and suggesting many useful ideas, Tayyabeh Bakhshi for being a great office mate and discussing research and lives, Jack Hopper for helping my research, Dr. Shou Zhao, Dr. Hao Luo, and Dr. Ram Pichaandi for advising my research.

I must express my greatest appreciation to my family in Korea. Their endless love, support and pray make me complete my graduate studies. Special thanks go to my brother Dr. Yong Hee Jang, for his encouragement, inspiration, and supports. I also thank my parents-in-law for their sincere love, support, and prays.

Last but most importantly, I thank my lovely wife, Hea Re An. You are always with me and extremely supportive of me throughout my studies. Your love and support were more than enough to continue and complete my studies and thesis. Without you, my life would not have been so meaningful.

VITA OF JUN HEE JANG

December 2020

EDUCATION

Bachelor of Science in Chemical Engineering, Korea University, August 2011 (magna cum laude)
Master of Science in Chemical Engineering, Seoul National University, August 2014
Doctor of Philosophy in Chemical Engineering, University of California, Santa Barbara, December 2020 (expected)

PROFESSIONAL EMPLOYMENT

2011-12: Researcher, Korea Institute of Science and Technology
2015-16: Research Assistant, Department of Chemistry, Purdue University, West Lafayette
2016-20: Teaching and Research Assistant, Department of Chemistry, University of California, Santa Barbara

PUBLICATIONS

"Deoxydehydration of Biomass-Derived Polyols with a Reusable Unsupported Rhenium Nanoparticles Catalyst," *ACS Sustainable Chemistry & Engineering* **2019**, 7 (13), 11438-11447
"Degradation Rates of Plastics in the Environment," *ACS Sustainable Chemistry & Engineering* **2020**, 8 (9), 3494-3511
"A Heterogeneous Pt-ReOx/C Catalyst for Making Renewable Adipates in One-Step from Sugar Acids," accepted in *ACS Catalysis*
"Deoxydehydration and Catalytic Transfer Hydrogenation: New Strategy to Valorize Tartaric Acid and Succinic Acid to γ-Butyrolactone and Tetrahydrofuran," accepted in *Energies*

FIELDS OF STUDY

Major Field: Catalysis & Sustainable Reaction Engineering

Studies in Heterogeneous catalysis for upgrading sugar alcohols and acids with Professor Mahdi M. Abu-Omar

ABSTRACT

Heterogeneous Monometallic and Bimetallic Catalysts for Deoxydehydration and Catalytic Transfer Hydrogenation: Valorization of Sugar Alcohols and Acids

by

Jun Hee Jang

Lignocellulosic biomass provides a renewable resource for sustainable routes to biofuels and biochemicals through catalytic conversion. Oxorhenium catalysts effectively transform biomass-derived polyols into olefins via deoxydehydration with a secondary alcohol reductant. In attempts to develop a reusable solid catalyst and to investigate a possible mechanism for deoxydehydration by a heterogeneous catalyst, unsupported rhenium oxide nanoparticles (ReO_x NPs) were prepared. The nanoparticle catalyst with 3-octanol as a reductant catalyzed deoxydehydration of various polyols to corresponding alkenes with high efficiency. In-situ and ex-situ X-ray spectroscopy analysis showed the changes in oxidation states and structures of ReO_x NPs during heterogeneous deoxydehydration reaction. This, combined with kinetic studies and kinetic isotope effect, proposed a possible mechanism involving a Re^{VII}/Re^{V} redox pair for deoxydehydration driven by heterogeneous ReO_x catalyst and alcohol reductants.

Multi-functional catalysis including deoxydehydration with monometallic and bimetallic heterogeneous catalysts was studied for the valorization of sugar acids. First, a combination of deoxydehydration and catalytic transfer hydrogenation by a bifunctional Pt-ReO_x/C

catalyst achieved a one-step conversion of mucic acid, a C6 sugar acid, to adipates in high yield (85%). Isopropanol was employed as a hydrogen donor for both reactions. The catalyst was reusable and regenerated multiple times. Spectroscopic studies of Pt-ReO_x/C demonstrated Re^{VII} and Pt^0 as the relevant species of deoxydehyration and catalytic transfer hydrogenation, respectively. Based on all observations, a bifunctional mechanism was proposed. This bifunctional catalysis was also achieved with Ir-ReO_x/C, allowing significantly reduced metal contents in the catalyst. Similarly, deoxydehydration and transfer hydrogenation of tartaric acid, a C4 sugar acid, converted to succinates with monometallic ReO_x NPs. Further dehydration/dealcoholization and transfer hydrogenation over ReO_x NPs produced γ-butyrolactone and tetrahydrofuran, realizing a one-step conversion of sugar acids to C4 commodity products.

TABLE OF CONTENTS

CHAPTER I. Introduction

A. Deoxydehydraion of biomass-derived polyols

Lignocellulosic biomass is one of the promising renewable energy resources to provide sustainable routes to biofuels and chemicals.[1,2] However, the establishment of new chemical processes to extract chemicals from biomass and to replace petroleum-based processes brings chemical and engineering challenges due to the structural differences between biomass and petroleum. Making chemicals from petroleum-derived synthons requires the addition of heteroatoms such as oxygen and nitrogen. In contrast, the removal of oxygen is a crucial challenge in making useful chemicals from biomass starting materials.[3,4] A range of deoxygenation methods (e.g., pyrolysis,[5] dehydration,[6] decarbonylation,[7] hydrogenolysis,[8] and deoxydehydration[9]) via homogeneous and heterogeneous catalysis have been reported to upgrade biomass-derived materials.[10] Catalytic deoxydehydration (DODH) is one attractive deoxygenation reaction, which converts vicinal diols to olefins (Scheme 1.1). Since Andrews and Cook reported the concept of DODH with Cp^*ReO_3 catalyst, up to this day, DODH has garnered much attention in biomass studies.[11] In this chapter, previous studies on rhenium catalyzed DODH will be introduced, followed by DODH with different metal catalysts including vanadium and molybdenum-based catalysts.

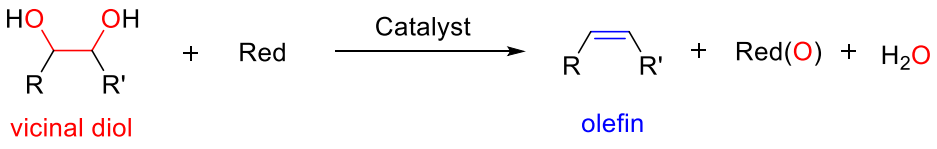

Scheme 1.1 Deoxydehydration of vicinal diol

1. Homogeneous Rhenium-based Catalysts

The first study on the transformation of diol to olefin over a rhenium complex was reported by Herrmann's group in 1987.[12] Sodium ethylene glycolate salt was converted to ethylene with a stoichiometric amount of Cp*ReO_3 at 150 ^oC under vacuum (Scheme 1.2). They observed Re-diolate (V) as an intermediate of the process. In 1996, Andrews and Cook reported a catalytic process with Cp*ReO_3 catalyst and triphenyl phosphine (PPh_3) as a reductant to convert bio-based polyols.[11] The catalytic process produced 67% yield of allyl alcohol from glycerol and 50 % yield of 1,3-butadiene was obtained from erythritol (Scheme 1.3).

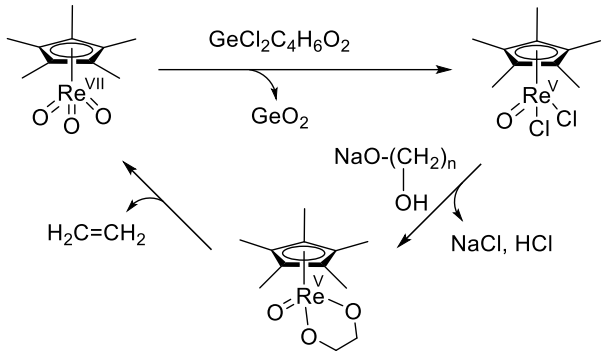

Scheme 1.2 Conversion of sodium ethylene glycolate salt to ethylene.

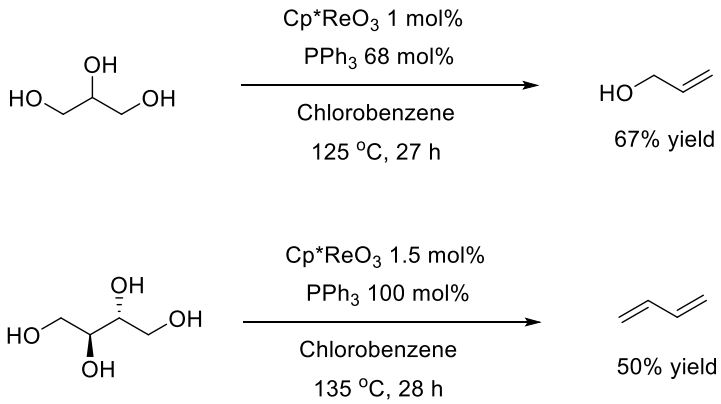

Scheme 1.3 DODH of glycerol and erythritol with Cp*ReO_3 and PPh_3.

In 2009, our group suggested DODH of diols to corresponding alkenes with methyltrioxorhenium (MTO) catalyst and molecular H_2 as a reductant (Scheme 1.4).[13] Under higher H_2 pressure, the produced alkenes were hydrogenated to alkanes. While MTO has air and water stability and H_2 is a cheap and convenient reductant, this system showed a low yield of C-C double bond product. 18% of 1-hexene was yielded from 1,2-hexanediol after 8 h reaction. Under the same conditions, DODH of cis-1,2-cyclohexanediol over MTO afforded cyclohexene, whereas trans-1,2-cyclohexanediol was not converted. This was explained by the formation of Re-diolate intermediate with only cis-diol compounds.[11,13]

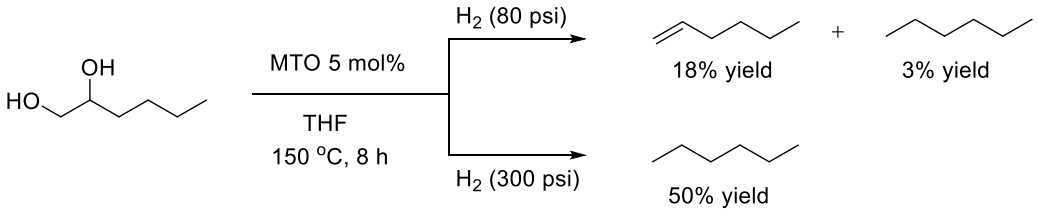

Scheme 1.4 DODH of vicinal diols with MTO and H_2.

Later Nicholas group tested perrhenate salts and MTO catalysts with sulfite reductant for DODH of vicinal diols.[14] Among several perrhenate salts, tetrabutylammonium perrhenate (Bu_4NReO_4) showed higher DODH activity with sulfite salt for the conversion of styrene glycol compared to MTO catalyst. In addition, they showed the possibility of DODH of glycerol under neat conditions while the yield of allyl alcohol was low (15%). Bu_4NReO_4 and Na_2SO_4 converted erythritol to 1,3-butadiene (27% yield) and a small amount of 2,5-dihydrofuran (6% yield) and cis-2-butene-1,4-diol (3% yield).

In 2010, Bergman and Ellman introduced rhenium carbonyl catalysts including $Re_2(CO)_{10}$ and $BrRe(CO)_5$ and a higher chain secondary alcohol as reductant and solvent (Scheme 1.5).[15] The carbonyl catalyst and sacrificial alcohol yielded a high amount of olefins, while

the sacrificial alcohol was oxidized to corresponding ketone. Upon optimization, DODH of erythritol gave 62% yield of 2,5-dihydrofuran in the presence of *p*-toluenesulfonic acid (TsOH) as a cocatalyst.

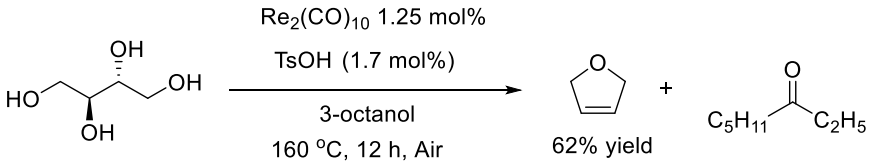

Scheme 1.5 DODH of erythritol with rhenium carbonyl catalyst and 3-octanol as reductant and solvent.

In 2012, our group and Toste's group extensively investigated DODH catalysis of various sugar alcohols (e.g. allyl alcohol, erythritol, xylitol, and sorbitol) with rhenium (VII) complexes such as MTO and ammonium perrhenate (NH_4ReO_4) in the presence of sacrificial alcohols (Scheme 1.6).[4,9] First of all, neat glycerol was converted to allyl alcohol (27% yield) and acrolein (6% yield) with MTO. Because glycerol worked as a reductant, the yield of olefins could not exceed 50%. In the presence of 1-heptanol reductant, MTO converted erythritol to 45% yield of 2,5-dihydrofuran and 13% yield of but-2-enal. Higher yield of allyl alcohol (90%) from glycerol was obtained with MTO/3-octanol, reported by Toste's group. The conversion of erythritol gave 1,3-butadiene (89% yield) as a major product and a small amount of 2,5-dihydrofuran. MTO catalyzed-DODH of xylitol and D-sorbitol with 3-pentanol as a reductant made moderate yields of corresponding olefins. Later, Toste group demonstrated that MTO/secondary alcohol system can catalyze DODH of 1,4-diols (1,4-DODH) and of 1,6-diols (1,6-DODH) as well as vicinal diols.[16]

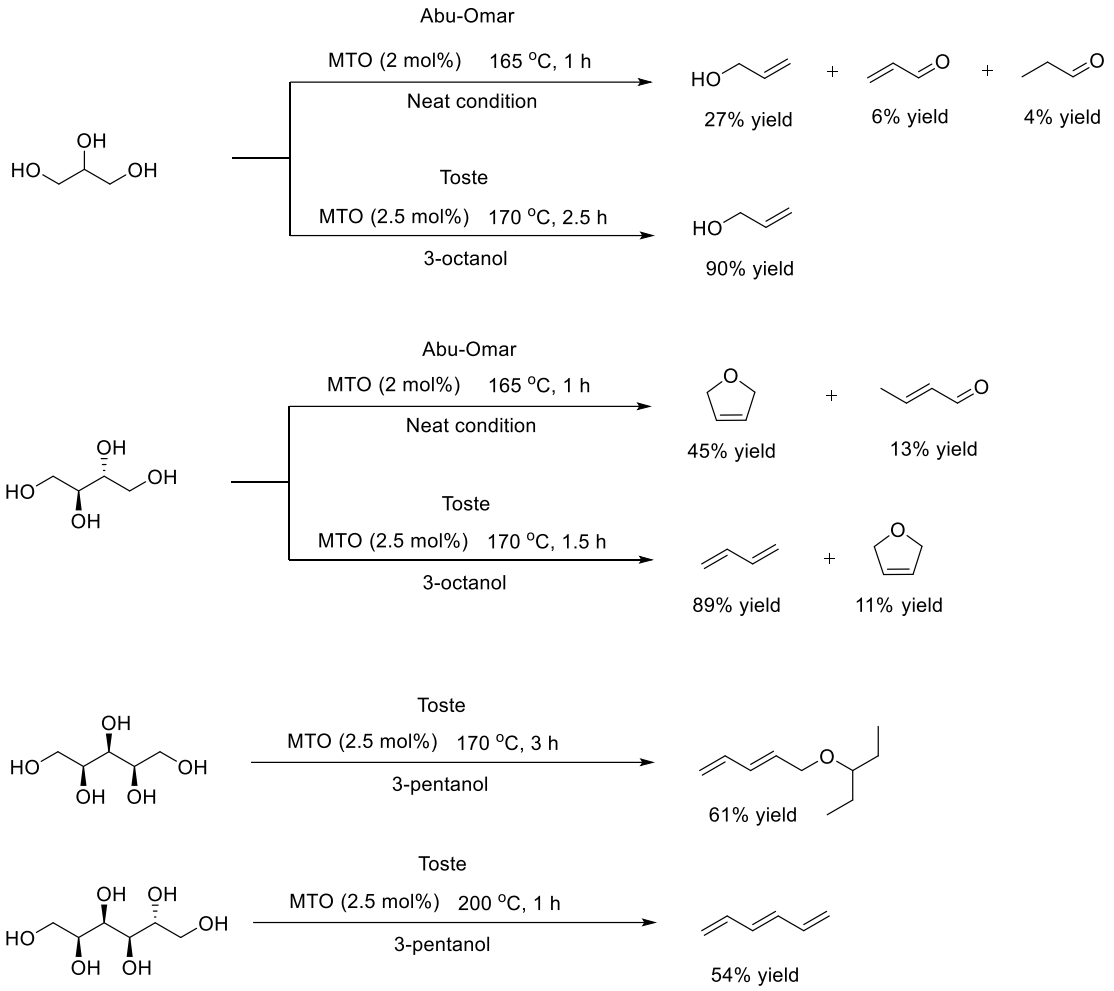

Scheme 1.6 DODH of C3-C6 sugar alcohols with MTO and sacrificial alcohol.

In 2018, de Vries group applied DODH reaction with Re_2O_7, NH_4ReO_4, and MTO catalysts to 1,2,6-hexanetriol and 1,2,5-hexanetriol.[17] In the presence of PPh_3 as a reductant, Re_2O_7 (0.5 mol%) converted 1,2,6-hexanetriol to 5-hexen-1-ol with a high yield (98%). Due to isomerization and cyclization, the conversion of 1,2,5-hexanetriol over Re_2O_7 (3 mol%) and PPh_3 produced several products including 5-hexen-2-ol, cis- and trans-2-hexene-5-ol, and 5-methyltetrahydrofurfurylic alcohol.

The proposed DODH mechanisms for homogeneous Re catalysis involve three steps: (1) reduction of high-valent Re species, (2) diol condensation to form Re diolate intermediates,

and (3) concerted alkene extrusion, the reverse of [3+2] addition. Our group proposed a possible mechanism that coordination of diol to rhenium occurs, followed by reduction of Re(VII) diolate to Re(V) diolate. The produced Re(V) diolate is active species for alkene extrusion (Scheme 1.7a).[9] A different mechanism with the same intermediate, Re(V) diolate, and different sequences was proposed by both Andrews and Toste group.[4,11] In the proposed mechanism, the reduction step occurs from MTO to methyldioxorhenium (MDO) before diol is attached to the rhenium catalyst (Scheme 1.7b). Besides the mechanisms proposed experimentally, DFT calculation suggested a different intermediate which is methyloxodihydroxyrhenium (Scheme 1.7c).[18] While theses mechanisms have different sequences or intermediate, they all involve Re^{VII}/Re^{V} redox pair. In 2013, our group suggested the possibility of Re^{V}/Re^{III} redox pair as a catalytic cycle based on the experimental results (Scheme 1.7d).[19]

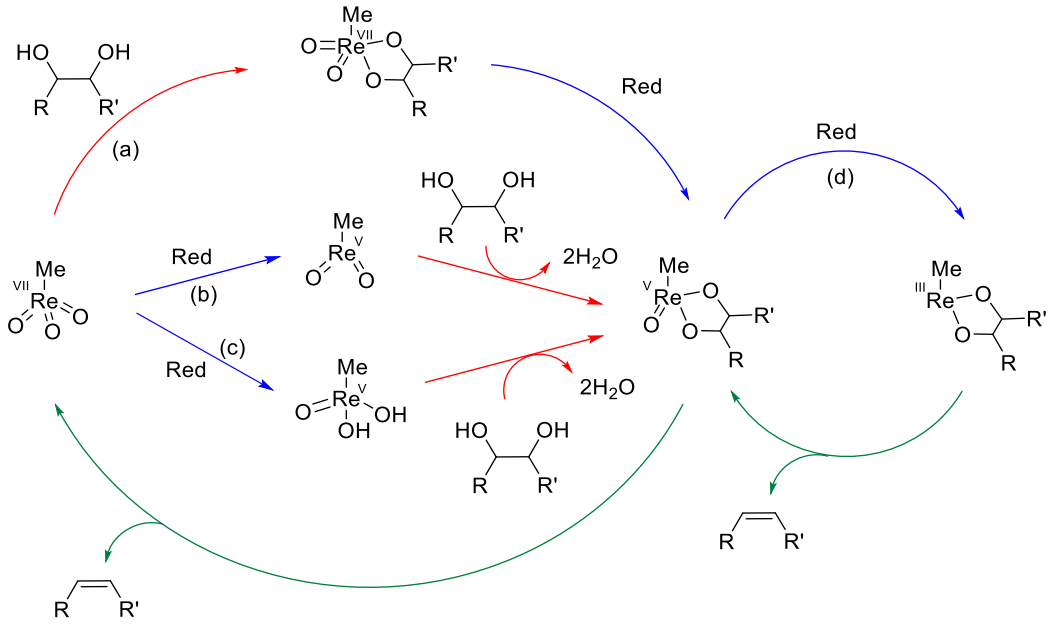

Scheme 1.7 The proposed mechanisms of MTO-catalyzed DODH. Red arrow: condensation of diol. Blue arrow: reduction. Green arrow: extrusion of olefins.

2. Heterogeneous Rhenium Catalysts

One major drawback of homogeneous catalysts is the difficulty in recycling the catalyst. Additionally, under the conditions necessary for DODH (T > 150 °C), homogeneous catalysts tend to degrade. As a result, heterogeneous Re catalysts are of interest and have recently been pursued. In 2013, oxo-rhenium supported on carbon (ReO_x-C) as the first heterogeneous catalyst for DODH with H_2 as a reductant was introduced by Nicholas group.[20] The adsorbed perrhenate on activated carbon catalyzed DODH of 1) L-(+)-diethyl tartarate to diethyl fumarate with a high yield (95%) and 2) 1,2-tetradecanediol to a moderate yield of tetradecane (36%). The recycling test showed significant leaching of rhenium, resulting in the reduced yield (10%) at the 4th cycle.

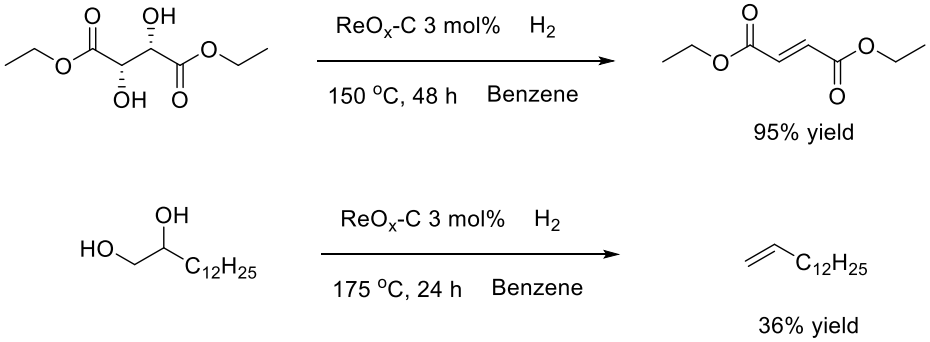

Scheme 1.8 DODH over ReO_x-C catalyst and H_2 as a reductant.

The stable solid catalyst for DODH was reported by Palkovits group (Table 1.1).[21] They prepared perrhenate on various supports (SiO_2, TiO_2, ZrO_2, and C) and the perrhenate/support was reduced to ReO_x/support involving Re^{VII}, Re^{IV}, and Re^0. Among them, ReO_x/TiO_2 exhibited good stability upto 7 consequence DODH runs. For example, DODH of glycerol over ReO_x/TiO_2 produced 48% yield of allyl alcohol in 1 h at 170 °C. Under the same conditions, the yield of allyl alcohol remained and the 7th cycle showed 54%

yield. Hot filtration demonstrated ReO_x/TiO_2 is stable under the reaction conditions. They showed an increase in Re^{IV} content by pre-reduction of supported ammonium perrhenate led to higher catalytic activity than Re^{VII}, demonstrating Re^{IV} as active species.

Table 1.1 DODH of diols with solid ReO_x/TiO_2 catalyst.

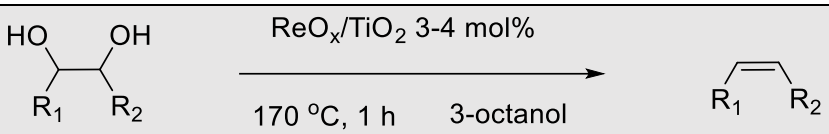

Run	R_1	R_2	Yield	
			1st cycle	7th cycle
1	H_2	CH_2OH	48	54
2	H_2	$CH_2CH_2CH_2CH_2OH$	38	35
3	H_2	CH_2CH_2OH	27	28

[a]Reaction conditions: 170 °C, 1 h, 3-octanol (21 eq.).

In 2017, Kon and Katryniok reported ReO_x/Al_2O_3 as a stable solid DODH catalyst.[22] In the presence of 2-hexanol as a reductant, DODH of glycerol produced 91% yield of ally alcohol and was reusable upto 3 runs without yield loss. In 2018, Nicholas group synthesized a rhenium complex containing dopamine ligand which is linked to 3-carboxypropyl silica gel and tested its activity and stability for DODH of L-(+)-diethyl tartarate.[23] In the first cycle, the synthesized catalyst and PPh_3 produced 94% yield of diethyl fumarate. The slightly reduced yield (83%) was observed in the 5th cycle, demonstrating stability of the synthesized catalyst.

In addition to monometallic ReO_x/support catalysts, bimetallic heterogeneous catalysts were used for DODH reaction. Tomishige group screened various ReO_x-M/CeO_2 (M: Rh, Pd,

Ir, Ru, Pt, Ag, and Au) catalysts, prepared by impregnating M/CeO_2 with an aqueous solution of NH_4ReO_4.[24] In the presence of H_2, glycerol was converted to allyl alcohol through DODH and further hydrogenation gave 1-propanol as a major product. Interestingly, ReO_x-Au/CeO_2 catalyst selectively retains allyl alcohol with a high yield (91%), suppressing further hydrogenation. Under the same conditions, DODH of erythritol, 1,2,4-butanetriol, 1,4-anhydroerythritol, and cis-1,2-cyclohexanediol afford corresponding olefins with high efficiency (Scheme 1.9). In 2019, this group used the same catalyst and reaction conditions to produce unsaturated sugars from methyl glycosides.[25]

The mechanism of ReO_x-Au/CeO_2 catalyzed DODH with H_2 reductant was studied based on experiments and DFT calculations.[26] The characterization of the catalyst demonstrated rhenium sites (Re^{VI} and Re^{IV}) were isolated on CeO_2 support while the size of gold nanoparticles is about 10 nm. Hydrogen, promoted by gold nanoparticles, was dissociated and transferred to the isolated Re^{VI} sites, resulting in reduced Re^{IV} sites. The proposed Re^{VI}/Re^{IV} redox cycle is different from previous homogeneous DODH mechanisms involving Re^{VII}/Re^{V} redox pair.

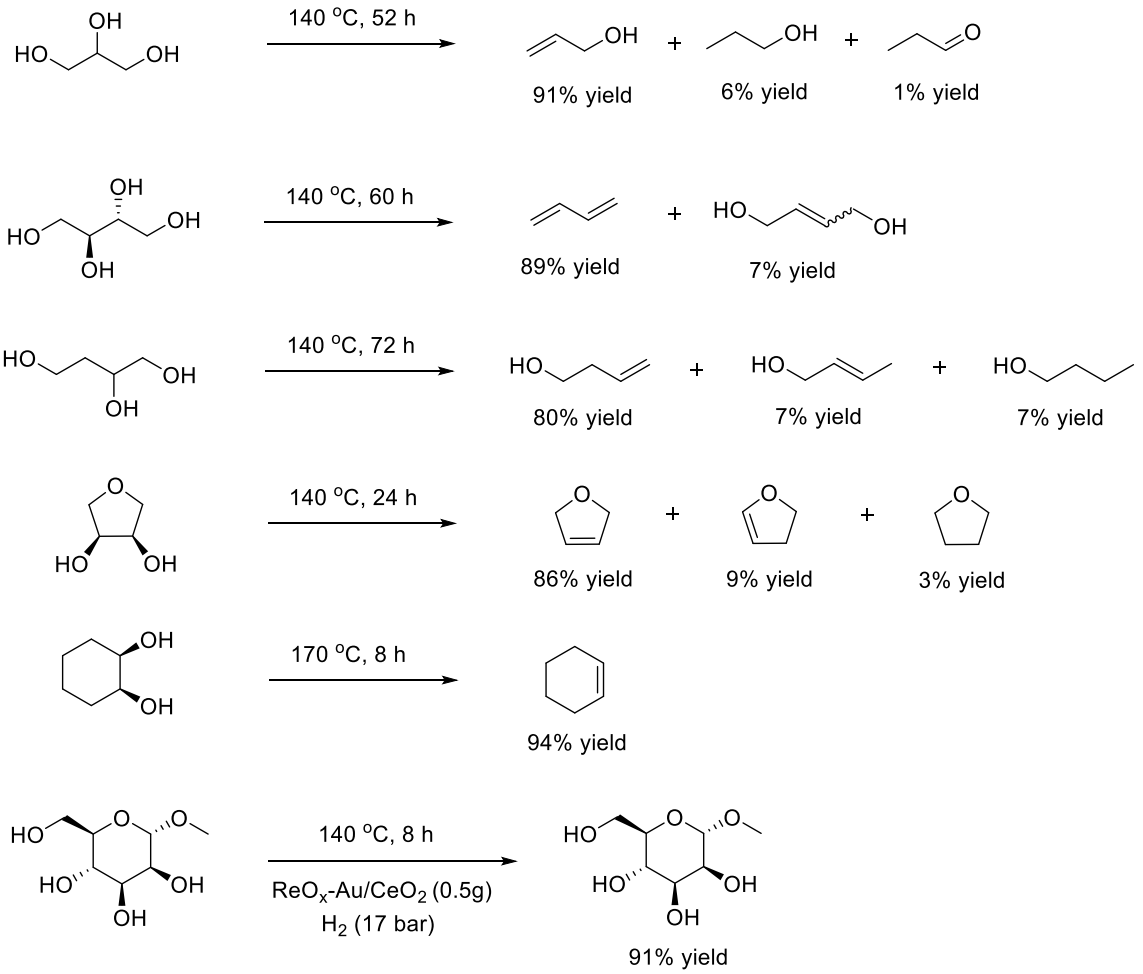

Scheme 1.9 DODH of various diols over ReO_x-Au/CeO_2 catalyst and H_2 as a reductant. Reaction conditions: 0.3 g (1 wt% Re, Au/Re=0.3mol/mol), substrate (0.5 g), 1,4-dioxane (4 g), and H_2 (80 bar). cis-1,2-hexanediol (0.25 g).

3. Other metal catalysts

Although rhenium-based catalysts have shown the highest efficiency, its use in industry is limited due to high costs. In this regard, DODH with more economical and abundant metals such as molybdenum and vanadium have been investigated. The first example of Mo-based catalyst that showed DODH activity was dioxomolybdenum(VI) complexes ($Mo(O)_2(Q^R)_2$, R = cyclohexyl, *n*-C_6H_{13}, and *n*-$CH_2C(CH_3)_3$).[27] The synthesized complexes converted styrene glycol to 55% yield of cyclooctene with PPh_3 as a reductant in toluene. Later,

commercially available ammonium heptamolybdate (AHM, $(NH_4)_6Mo_7O_{24}4H_2O$) revealed good activity for DODH reaction with various reductants including isopropanol, Na_2SO_3, PPh_3, and KI.[28,29] Mo-based heterogeneous catalysts including AHM/support and MoO_x/support catalysts were also tested for DODH of diols, affording olefins with moderate yields.[23,30]

Recently, both vanadium-based complexes and solid catalysts also attributed attention for DODH. Nicholas group used both commercially available vanadium catalysts ($NaVO_3$, NH_4VO_3, and *n*-Bu_4NVO_3) and synthesized oxo-vanadium complexes for DODH.[31,32] Commercially available metavanadate (VO_3^-) catalyzed DODH was also reported by Fristrup's group.[33] In 2017, Chen's group synthesized VO_x/SiO_2 solid catalyst and used it to convert 2,3-butanediol to butenes with a yield of 45% in a continuous system.[34] Another continuous DODH reaction was reported that V_2O_5/β-zeolite catalyst produced acrolein (38%) and allyl alcohol (10%) from glycerol.[35]

B. Deoxydehydration and hydrogenation for sugar acids valorization

A combination of catalytic deoxydehydration and hydrogenation has been utilized to valorize biomass-derived sugar acids or lactones to dicarboxylic acid and its esters. As described above, DODH reaction affords olefins from diols. The resulting C-C double bonds can be saturated through catalytic hydrogenation. The first example of DODH + hydrogenation to produce adipates from mucic acid was reported by Toste's group.[16] Mucic acid (also known as galactaric acid) is an aldaric acid that can be produced by the oxidation of galactose.[36] In the presence of *n*-butanol as a reductant, $HReO_4$ catalyzed DODH of mucic acid, making dibutyl muconate with a yield of 62% under air or 71% under N_2 atmosphere (Scheme 1.10).[16] After DODH reaction, Pd/C catalyst and H_2 were added to

hydrogenate the produced dibutyl muconate to dibutyl adipate. This one-pot two-step reaction converted mucic acid to 62% yield of adipate.

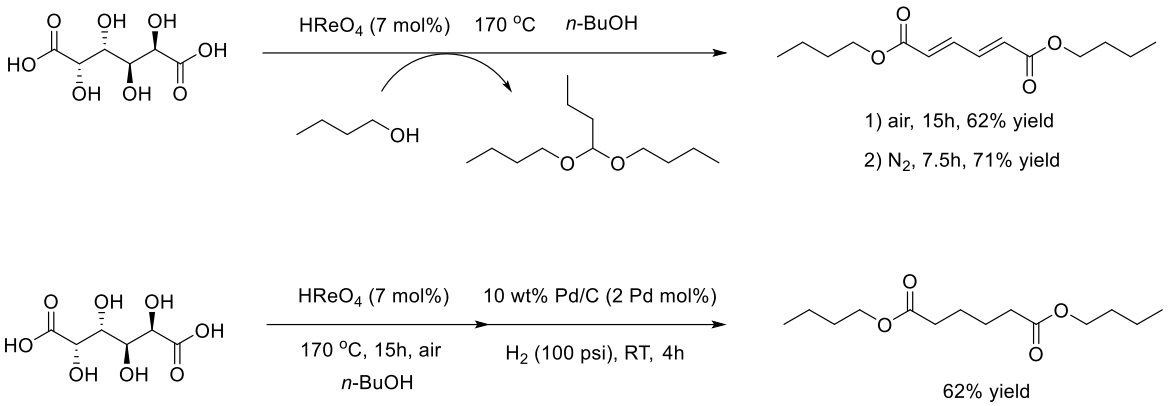

Scheme 1.10 DODH of mucic acid and DODH-hydrogenation one-pot reaction of mucic acid.

Later, Zhang's group reported a similar reaction pathway, but a much higher yield of adipates through two-step DODH and transfer hydrogenation reaction.[36] At 120 °C, MTO converted mucic acid to muconates (99% yield) in 3-pentanol (Scheme 1.11). Because esterification also proceeds, resulting in a mixture of monoester and diester as a final product. In the presence of TsOH, esterification was promoted, resulting in the enhanced solubility of mucic acid in 3-pentanol and the reduced reaction time. Re_2O_7 catalyzed-conversion of mucic acid selectively yielded a diester compound with *n*-butanol as a reductant. The resulting muconates were saturated to adipates through transfer hydrogenation over Ru/C, Pd/C, and Pt/C catalysts with 3-pentanol as a hydrogen donor. DODH and transfer hydrogenation two-step reaction gave 99% yield of adipates. A one-step process with a mixture of MTO, TsOH, Pt/C, and 3-pentanol yielded up to 75% at 200 °C. DFT calculation of DODH of mucic acid suggested methyloxodihydroxyrhenium as an intermediate shown in Scheme 1.7c. In 2016, the same authors used NH_4ReO_4 (5 mol%) for

DODH of L-(+)-tartaric acid, a C4 sugar acid, to maleic acid in 3-pentanol with 91% yield. Subsequently, hydrogenation of the produced maleic acid with Pt/C and H_2 yielded succinic acid.[37]

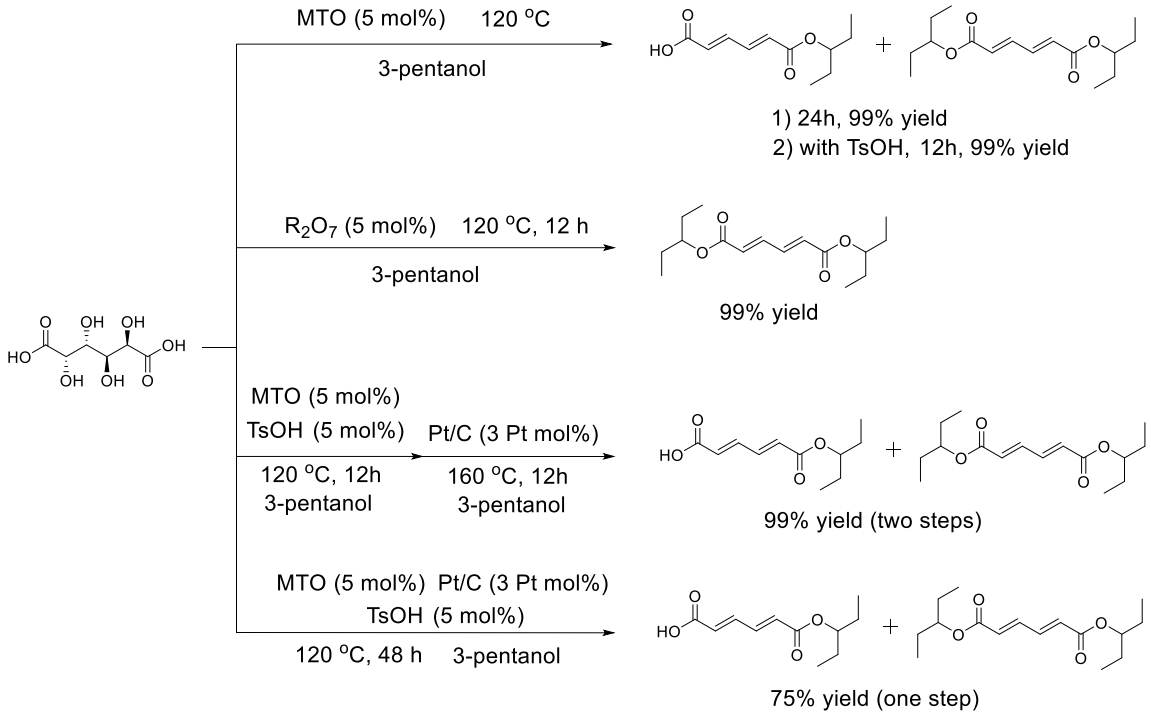

Scheme 1.11 DODH-transfer hydrogenation of mucic acid.

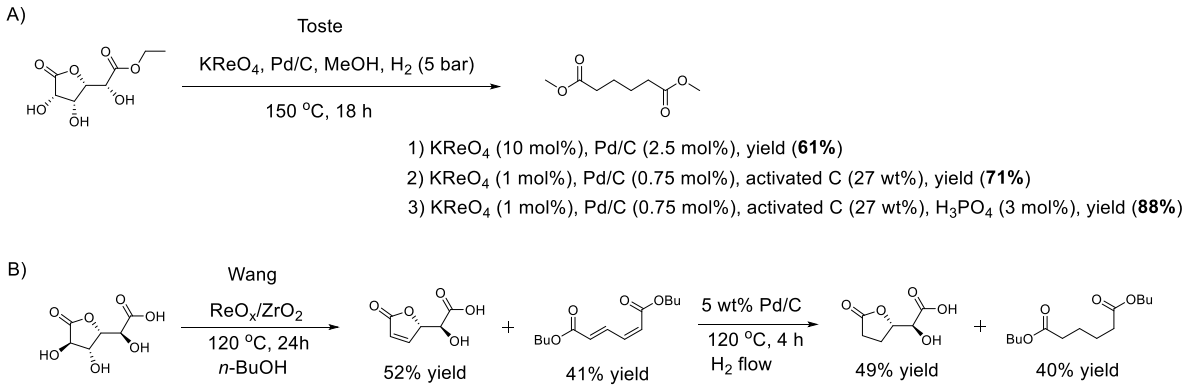

Scheme 1.12 DODH-hydrogenation of A) ethyl ester of D-glucarate-6,3-lactone and B) D-glucaric acid-1,4-lactone.

In addition to mucic acid, D-glucaric acid lactone or its ester was used to produce adipates through DODH-hydrogenation reaction (Scheme 1.12). In 2017, Toste's group employed a physical mixture of $KReO_4$ and Pd/C for DODH and hydrogenation, respectively.[38] Molecular H_2 worked as a hydrogen donor for both reactions. This one-step reaction produced 61% yield of adipates at 150 ^oC. With an additive of activated carbon, H_3PO_4 cocatalyst, and the reduced amount of Re and Pd catalysts, a higher yield (88%) of adipates was obtained (Scheme 1.12A). Recently, Wang et al. investigated DODH of glucaric acid lactone over ReO_x/support catalysts.[39] Among them, ReO_x/ZrO_2 catalyst exhibited the highest yield of olefins with *n*-butanol as a reductant. DODH products consisted of muconate and five-membered ring lactone with one OH group and one C-C double bond (Scheme 1.12B). Further hydrogenation of the products with Pd/C gave hydrogenated five-membered ring lactone (49% yield) and adipate (40% yield).

C. Transfer hydrogenation with heterogeneous catalysts for upgrading of biomass model compounds

Catalytic transfer hydrogenation (CTH) reaction is an effective method that adds hydrogen to the substrate without using molecular H_2 gas.[40] CTH reaction uses liquid phase hydrogen donor including simple alcohols and formic acid, providing several advantages over direct hydrogenation: 1) minimizing possible hazards without using flammable gas, 2) avoiding high-pressure affordable infrastructure, and 3) enhancing the solubility of the hydrogen donor.[41] Since Knoevenagel proposed CTH reaction a century ago, a wide range of homo- and heterogeneous catalysts and hydrogen donors have been developed for CTH of unsaturated bonds (e.g. C=C, C=O, N=O, N=N, C≡N, and C≡C) or for single bonds

resulting in bond cleavage (C-O, C-N, and C-S).[40,42] In the last two decades, CTH with C1-C3 alcohols or formic acid has been employed to provide hydrogen for hydrodeoxygenation (HDO) of biomass-derived chemicals, lowering their oxygen contents. HDO processes with CTH over heterogeneous catalysts include hydrogenation of olefins and carbonyl groups, hydrogenolysis of C-O bonds.

In 2010, Thananatthanachon and Rauchfuss proposed the use of CTH reaction with formic acid as a hydrogen donor to convert 5-hydroxymethylfurfural (HMF) into 2,5-dimethylfuran (DMF) with 5 wt% Pd/C catalyst and sulfuric acid.[43] Later, the same transformation was conducted with 5 wt% Ru/C catalyst and isopropanol, reported by Vlachos group.[44] Other metal catalysts such as Pd/Fe_2O_3,[45] Cu/porous metal oxides,[46] and Ni-Co/C[47] were also used to produce DMF from HMF through CTH reaction. This conversion of HMF to DMF follows CTH of C=O bond and two separate C-O hydrogenolysis shown in Scheme 1.13. Similarly, a combination of CTH/hydrogenolysis transformed furfural to 2-methylfuran.[45,48]

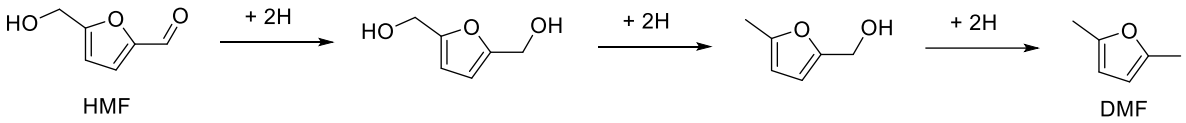

Scheme 1.13 Transformation of HMF to DMF.

CTH-assisted HDO over metal catalysts was also utilized to produce γ-valerolactone (GVL) from levulinic acid (LA). In 2013, Fu's group reported Raney Ni exhibited 99% yield of GVL from LA in the presence of isopropanol as a hydrogen donor while other Ni nanoparticle catalysts did not afford GVL.[49] The possible mechanism is CTH of LA to 4-hydroxypentanoic (HPA) acid, followed by lactonization to GVL (Scheme 1.14). The other possible mechanism that LA undergoes lactonization, followed by CTH of the resulting C=C bond was proposed by Hasan's group.[50] They obtained 89% yield of GVL over Pd/C catalyst in ethanol with KOH. In the absence of base, Pd/C catalyst did not afford GVL.

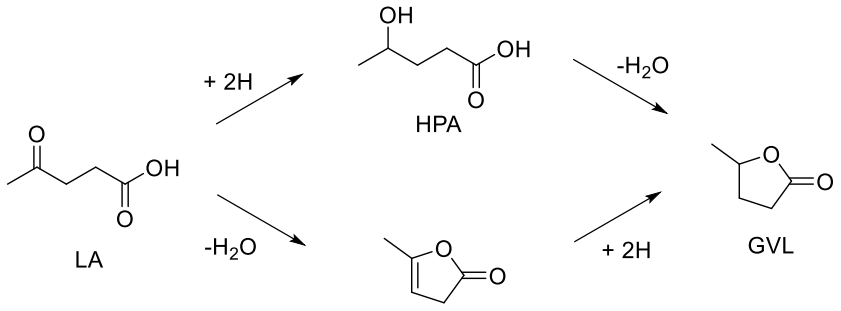

Scheme 1.14 Transformation of LA to GVL.

In addition to the conversion of cellulose-derived materials, HDO-CTH reaction of aromatic compounds has been also investigated. CTH assisted C-O bond cleavage of lignin-derived monomeric and dimeric phenolics can be an alternative H_2-driven HDO of the phenolics.[51] Jae's group tested monometallic Ru and bimetallic Ru-Re catalysts for the conversion of guaiacol into cyclohexanol and cyclohexane through CTH with isopropanol.[52] Ring saturation of guaiacol and the removal of methoxy group through C-O hydrogenolysis were catalyzed by Ru, producing cyclohexanol as a major product. Further deoxygenation from cyclohexanol and cyclohexane was realized with bimetallic RuRe/C catalyst (Scheme 1.15). Similarly, various metal catalysts for HDO-CTH reaction of other phenolics including p-cresol,[53] phenol,[54] vanillin,[55] and 2-(2-methoxyphenoxy)-1-phenyl ethanol[56] as a β-O-4 model compound with isopropanol or formic acid were developed.

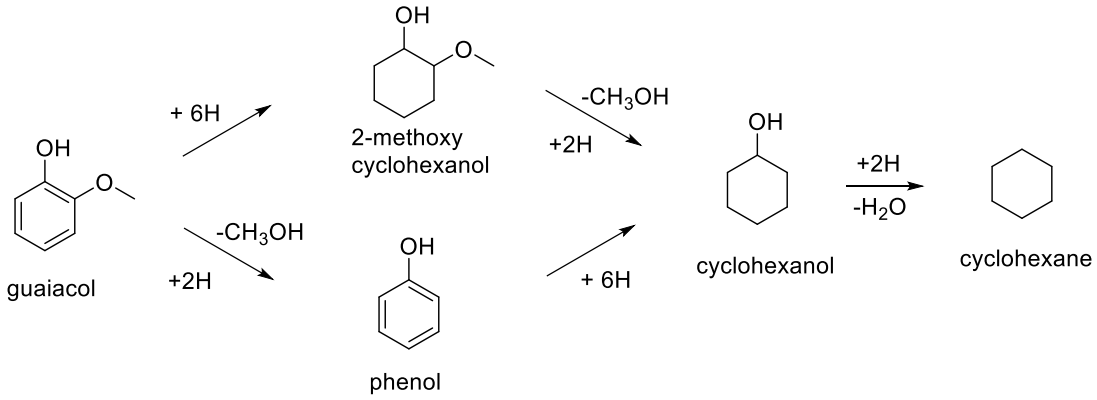

Scheme 1.15 Transformation of guaiacol to cyclohexanol and cyclohexane.

D. Chapter overview

This chapter is a brief introduction of literature regarding catalysis of deoxydehydration, hydrogenation, and catalytic transfer hydrogenation as effective strategies to valorize biomss-drived sugar alcohols and acids. Chapter 2 describes deoxydehydration of polyols with unsupported rhenium oxide nanoparticles, which is reusable as a heterogeneous catalyst. Changes in the speciation and structure of ReO_x during catalysis are shown through various in-situ and ex-situ characterization tools. In addition to the characterization results, kinetic isotope effect tests provide the mechanistic insights in deoxydehydration over heterogeneous rhenium oxide catalysts. Chapter 2 is reproduced with permission from *ACS Sustainable Chemistry and Engineering*, **2019**, 7, 11438-11447. Copyright 2019 American Chemical Society.

Chapters 3 and 4 describe bimetallic bifunctional catalysts for one-step conversion of mucic acid to adipates through a combination of deoxydehydration and catalytic transfer hydrogenation. Isopropanol is used as both solvent and hydrogen donor for both deoxydehydration and catalytic transfer hydrogenation. The reusability and regeneration of the catalysts are investigated. Based on the characterization of the catalyst and isotope labeling experiments, the possible mechanism is proposed. Chapter 3 is reproduced with permission from *ACS Catalysis*, in press. Unpublished work copyright **2020** American Chemical Society.

In Chapter 5, catalytic transfer hydrogenation assisted hydrodeoxygenation of succinic acid to γ-butyrolactone and tetrahydrofuran with rhenium oxide nanoparticle is investigated. This, combined with deoxydehydration and C=C bond saturation through catalytic transfer hydrogenation, enables to convert tartaric acid to γ-butyrolactone in one-step. The possible pathways are described based on experimental observations. Chapter 5 is reproduced with permission from *Energies*, in press. Unpublished work copyright **2020** MDPI.

E. References

(1) Rinaldi, R.; Jastrzebski, R.; Clough, M. T.; Ralph, J.; Kennema, M.; Bruijnincx, P. C. A.; Weckhuysen, B. M. Paving the Way for Lignin Valorisation: Recent Advances in Bioengineering, Biorefining and Catalysis. *Angew. Chem. Int. Ed.* **2016**, *55* (29), 8164–8215.

(2) Lin, Y.-C.; Huber, G. W. The Critical Role of Heterogeneous Catalysis in Lignocellulosic Biomass Conversion. *Energy Environ. Sci.* **2009**, *2* (1), 68–80.

(3) Dodds, D. R.; Gross, R. A. Chemicals from Biomass. *Science* **2007**, *318*, 1250–1251.

(4) Shiramizu, M.; Toste, F. D. Deoxygenation of Biomass-Derived Feedstocks: Oxorhenium-Catalyzed Deoxydehydration of Sugars and Sugar Alcohols. *Angew. Chem. Int. Ed.* **2012**, *51* (32), 8082–8086.

(5) Mettler, M. S.; Vlachos, D. G.; Dauenhauer, P. J. Top Ten Fundamental Challenges of Biomass Pyrolysis for Biofuels. *Energy Environ. Sci.* **2012**, *5* (7), 7797.

(6) Akien, G. R.; Qi, L.; Horvath, I. T.; Horváth, I. T. Molecular Mapping of the Acid Catalysed Dehydration of Fructose. *Chem. Comm.* **2012**, *48* (47), 5850–5852.

(7) Miranda, M. O.; Pietrangelo, A.; Hillmyer, M. A.; Tolman, W. B. Catalytic Decarbonylation of Biomass-Derived Carboxylic Acids as Efficient Route to Commodity Monomers. *Green Chem.* **2012**, *14* (2), 490.

(8) Ruppert, A. M.; Weinberg, K.; Palkovits, R. Hydrogenolysis Goes Bio: From Carbohydrates and Sugar Alcohols to Platform Chemicals. *Angew. Chem. Int. Ed.* **2012**, *51* (11), 2564–2601.

(9) Yi, J.; Liu, S.; Abu-Omar, M. M. Rhenium-Catalyzed Transfer Hydrogenation and Deoxygenation of Biomass-Derived Polyols to Small and Useful Organics. *ChemSusChem* **2012**, *5* (8), 1401–1404.

(10) Raju, S.; Moret, M. E.; Klein Gebbink, R. J. M. Rhenium-Catalyzed Dehydration and Deoxydehydration of Alcohols and Polyols: Opportunities for the Formation of Olefins from Biomass. *ACS Catal.* **2015**, *5* (1), 281–300.

(11) Cook, G. K.; Andrews, M. A. Toward Nonoxidative Routes to Oxygenated Organics: Stereospecific Deoxydehydration of Diols and Polyols to Alkenes and Allylic Alcohols Catalyzed by the Metal Oxo Complex (C5Me5)ReO3. *J. Am. Chem. Soc.* **1996**, *118* (39), 9448–9449.

(12) Herrmann, W. A.; Marz, D.; Herdtweck, E.; Schäfer, A.; Wagner, W.; Kneuper, H.-J. Glycolate and Thioglycolate Complexes of Rhenium and Their Oxidative Elimination of Ethylene and of Glycol. *Angew. Chem. Int. Ed. Engl.* **1987**, *26* (5), 462–464.

(13) Ziegler, J. E.; Zdilla, M. J.; Evans, A. J.; Abu-Omar, M. M. H2-Driven Deoxygenation of Epoxides and Diols to Alkenes Catalyzed by Methyltrioxorhenium. *Inorg. Chem.* **2009**, *48* (21), 9998–10000.

(14) Ahmad, I.; Chapman, G.; Nicholas, K. M. Sulfite-Driven, Oxorhenium-Catalyzed Deoxydehydration of Glycols. *Organometallics* **2011**, *30* (10), 2810–2818.

(15) Arceo, E.; Ellman, J. A.; Bergman, R. G. Rhenium-Catalyzed Didehydroxylation of Vicinal Diols to Alkenes Using a Simple Alcohol as a Reducing Agent. *J. Am. Chem. Soc.* **2010**, *132* (33), 11408–11409.

(16) Shiramizu, M.; Toste, F. D. Expanding the Scope of Biomass-Derived Chemicals through Tandem Reactions Based on Oxorhenium-Catalyzed Deoxydehydration. *Angew. Chem. Int. Ed.* **2013**, *52* (49), 12905–12909.

(17) Wozniak, B.; Li, Y.; Tin, S.; de Vries, J. G. Rhenium-Catalyzed Deoxydehydration of Renewable Triols Derived from Sugars. *Green Chem.* **2018**, *20* (19), 4433–4437.

(18) Qu, S.; Dang, Y.; Wen, M.; Wang, Z.-X. Mechanism of the Methyltrioxorhenium-Catalyzed Deoxydehydration of Polyols: A New Pathway Revealed. *Chem. Eur. J.* **2013**, *19* (12), 3827–3832.

(19) Liu, S.; Senocak, A.; Smeltz, J. L.; Yang, L.; Wegenhart, B.; Yi, J.; Kenttämaa, H. I.; Ison, E. A.; Abu-Omar, M. M. Mechanism of MTO-Catalyzed Deoxydehydration of Diols to Alkenes Using Sacrificial Alcohols. *Organometallics* **2013**, *32* (11), 3210–3219.

(20) Denning, A. L.; Dang, H.; Liu, Z.; Nicholas, K. M.; Jentoft, F. C. Deoxydehydration of Glycols Catalyzed by Carbon-Supported Perrhenate. *ChemCatChem* **2013**, *5* (12), 3567–3570.

(21) Sandbrink, L.; Klindtworth, E.; Islam, H.-U.; Beale, A. M.; Palkovits, R. ReOx/TiO2: A Recyclable Solid Catalyst for Deoxydehydration. *ACS Catal.* **2016**, *6* (2), 677–680.

(22) Kon, Y.; Araque, M.; Nakashima, T.; Paul, S.; Dumeignil, F.; Katryniok, B. Direct Conversion of Glycerol to Allyl Alcohol Over Alumina-Supported Rhenium Oxide. *ChemistrySelect* **2017**, *2* (30), 9864–9868.

(23) Sharkey, B. E.; Denning, A. L.; Jentoft, F. C.; Gangadhara, R.; Gopaladasu, T. V.; Nicholas, K. M. New Solid Oxo-Rhenium and Oxo-Molybdenum Catalysts for the Deoxydehydration of Glycols to Olefins. *Catal. Today* **2018**, *310*, 86–93.

(24) Tazawa, S.; Ota, N.; Tamura, M.; Nakagawa, Y.; Okumura, K.; Tomishige, K. Deoxydehydration with Molecular Hydrogen over Ceria-Supported Rhenium Catalyst with Gold Promoter. *ACS Catal.* **2016**, *6* (10), 6393–6397.

(25) Cao, J.; Tamura, M.; Nakagawa, Y.; Tomishige, K. Direct Synthesis of Unsaturated Sugars from Methyl Glycosides. *ACS Catal.* **2019**, *9* (4), 3725–3729.

(26) Nakagawa, Y.; Tazawa, S.; Wang, T.; Tamura, M.; Hiyoshi, N.; Okumura, K.; Tomishige, K. Mechanistic Study of Hydrogen-Driven Deoxydehydration over Ceria-Supported Rhenium Catalyst Promoted by Au Nanoparticles. *ACS Catal.* **2018**, *8* (1), 584–595.

(27) Hills, L.; Moyano, R.; Montilla, F.; Pastor, A.; Galindo, A.; Álvarez, E.; Marchetti, F.; Pettinari, C. Dioxomolybdenum(VI) Complexes with Acylpyrazolonate Ligands: Synthesis, Structures, and Catalytic Properties. *Eur. J. Inorg. Chem.* **2013**, *2013* (19), 3352–3361.

(28) Dethlefsen, J. R.; Lupp, D.; Teshome, A.; Nielsen, L. B.; Fristrup, P. Molybdenum-Catalyzed Conversion of Diols and Biomass-Derived Polyols to Alkenes Using Isopropyl Alcohol as Reductant and Solvent. *ACS Catal.* **2015**, *5* (6), 3638–3647.

(29) Navarro, C. A.; John, A. Deoxydehydration Using a Commercial Catalyst and Readily Available Reductant. *Inorg. Chem. Comm.* **2019**, *99*, 145–148.

(30) Sandbrink, L.; Beckerle, K.; Meiners, I.; Liffmann, R.; Rahimi, K.; Okuda, J.; Palkovits, R. Supported Molybdenum Catalysts for the Deoxydehydration of 1,4-Anhydroerythritol into 2,5-Dihydrofuran. *ChemSusChem* **2017**, *10* (7), 1375–1379.

(31) Chapman, G.; Nicholas, K. M. Vanadium-Catalyzed Deoxydehydration of Glycols. *Chem. Commun.* **2013**, *49* (74), 8199.

(32) Gopaladasu, T. V.; Nicholas, K. M. Carbon Monoxide (CO)- and Hydrogen-Driven, Vanadium-Catalyzed Deoxydehydration of Glycols. *ACS Catal.* **2016**, 6 (3), 1901-1904.

(33) Petersen, A. R.; Nielsen, L. B.; Dethlefsen, J. R.; Fristrup, P. Vanadium-Catalyzed Deoxydehydration of Glycerol Without an External Reductant. *ChemCatChem* **2018**, 10, 769-778.

(34) Kwok, K. M.; Choong, C. K. S.; Ong, D. S. W.; Ng, J. C. Q.; Gwie, C. G.; Chen, L.; Borgna, A. Hydrogen-Free Gas-Phase Deoxydehydration of 2,3-Butanediol to Butene on Silica-Supported Vanadium Catalysts. *ChemCatChem* **2017**, *9* (13), 2443–2447.

(35) Almeida, R.; Ribeiro, M. F.; Fernandes, A.; Lourenço, J. P. Gas-Phase Conversion of Glycerol to Allyl Alcohol over Vanadium-Supported Zeolite Beta. *Catal. Comm.* **2019**, *127*, 20–24.

(36) Li, X.; Wu, D.; Lu, T.; Yi, G.; Su, H.; Zhang, Y. Highly Efficient Chemical Process To Convert Mucic Acid into Adipic Acid and DFT Studies of the Mechanism of the Rhenium-Catalyzed Deoxydehydration. *Angew. Chem. Int. Ed.* **2014**, *53* (16), 4200–4204.

(37) Li, X.; Zhang, Y. Highly Selective Deoxydehydration of Tartaric Acid over Supported and Unsupported Rhenium Catalysts with Modified Acidities. *ChemSusChem* **2016**, *9* (19), 2774–2778.

(38) Larson, R. T.; Samant, A.; Chen, J.; Lee, W.; Bohn, M. A.; Ohlmann, D. M.; Zuend, S. J.; Toste, F. D. Hydrogen Gas-Mediated Deoxydehydration/Hydrogenation of Sugar Acids: Catalytic Conversion of Glucarates to Adipates. *J. Am. Chem. Soc.* **2017**, *139* (40), 14001–14004.

(39) Lin, J.; Song, H.; Shen, X.; Wang, B.; Xie, S.; Deng, W.; Wu, D.; Zhang, Q.; Wang, Y. Zirconia-Supported Rhenium Oxide as an Efficient Catalyst for the Synthesis of Biomass-Based Adipic Acid Ester. *Chem. Commun.* **2019**, *55* (74), 11017–11020.

(40) Wang, D.; Astruc, D. The Golden Age of Transfer Hydrogenation. *Chem. Rev.* **2015**, *115* (13), 6621–6686.

(41) Gilkey, M. J.; Xu, B. Heterogeneous Catalytic Transfer Hydrogenation as an Effective Pathway in Biomass Upgrading. *ACS Catal.* **2016**, *6* (3), 1420–1436.

(42) Brieger, G.; Nestrick, T. J. Catalytic Transfer Hydrogenation. *Chem. Rev.* **1974**, *74*, 567–580.

(43) Thananatthanachon, T.; Rauchfuss, T. B. Efficient Production of the Liquid Fuel 2,5-Dimethylfuran from Fructose Using Formic Acid as a Reagent. *Angew. Chem. Int. Ed.* **2010**, *49* (37), 6616–6618.

(44) Jae, J.; Zheng, W.; Lobo, R. F.; Vlachos, D. G. Production of Dimethylfuran from Hydroxymethylfurfural through Catalytic Transfer Hydrogenation with Ruthenium Supported on Carbon. *ChemSusChem* **2013**, *6* (7), 1158–1162.

(45) Scholz, D.; Aellig, C.; Hermans, I. Catalytic Transfer Hydrogenation/Hydrogenolysis for Reductive Upgrading of Furfural and 5-(Hydroxymethyl)Furfural. *ChemSusChem* **2014**, *7* (1), 268–275.

(46) Hansen, T. S.; Barta, K.; Anastas, P. T.; Ford, P. C.; Riisager, A. One-Pot Reduction of 5-Hydroxymethylfurfural via Hydrogen Transfer from Supercritical Methanol. *Green Chem.* **2012**, *14* (9), 2457.

(47) Yang, P.; Xia, Q.; Liu, X.; Wang, Y. Catalytic Transfer Hydrogenation/Hydrogenolysis of 5-Hydroxymethylfurfural to 2,5-Dimethylfuran over Ni-Co/C Catalyst. *Fuel* **2017**, *187*, 159–166.

(48) Panagiotopoulou, P.; Vlachos, D. G. Liquid Phase Catalytic Transfer Hydrogenation of Furfural over a Ru/C Catalyst. *Appl. Catal. A-Gen* **2014**, *480*, 17–24.

(49) Yang, Z.; Huang, Y.-B.; Guo, Q.-X.; Fu, Y. RANEY® Ni Catalyzed Transfer Hydrogenation of Levulinate Esters to γ-Valerolactone at Room Temperature. *Chem. Commun.* **2013**, *49* (46), 5328.

(50) Amarasekara, A. S.; Hasan, M. A. Pd/C Catalyzed Conversion of Levulinic Acid to γ-Valerolactone Using Alcohol as a Hydrogen Donor under Microwave Conditions. *Catal. Comm.* **2015**, *60*, 5–7.

(51) Jin, W.; Pastor-Pérez, L.; Shen, D.; Sepúlveda-Escribano, A.; Gu, S.; Ramirez Reina, T. Catalytic Upgrading of Biomass Model Compounds: Novel Approaches and Lessons Learnt from Traditional Hydrodeoxygenation - a Review. *ChemCatChem* **2019**, *11* (3), 924–960.

(52) Kim, M.; Ha, J.-M.; Lee, K.-Y.; Jae, J. Catalytic Transfer Hydrogenation/Hydrogenolysis of Guaiacol to Cyclohexane over Bimetallic RuRe/C Catalysts. *Catal. Comm.* **2016**, *86*, 113–118.

(53) Guo, T.; Xia, Q.; Shao, Y.; Liu, X.; Wang, Y. Direct Deoxygenation of Lignin Model Compounds into Aromatic Hydrocarbons through Hydrogen Transfer Reaction. *Appl. Catal. A-Gen.* **2017**, *547*, 30–36.

(54) Zeng, Y.; Wang, Z.; Lin, W.; Song, W. In Situ Hydrodeoxygenation of Phenol with Liquid Hydrogen Donor over Three Supported Noble-Metal Catalysts. *Chem. Eng.* **2017**, *320*, 55–62.

(55) Singh, A. K.; Jang, S.; Kim, J. Y.; Sharma, S.; Basavaraju, K. C.; Kim, M.-G.; Kim, K.-R.; Lee, J. S.; Lee, H. H.; Kim, D.-P. One-Pot Defunctionalization of Lignin-Derived Compounds by Dual-Functional $Pd_{50}Ag_{50}/Fe_3O_4$/N-RGO Catalyst. *ACS Catal.* **2015**, *5* (11), 6964–6972.

(56) Zhang, B.; Qi, Z.; Li, X.; Ji, J.; Zhang, L.; Wang, H.; Liu, X.; Li, C. Cleavage of Lignin C–O Bonds over a Heterogeneous Rhenium Catalyst through Hydrogen Transfer Reactions. *Green Chem.* **2019**, *21* (20), 5556–5564.

CHAPTER II. Deoxydehydration (DODH) of Biomass-Derived Polyols with Reusable Unsupported Rhenium Nanoparticles Catalyst

A. Introduction

Making chemicals from petroleum derived synthons requires addition of heteroatoms such as oxygen and nitrogen. In contrast, removal of oxygen is necessary in making useful chemicals from biomass starting materials.[1,2] One attractive deoxygenation reaction is catalytic deoxydehydration (DODH),[3] which converts vicinal diols to alkenes. Several DODH metal catalysts have been reported including Re,[4] V,[5] and Mo.[6] In particular, Re-based homogeneous catalysts have been extensively studied and their efficacy attributed to oxophilicity[7] and a wide range of accessible oxidation states.[4] Many reductants have been used with rhenium catalysts including organophosphines,[8,9] H_2,[10–12] inorganic sulfites,[13–15] and alcohols.[2,3,16–21] Based on experimental and computational investigations, the DODH mechanism for homogeneous Re catalysis involves three steps: (1) reduction of high-valent Re species, (2) diol condensation to form Re diolate intermediates, and (3) concerted alkene extrusion, the reverse of [3+2] addition (Eq 1).[4,22]

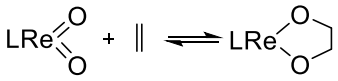

(1)

One major drawback of homogeneous catalysts is the difficulty in recycling the catalyst. Additionally, under the conditions necessary for DODH (T > 150 °C), homogeneous catalysts tend to degrade. As a result, heterogeneous Re catalysts are of interest and have recently been pursued. In 2013, oxo-rhenium supported on carbon (ReO_x-C) was introduced as the first heterogeneous catalyst for DODH with H_2 as a reductant.[23] For this catalyst, significant metal leaching was observed.[24] A recent study of ReO_x/TiO_2 showed glycerol conversion into allyl alcohol in 58% yield with 3-octanol as a reductant.[25] Yet a higher yield

of allyl alcohol (91%) was achieved by ReO_x/Al_2O_3 with 2-hexanol and by ReO_x-Au/CeO_2 in 1,4-dioxane using H_2 as a reductant.[26,27]

Despite these recent advances on heterogeneous DODH catalysts, the reaction mechanism and oxidation states of rhenium remain poorly understood. Tomishige suggested a mechanism for H_2-driven heterogeneous DODH involving Re^{VI}/Re^{IV} cycle and analogous elementary steps to homogeneous systems.[28,29] Mechanistic and kinetic studies of heterogeneous DODH catalysis with alcohol as a reductant have not been reported.

It has been found that unsupported ReO_x nanoparticles reported earlier by our group for alcohol dehydrogenation[30] afford heterogeneous DODH of polyols with high recyclability and provide a good system to study for mechanistic insights without the influence of a support. Investigations of ReO_x NPs in DODH via *in situ* and *ex situ* X-ray spectroscopic analysis, kinetics studies, and kinetic isotope effect measurements have been conducted to elucidate heterogeneous DODH mechanism driven by alcohol reductants. The postulated mechanism suggests a Re(V) desoxo species as the active site for alkene extrusion.

B. Experimental details

1. Synthesis

All commercial materials were used as received without further purification. Ammonium perrhenate (NH_4ReO_4) was purchased from Strem Chemicals. 1,1,2,3,3-d_5-Glycerol and $(OD)_3$-glycerol were purchased from Cambridge Isotope Laboratory. All other reagents were purchased from Sigma-Aldrich or Alfa Aesar. Unsupported rhenium oxide nanoparticles (ReO_x NPs) were prepared in neat alcohol as reported previously.[30] In order to simplify synthesis process and avoid formation of metallic rhenium, the nanoparticles were prepared under ambient atmosphere instead of under nitrogen.

Catalyst preparation. Ammonium perrhenate (NH_4ReO_4, 134 mg, 0.5 mmol) and 3-octanol (10 mL, 63 mmol) were refluxed at 180 °C for 12 h in open air. After 10 min the color of solution changed to yellow, and finally dark brown. The synthesized unsupported ReO_x NPs were obtained by centrifugation (11,000 rpm for 1.5 h). In order to remove unreacted ammonium perrhenate, the resulting ReO_x NPs were washed with ethanol and hexane solution (1:1 wt %) followed by further centrifugation. After repeating the washing step, the ReO_x NPs were dispersed in ethanol and kept for future use.

2. General catalytic procedure

Catalytic tests for DODH reactions were performed in a 50 mL one neck round-bottom flask connected to a column, collecting flask, heating band, and thermometer. 10.9 mmol (1.0 g) of glycerol, 109 mmol (17.3 mL) of 3-octanol, and 10 mg (1.0 wt %) of the synthesized ReO_x NPs were placed into the round-bottom flask. The flask was heated in a preheated 170 °C oil bath. The produced volatile products such as allyl alcohol and acrolein were collected over a water bath. The products in the collection flask and the remaining solution in the reaction flask were added to d_6-DMSO and analyzed by NMR with mesitylene as an internal standard. ^{1}H-NMR and ^{13}C-NMR spectra were measured on a Bruker Avance 500MHz spectrometer. Due to high volatility of products at room temperature, the catalytic tests of meso-erythritol and cis-but-2-ene-1,4-diol were performed in 120 mL pressure glass vessel sealed with a Teflon lined screw cap. For recycling experiments, the used catalyst was separated by centrifugation, followed by washing with ethanol and hexane solution and drying under vacuum.

3. Characterization

Transmission electron microscope (TEM) images were acquired on FEI Tecnai G2 Microscope. Averaged particle size was calculated by $\Sigma n_i d_i^3/\Sigma n_i d_i^2$ (d_i: particle size, n_i: number of particles with d_i). Elemental analysis was carried out via inductively coupled plasma (ICP) (Thermo iCAP 6300) and on CHN analyzer (CEC 440HA). IR spectra were obtained on Thermo-Nicolet iS10 FTIR. X-ray diffraction (XRD) patterns were recorded on a PANalytical Empyrean X-ray diffractometer using Cu K_α source. The software package HighScore 3.0 was used to identify the phases. In order to quantify amorphous phase fraction, the XRD data of a 1:1 (wt%) mixture of the power sample and fully crystalline silicon as an internal standard was analyzed by Rietveld method with the software package.

Ex-situ X-ray photoelectron spectroscopy (XPS) analyses were performed on a Kratos Axis Ultra spectrometer with an Al K monochromic X-ray radiation. The survey spectra 160 eV) and the high-resolution spectra (20 eV) of the Re 4f, C 1s, and O 1s were collected. Binding energies were calibrated by setting the C 1s peak to 284.5 eV. The CasaXPS software package was used for curve fitting. The oxidation states of as-prepared and recycled ReO_x NPs were determined.[31,32] The catalysts reduced or oxidized in a flow of 3% H_2/He (50 mL/min) or air (50 mL/min) at different temperatures of 200 and 300 °C for 1 h were cooled down to room temperature first and then analyzed by XPS.

X-ray absorption spectroscopy (XAS) experiments were conducted at Sector 10-ID (insertion device) beamline in collaboration with the Materials Research Collaborative Access Team (MR-CAT) at the Advanced Photon Source (APS) of Argonne National Laboratory (ANL). Prior to the XAS measurements, the samples were finely ground with addition of boron nitride as a diluent using a mortar and pestle. The amount of boron nitride was calculated separately for each sample in order to obtain a good edge step close to 1. The

sample was then pressed into a six-hole, cylindrical-shaped holder where each hole has a radius of 2.0 mm, forming a self-supporting wafer. The six-hole sample holder was placed in a quartz tube (1 in. OD, 10 in. length) sealed with Kapton windows by two Ultra-Torr fittings. The quartz tube was then transferred to the beamline hutch and positioned at the center of a lab-scale furnace. Both the inlet and the outlet of the quartz tube were connected to stainless-steel tubing allowing gases to flow through the sample holder. For measurements involving treatment with H_2, the as-prepared ReO_x NPs were first heated to the target temperature (100, 200 and 300 °C) with a 50 mL/min flow of a 3% H_2/He feed, and the temperature was maintained until the oxidation state of Re reached equilibrium. It should be noted that multiple scans were collected at an average rate of 1 scan /5 min at each temperature. After collecting the last EXAFS spectrum at RT, the ReO_x NPs were exposed to air for 30 min and subsequently treated with 1% O_2/He for 1 h at 300 °C.

With respect to the solution-phase measurements, the sample was suspended in 1:3 (vol/vol) glycerol + 3-octanol and shaken vigorously to achieve uniform dispersion prior to the measurements. The suspension was then transferred to an NMR tube and was heated in a preheated 170 °C mineral oil bath. The XAS spectra were collected by aligning the beam at the center of the NMR tube. All XAS measurements were carried out in transmission mode. A Si (111) monochromator with a cryo-cooled first crystal and a 250-mm long second crystal was used to provide Re-L3 edge energy (10535 eV). Harmonic interference was removed by using a 60-cm long flat harmonic rejection mirror with Pt and Rh coatings. The beamline was calibrated using a Re foil and the foil spectrum was collected simultaneously with the samples to correct the edge energies of each sample. Background removal and normalization procedures were carried out using the Athena software package. EXAFS fitting was conducted using Artemis.[33]

C. Results and discussion

1. Deoxydehydration (DODH) of biomass-derived substrates

According to previous DODH catalysis studies, rhenium catalysts convert glycerol into useful organics such as allyl alcohol, propanal, and acrolein through both homogeneous and heterogeneous catalysis with specific reductants including alcohols and H_2.[34] In this chapter, glycerol (10 mmol) DODH is catalyzed by unsupported ReO_x NPs (1 wt % of glycerol) with 3-octanol as reductant, producing allyl alcohol under batch conditions combined with a distillation apparatus for removal of volatile products as they are formed (i.e. reactive distillation shown in Figure 2.1). Besides separation of volatile products from the reactor, this distillation system removes water, a byproduct of DODH, resulting in a higher reaction rate than a simple batch reactor (run 1-3 in Table 2.1). First, the most effective sacrificial alcohol and reaction conditions including reaction temperature and concentrations were determined (Figure 2.2). Among several candidate alcohols as sacrificial reductants for glycerol DODH, 3-octanol, a secondary alcohol, showed high activity and yield (Figure 2.2a). Primary alcohols and diols were not as effective. This is in agreement with ReO_x NPs acting as a dehydrogenation catalyst for alcohols and having the highest activity with secondary alcohols as has been noted previously.[30] The effect of 3-octanol versus glycerol concentrations on the DODH reaction was investigated in the range of [glycerol] = 0.6-4.2 M (Figure 2.2b). It should be noted that since 3-octanol is a solvent as the concentration of glycerol is increased, the concentration of 3-octanol is decreased. The optimal [glycerol] in 3-octanol was found to be 1.1 M. Higher concentration than 1.1 M led to a miscibility issue between 3-octanol and glycerol, resulting in the lower reaction rate (Figure 2.2b).

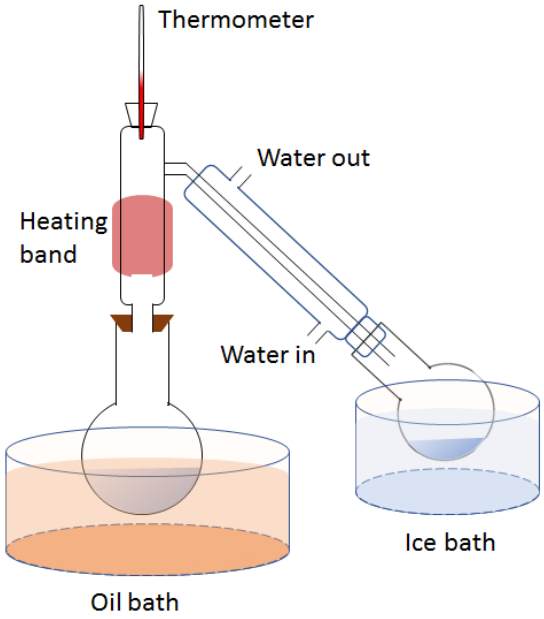

Figure 2.1 scheme of the reaction system. Temperature of oil bath is 170 °C. Heating band was used to collect volatile products efficiently.

Table 2.1 DODH Reaction of various substrates with ReO_x NPs

Run[a]	Substrate	t(h)	conv.[b] (%)	yield[d] (%)
1[d]	glycerol	3	56[c]	allyl alcohol (40) + acrolein (0.7)
2[d]	glycerol	10	89[c]	allyl alcohol (76) + acrolein (1.4)
3[e]	glycerol	3	40	allyl alcohol (22)
4[d]	1,2-hexanediol	10	91	1-hexene (80)
5[e]	meso-erithritol	3	72	1,3-butadiene (18) + 2,5-dihydrofuran (2)
6[e]	meso-erithritol	10	100	1,3-butadiene (34) + 2,5-dihydrofuran (7)
7[e]	cis-but-2-ene-1,4-diol	3	97	1,3-butadiene (41) + 2,5-dihydrofuran (9)

[a]Conditions: ReO_x 1 wt % of substrate, 3-octanol/substrate 10/1 mole ratio, T = 170 °C. [b]Conversion and yield are calculated by ^1H NMR [c]Conversion is calculated by HPLC. [d]substrate 1 g, using distillation system. [e]substrate 0.5 g, using pressure glass vessel.

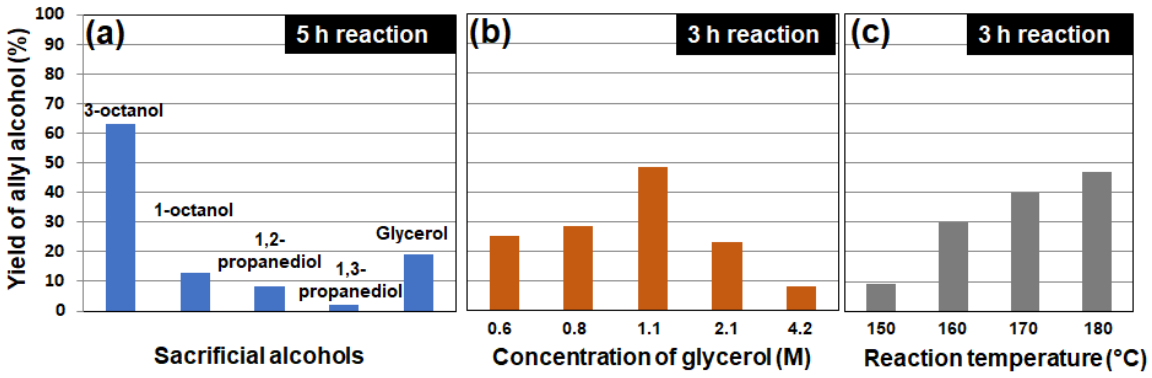

Figure 2.2 Optimal DODH conditions. (a) sacrificial alcohol reductants (reductant/glycerol is 10 equiv.), (b) concentration of glycerol (changing the amount of 3-octanol and fixing the amount of glycerol and catalysts), and (c) reaction temperature

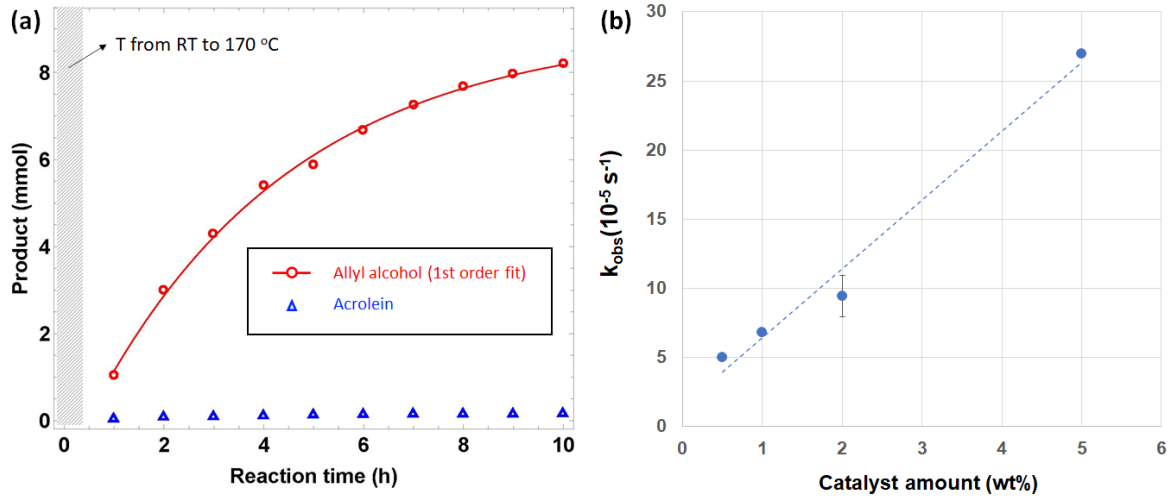

Figure 2.3 (a) Reaction profile for glycerol heterogeneous DODH to allyl alcohol and acrolein. Conditions: 1, 2, and 5 wt % ReO_x NPs of glycerol, 170 °C, 10 equiv of 3-octanol to glycerol, and air. The formation of allyl alcohol is fitted with pseudo-first-order kinetics (solid line). (b) Effect of the amount of ReO_x on glycerol DODH reaction.

At the optimized concentration and temperature (1.1 M glycerol and 170 °C), the time profile for DODH catalyzed by unsupported ReO_x NPs (1 wt% relative to glycerol) was collected and displayed in Figure 2.3a. 76 % yield of allyl alcohol was achieved and separated over the course of 10 h. The rate of formation of allyl alcohol follows first-order

kinetics in the limiting reagent [glycerol] with an observed rate constant of 6.8 x 10^{-5} s^{-1} at 1 wt% ReO_x NPs. At different catalyst loadings the observed rate constant shows dependence on ReO_x NPs (Figure 2.3b). During DODH, 3-octanol was dehydrogenated resulting in 3-octanone. The higher amount of 3-octanone (11.7 mmol) produced over the course reaction versus that of allyl alcohol (8.4 mmol) is due to independent dehydrogenation of 3-octanol by ReO_x NPs.

The question of whether the active catalyst is a homogeneous rhenium complex resulting from dissolution of the NPs was addressed through hot filtration test (Figure 2.4). During the course of the reaction, the catalyst was filtered hot and the filtrate was followed showing no further increase in yield of allyl alcohol with 4 % further conversion. It should be noted that the small conversion in starting material was also observed in a control experiment without catalyst, excluding the possibility of leaching of rhenium (Figure 2.4c). Furthermore, the heterogeneous ReO_x NPs were recycled seven times without showing significant loss of activity (Figure 2.5). The stability of solid Re catalysts is highly dependent on the support materials; ReO_x/TiO_2 showed high stability while a clear deactivation was detected for Re catalysts on activated carbon, zirconia, and silica.[23,25] Unsupported ReO_x nanoparticles exhibited long-term stability without any effect of supporting materials.

In addition to glycerol, other substrates including 1,2-hexanediol, meso-erythritol, and cis-but-2-ene-1,4-diol were investigated. The results are summarized in Table 2.1. The DODH of 1,2-hexanediol catalyzed by ReO_x NPs gave 1-hexene as the major product with moderate yields (52 % in 10 h). As previously studied in other reports for homogeneous Re-based catalysts,[2] ReO_x NPs produce butadiene by DODH from erythritol and 2,5-dihydrofuran by combination of DODH and dehydration. Recently, Toste and co-workers reported oxorhenium complexes catalyze also 2-ene-1,4-diols (1,4-DODH) and 2,4-diene-1,6-diols

(1,6-DODH).[20] DODH of cis-but-2-ene-1,4-diol by ReO_x NPs indicates that heterogeneous Re catalysts are also capable of 1,4-DODH, which has not been shown before for heterogeneous systems.

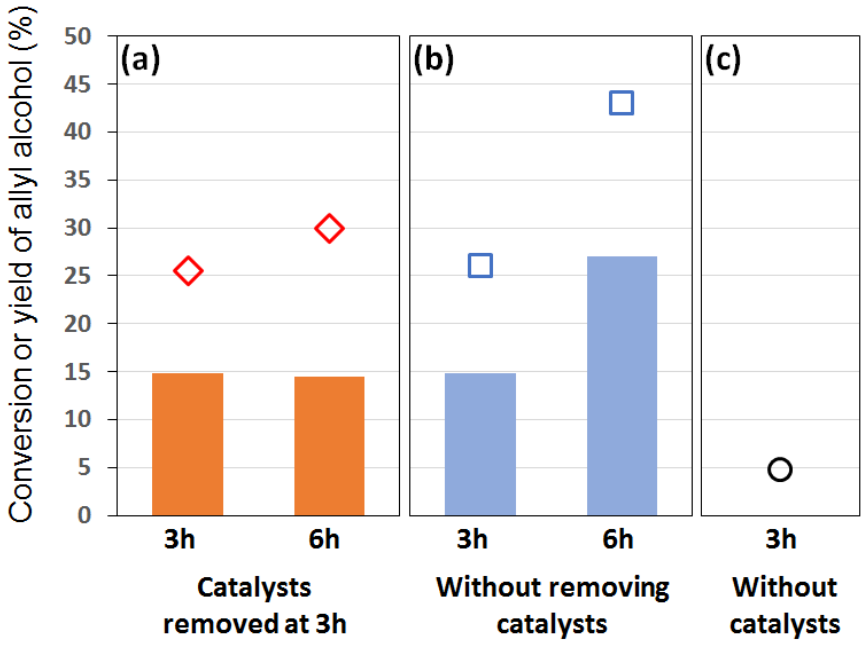

Figure 2.4 Hot filtration test. (a) ReO_x NPs (2 wt%) undergo glycerol DODH with 3-ocatnol in pressure glass vessel for 3 h at 160 °C. ReO_x NPs were removed by filtration at high temperature and the filtrate without ReO_x NPs was heated to 160 °C for additional 3 h. (b) Glycerol conversion and yield of allyl alcohol for 6 h without removing ReO_x NPs were recorded at 3h and 6h for control test. (c) Glycerol conversion without catalysts was studied for another control test.

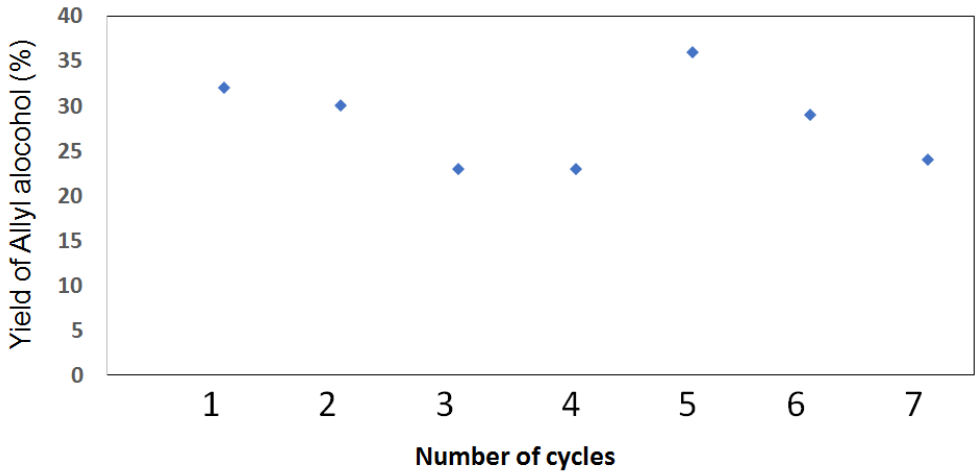

Figure 2.5 Recycling study for glycerol DODH by ReO_x NPs Conditions: 5 wt% ReO_x NPs of glycerol, 170 ºC, 1h, 10 equiv of 3-octanol to glycerol, and air. The used catalyst was separated and washed for recycling.

2. Catalyst characterization and reaction mechanism

The general DODH mechanism for homogeneous Re catalysts has been suggested to involve two electron redox cycles of Re^{VII}/Re^{V} [2,17] or Re^{V}/Re^{III}.[18] Heterogeneous DODH driven by H_2 with ReO_x-Au/CeO_2 has been suggested to follow similar mechanistic steps but via a different redox pair of Re^{VI}/Re^{IV}.[27] In this chapter, the changes of unsupported ReO_x NPs as-prepared and after (spent) DODH reaction were investigated.

2.1 The catalyst as prepared

Figure 2.7 shows the unsupported ReO_x nanoparticles as synthesized in this chapter. Based on estimation with 100 particles in the TEM images, the average size of nanoparticles prepared from NH_4ReO_4 in 3-octanol is 1.8 nm. The X-ray diffractogram of the prepared ReO_x NPs has only the diffraction peaks of ammonium perrhenate (Figure 2.6a). However, the quantitative analysis using internal standard method indicates that the prepared nanoparticles are heterogeneous materials, composed of 90 wt% of amorphous rhenium

oxides and 10 wt% of perrhenate structure (Figure 2.6b). Despite several washing steps, both NH_4^+ cations and 3-octanol are present in the prepared nanoparticles as shown by solid-state NMR (Figure 2.8). 3-octanol serves as a capping agent and it prevents the nanoparticles from growing into larger clusters. ICP and CHN elemental analysis showed that the approximate elemental composition is one ammonium (N) for every three Re atoms and the ratio of Re:O is 1:3 (Table 2.2).

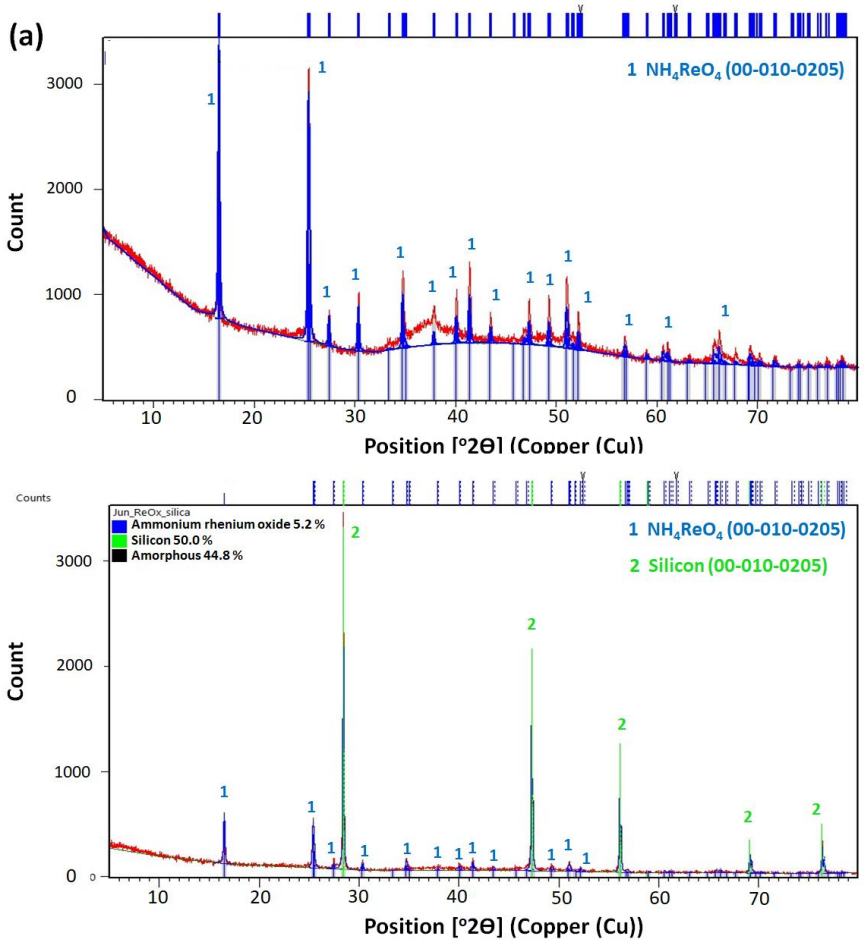

Figure 2.6 XRD patterns of (a) as-prepared ReO_x NP (b) a 1:1 mixture of ReO_x NPs and fully crystalline silicon as an internal standard. Rietveld refinement fits of ammonium perrhenate (blue lines) and fully crystalline silicon (green lines) were overlaid on the patterns.

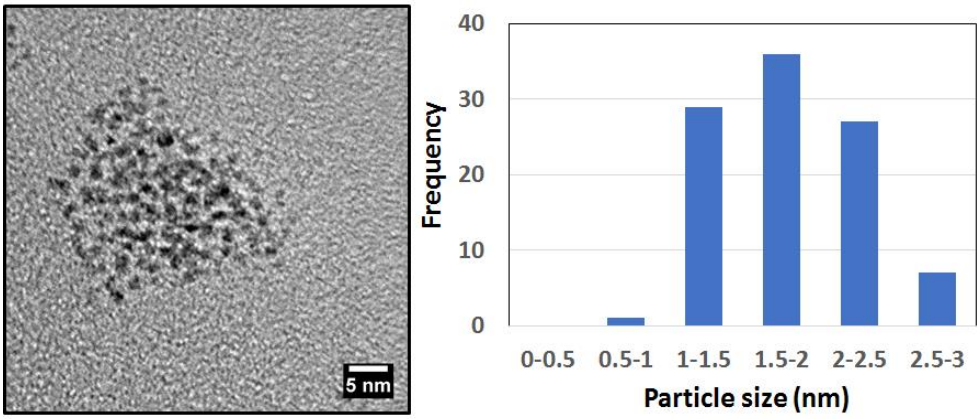

Figure 2.7 TEM image of as-prepared ReO_x NPs and size distribution.

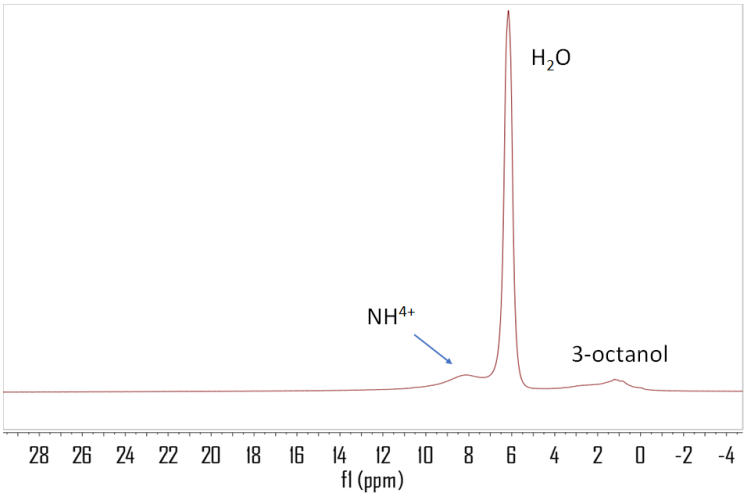

Figure 2.8 Solid-state ^1H MAS NMR spectra of ReO_x NPs.

Table 2.2 Elemental analysis based on ICP and CHN analyzer

Sample		Re[a]	C[b]	H	N	O[c]	O[b] (3-octanol)	O[d] (ReO_x)	O/Re (ReO_x)
As-prepared ReO_x NPs	Wt%	73.1	6.5	1.3	1.7	17.4	2.0	29.2	2.58
	Atomic%	11.3	15.7	38.2	3.6	31.2			

[a] ICP analysis, [b] C is from 3-octanol capping or in ReO_x NPs, [c] 100 - (Re+C+H+N) %, [d] O(total) – O (3-octanol) %,

2.2 In-situ and ex-situ XAS

XAS was employed to understand oxidation states and structural features of the ReO_x NPs under different treatment/reaction conditions. Figure 2.9a,b show the XANES spectra of as-prepared (before reaction) and spent (after DODH reaction) ReO_x NPs as well as the spectrum collected under catalytic DODH conditions ([3-octanol]/[glycerol] = 3, 1 wt% ReO_x NP at 170 °C). All the edge energies are summarized in Table 2.3. The edge energy of the as-prepared ReO_x NPs (10538.65 eV) indicates an average Re oxidation state between Re^{6+} and Re^{7+}, based on the edge energies of different Re standards (Figure 2.9d). Under reaction conditions (glycerol and 3-octanol), ReO_x NPs were slightly reduced, showing an average oxidation state between Re^{5+} and Re^{6+} (10538.13 eV). Two spent ReO_x NP catalysts, recovered after one and three catalytic cycles, showed an oxidation state between Re^{6+} and Re^{7+}, a value similar to that observed for the as-prepared ReO_x NPs.

EXAFS spectra of the as-prepared and post catalysis ReO_x NPs samples are shown in Figure 2.9c, and the corresponding fitting results are listed in Table 2.3. The EXAFS spectrum of the as-prepared ReO_x NPs revealed three different scattering paths which include two Re-O bond lengths of 1.73 ± 0.01 Å (consistent with Re=O double bond) and 2.02 ± 0.01 Å (consistent with Re-O single bond), and a Re-Re scattering at 2.57 ± 0.01 Å. Based on the reported range of rhenium standards, the longer Re-O path and Re-Re scattering might represent Re^{5+} oxorhenium cluster,[31] while the shorter Re-O bond length is close to Re^{7+} standards (i.e., 1.73 Å).[30,35] It is reported that EXAFS analysis of oxorhenium (V) clusters in Re-Pd/C catalysts showed Re-O path and Re-Re path with bond lengths of 2.03 and 2.57 Å.[31] As the catalyst goes through more reaction cycles, the shorter Re-O path (1.73-1.76 Å) decreases in intensity while the longer Re-O scattering (2.02 Å) increases in amplitude. This is indicative of a possible phase change in the Re catalyst, with perrhenate

type phases converting to ReO_x (Re^{5+}) type; this, coupled with the observed increase in coordination number of the Re-Re scattering corroborates the increasing degree of Re reduction after catalysis.

Reduction of ReO_x NPs after DODH reaction shown in XAS results was elaborated by FT-IR analysis. In the FT-IR spectra (Figure 2.10), the recycled ReO_x NPs (1 cycle) has reduced peaks between 800-1000 cm^{-1}, which are frequencies of Re=O multiple bonds.

Table 2.3 XANES edge energies of ReO_x NPs samples. EXAFS fitting results of Re-L3 edge are listed as N (coordination number), ss (Debye-Waller factor) and R (bond distance).[a]

Samples	Oxidation state	Edge Energy (eV)	Path	N	ss (Å)	R (Å)
In-situ	5+ < X < 6+	10538.13	N/A	N/A	N/A	N/A
As-prepared	6+ < X < 7+	10538.65	Re-O	1.7 (2)	0.0024	1.73 (1)
			Re-O	3.7 (3)	0.0056	2.02 (1)
			Re-Re	1.8 (3)	0.0056	2.57 (1)
Post-catalysis (1cycle)	6+ < X < 7+	10538.55	Re-O	1.3 (3)	0.0050	1.75 (2)
			Re-O	5.0 (8)	0.0055	2.02 (1)
			Re-Re	2.3 (5)	0.0046	2.57 (1)
Post-catalysis (3cycle)	6+ < X < 7+	10538.43	Re-O	0.8 (3)	0.0050	1.76 (2)
			Re-O	5.5 (7)	0.0056	2.02 (1)
			Re-Re	2.4 (4)	0.0042	2.55 (1)

[a] k-range: 3.3~3.4 < k < 15.5 $Å^{-1}$ (k2 weighting), r-range: 1.1~1.2 < R < 3.1 Å, $S_o^2 = 0.9$

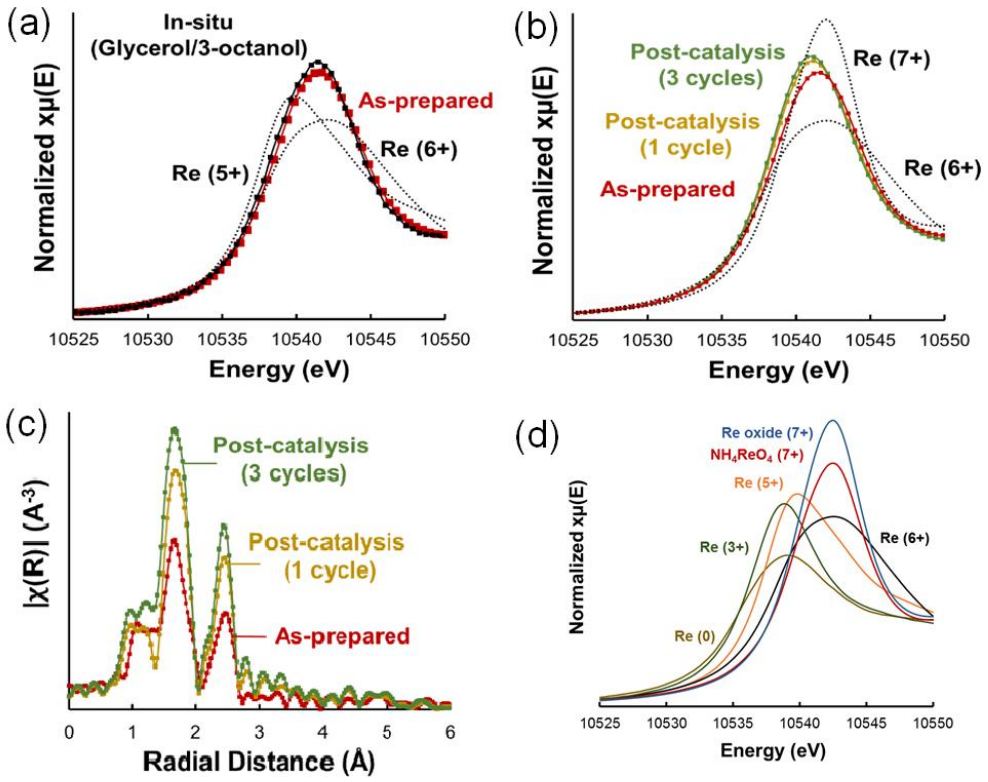

Figure 2.9 Re-L3 edge XANES spectra of (a) as-prepared (red solid line), in-situ (black solid line) and (b) post-catalysis ReO_x NPs (Green and yellow solid lines). (c) EXAFS spectra of as-prepared and post-catalysis ReO_x NPs. (d) XANES spectra rhenium standards.

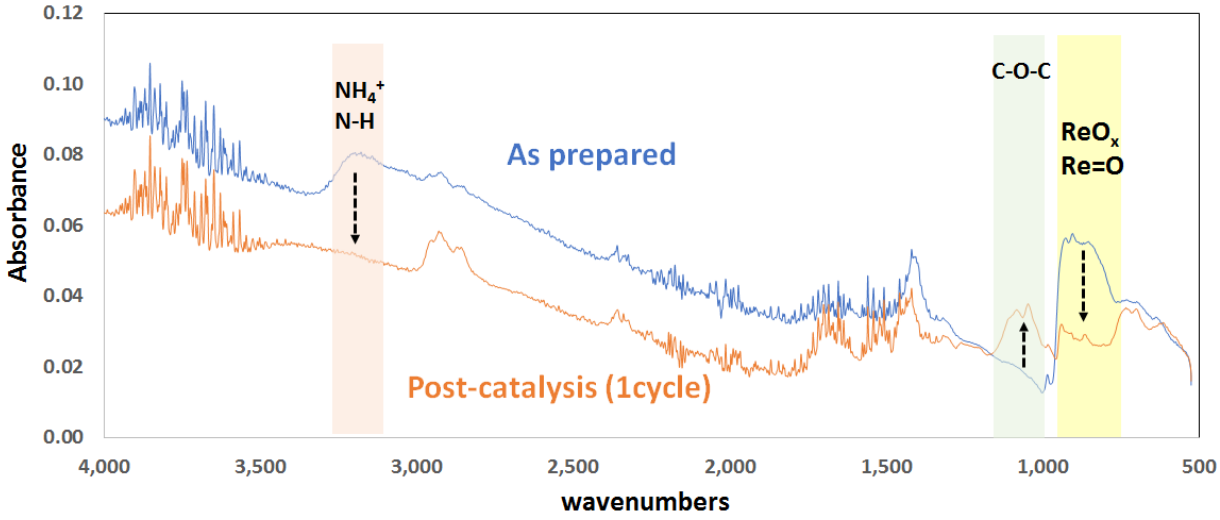

Figure 2.10 FT-IR spectra of as-prepared and recycled ReO_x NPs (1 cycle).

2.3 XPS

The change in oxidation states of Re species during glycerol DODH reaction was also investigated by ex-situ XPS. Figures 2.11a,b represent Re 4f spectra of before and after DODH reaction and their curve-fitted results are shown in Table 2.4. The major contribution of Re 4f doublets of as-prepared ReO_x NPs at binding energy of 45.6 and 47.9 indicates Re^{7+} (68 %), followed by Re^{5+} (32 %) at binding energy of 42.8 and 45.2.[31,32] After DODH reaction, a large increase in the amount of Re^{5+} concurrent with a decrease in the amount of Re^{7+} was observed. It is evident from the XPS data that the oxidation states of ReO_x NPs were reduced during DODH reaction, which is consistent with the XANES and EXAFS results. However, the extent of reduction is more pronounced in the XPS data than XAS. While XPS is a surface technique and it can be argued that XAS represents the bulk average, given the small size of our ReO_x NPs, it is expected that XPS penetrates enough to provide a picture of the bulk material. Nevertheless, both techniques provide a consistent, emerging picture of involvement of two oxidation states with EXAFS providing more detail on the structure of oxorhenium sites.

Spent ReO_x NPs (after one cycle) were recovered and used with a fresh glycerol for a second cycle which was stopped at 3 h. Figure 2.11c shows the XPS spectrum of the ReO_x NPs separated from the second cycle after 3 h of reaction. The overall picture of the Re catalyst at 3 h was similar to that after cycle one. These results are consistent with oxorhenium having two oxidation states and reduction to metallic rhenium or low oxidation state rhenium is not observed.

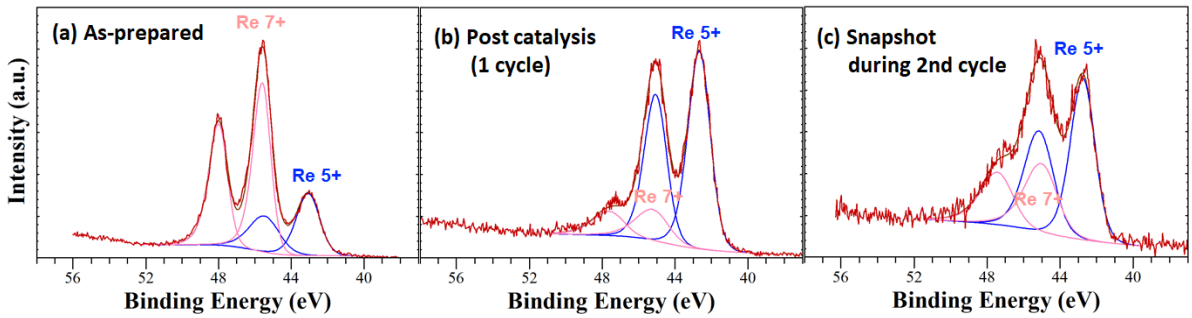

Figure 2.11 Re 4f spectra of (a) As-prepared ReO_x NPs (b) Post catalysis and recycled ReO_x (one cycle) (c) Further 3 h reaction with new a glycerol before completion and recycled ReO_x. The fitting line (brown solid line) was overlaid on the raw XPS data (red solid line).

Table2.4 The fractions of the different Re oxidation states obtained by the curve fitting of the Re 4f spectra.

Samples	Re 5+ %	Re 7+ %
As-prepared	32	68
Post-catalysis (1 cycle)	81	19
3 h further reaction with 1 cycle	63	37

2.4 Kinetic isotope effect and activation parameters

The kinetic isotope effect (KIE) of glycerol was determined using $CH_2(OD)CH(OD)CH_2(OD)$ and $CD_2(OH)CD(OH)CD_2(OH)$. For the homogeneous methyltrioxorhenium (MTO) DODH catalyst with glycerol as both substrate and reductant, the KIE of d_5-glycerol-$(OH)_3$ was reported to be 2.4, indicating involvement of the C-H/D bond of glycerol in the rate-determining step.[17] Reduction of Re species in DODH reaction in the presence of 3-octanol is associated with dehydrogenation of 3-octanol by ReO_x NPs to give 3-octanone.[30] In this chapter, glycerol-$(OD)_3$ in the presence of either 3-octanol or 3-(OD)-octanol showed no kinetic isotope effect (Table 2.5). On the other hand, 3-d-3-octanol gave a large KIE = 4.2. This is indicative that the reduction of ReO_x NPs by 3-octanol via C-

H bond activation is part of the catalytic rate-determining step(s). Also d_5-glycerol-$(OH)_3$ gave a modest KIE, indicating that a certain amount of glycerol was involved as reductant like 3-octanol via the C-H/D activation (Table 2.5).[17]

Thermodynamic activation parameters were determined from observed rate constants at different temperatures (150-180 °C). Least-squares fitting of data to the Eyring equation gave the following activation parameters: $\Delta H^{\ddagger} = 97 \pm 9$ kJ mol^{-1}, $\Delta S^{\ddagger} = -111 \pm 5$ J mol^{-1} K^{-1}, and $\Delta G^{\ddagger} = 145 \pm 11$ kJ mol^{-1} (Figure 2.12). The activation energy in this reaction is higher than that observed for homogeneous glycerol DODH as estimated by DFT calculation.[19] The large and negative entropy of activation is consistent with a bimolecular reaction.

Table 2.5 DODH Reaction of various substrates with ReO_x NPs

Run[a]	glycerol	3-octanol	k, rate constant ($10^{-4}s^{-1}$)	KIE[b]
1	glycerol	3-octanol	1.1	-
2	glycerol-$(OD)_3$	3-octanol	1.2	0.94
3	d_5-glycerol-$(OH)_3$	3-octanol	0.40	2.78
4	glycerol	2,2,4,4,-d_4-3-octanol	0.92	1.19
5	glycerol-$(OD)_3$	3-(OD)-octanol	0.89	1.24
6	glycerol	3-d-3-octanol	0.26	4.23

[a]Conditions: ReO_x 2 wt % of glycerol, 1g of glycerol, 3-octanol/glycerol 10/1 mole ratio, T = 170 ^{o}C. [b]k_{Run1}/k_{Runx}

$$\ln\frac{k}{T} = \frac{-\Delta H^{\ddagger}}{R}\cdot\frac{1}{T} + ln\frac{k_B}{h} + \frac{\Delta S^{\ddagger}}{R}$$

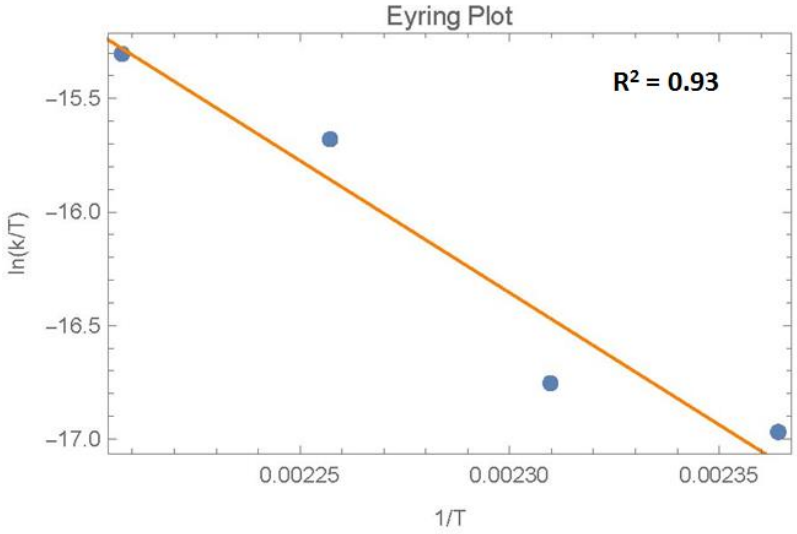

Figure 2.12 Least-squares fitting of data to the Eyring equation. Raw data (blue dot), fitting lined (orange solid line).

3. Effect of oxidation state of rhenium on catalytic activity of ReO_x NPs

First, the reduction behavior of ReO_x NPs was probed by in-situ XAS experiments with a 3% H_2/He feed as a reducing agent. The as-prepared ReO_x NPs were treated at three different temperatures 100 °C, 200 °C and 300 °C, and multiple XANES spectra (average 60 scans/temperature) were collected until no change in the oxidation state of Re was observed. The EXAFS spectra were collected at RT by cooling down the reactor after each treatment. XANES and EXAFS fitting results are summarized in Table 2.6.

Hydrogen treatment at 100 °C showed negligible effect on the Re oxidation state based on the edge energy (10538.69 eV) and EXAFS spectra features were identical to that of as-prepared ReO_x NPs (10538.65 eV). However, as the temperature was raised to 200 °C, significant reduction of Re was observed, with a final oxidation state between Re^{+3} and Re^{+4}. Further hydrogen treatment at 300 °C led to formation of metallic Re, evident by the

observed increase in coordination number of Re-Re EXAFS feature. Upon exposure of the reduced sample to air at RT for 30 min, no significant changes in the XANES and EXAFS were observed, confirming the stability of reduced rhenium NPs under ambient atmosphere.

Table 2.6 XANES edge energies of ReO_x NPs treated with hydrogen at different temperatures of 100 °C,[a] 200 °C,[b] and 300 °C.[c] EXAFS fitting results of Re-L3 edge are listed as N (coordination number), ss (Debye-Waller factor) and R (bond distance).

Samples	Oxidation state	Edge Energy (eV)	Path	N	ss (Å)	R (Å)
Hydrogen 100 °C	6+ < X < 7+	10538.69	Re-O	1.5 (2)	0.0017	1.73 (1)
			Re-O	3.7 (5)	0.0061	2.02 (1)
			Re-Re	1.8 (4)	0.0057	2.58 (1)
Hydrogen 200 °C	3+ < X < 5+	10536.96	Re-O	0.7 (1)	0.0057	1.77 (2)
			Re-O	3.3 (4)	0.0058	2.02 (1)
			Re-Re	3.2 (5)	0.0118	2.62 (1)
Hydrogen 300 °C	0 < X < 3+	10536.49	Re-O	0.3 (1)	0.0050	1.73 (2)
			Re-O	2.1 (8)	0.0134	2.03 (1)
			Re-Re	7.7(13)	0.0167	2.68 (1)

[a] k-range: 3.4 < k < 15.5 $Å^{-1}$ (k2 weighting), r-range: 1 < R < 3.1 Å, S_o^2 = 0.9 [b]k-range: 3.3 < k < 12.5 $Å^{-1}$ (k2 weighting), r-range: 1 < R < 3.1 Å, S_o^2 = 0.9 [c]k-range: 3.3 < k < 12.0 $Å^{-1}$ (k2 weighting), r-range: 1 < R < 3.6 Å, S_o^2 = 0.9

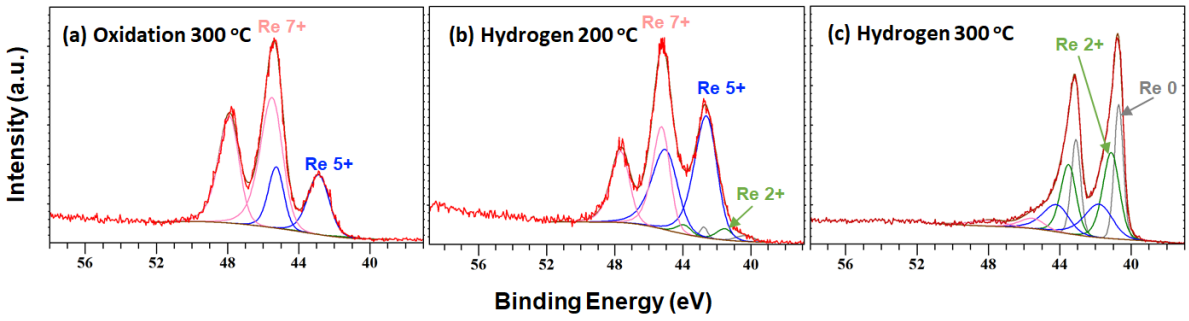

Figure 2.13 Re 4f spectra of ReO_x NPs treated with (a) Oxygen at 300 °C, (b) Hydrogen at 200 °C, and (c) Hydrogen at 300 °C

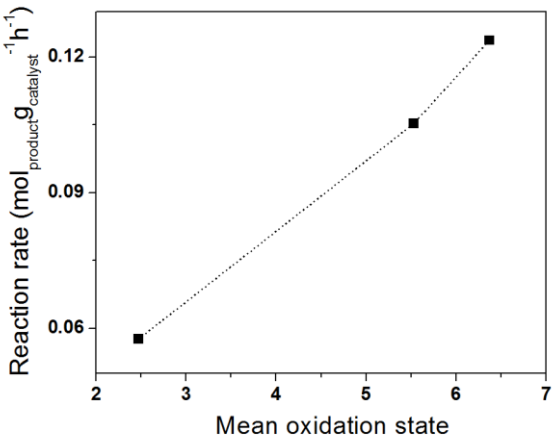

Figure 2.14 Effect of mean oxidation state of ReO_x NPs on reaction rate of heterogenous glycerol DODH.

Based on reduction and oxidation behavior of ReO_x NPs observed by XAS techniques, catalysts with different oxidation states were prepared and investigated for glycerol DODH. The chosen representatives were after reduction with H_2 at 200 and 300 °C as well as the restored ReO_x NPs after oxidation with O_2 at 300 °C. The oxidation states of each representative are analyzed by XPS (Figure 2.13). ReO_x NPs, oxidized with oxygen at 300 ^oC, showed quite similar oxidation states to as-prepared NPs; the major oxidation state is Re^{7+}. Reduction with H_2 at 200 ^oC led to decrease in the amount of Re^{7+} and increase in that of Re^{5+}. Lower oxidation states including metallic rhenium were observed after reduction with H_2 at 300 ^oC. The DODH reaction was run for the first 3 hours under the standard reaction conditions such as 1 wt% reduced or oxidized ReO_x NPs, 170 ^oC, and 10 equivalents of 3-octanol to glycerol. When the rate of reaction as determined by initial rate was plotted versus the average oxidation state (Figure 2.14), it is evident that lower rhenium oxidation state in the ReO_x NPs catalyst, the lower the activity. These findings are important because they preclude metallic rhenium nanoparticles as the active species and are

consistent with the observed XAS showing that oxorhenium in high oxidation state is the prevalent catalytic species.

4. Reaction mechanism

The as-prepared (pre-catalyst) ReO_x NPs display structural features similar to perrhenate with approximately two Re=O double bonds and three Re-O single bonds. Both XAS and XPS demonstrate that under reaction conditions and after recycling oxorhenium centers in the NPs show some reduction in oxidation state by roughly two oxidation units. Rate dependences and KIE show the C-H bond on the secondary alcohol in 3-octanol is involved in the RDS. The rate law can be expressed as

$$-d[\text{glycerol}]/dt = d[\text{allyl alcohol}]/dt = k\,[\text{glycerol}]\,[Re]_T\,[\text{3-octanol}] = k_{obs}\,[\text{glycerol}]$$

Based on all of these observations and building on the knowledge from the homogeneous catalysts that rhenium(V) diolate is capable of undergoing alkene extrusion,[2,13,17,21,36] the mechanism is offered in Scheme 2.1 below. The pre-catalyst is perrhenate like species with oxidation state Re^{VII}. Glycerol dependence arises from its coordination to afford mono-oxo rhenium(VII) diolate. Coordination of 3-octanol sets the stage for rhenium(VII) reduction to rhenium(V) diolate and formation of 3-octanone; this irreversible step is part of the rate determining states/steps. The C-H of 3-octanol undergoes what can be thought of conceptually as hydride transfer to oxorhenium.[17,19] The resulting desoxo rhenium(V) regenerates the dioxo rhenium(VII) species by extrusion of allyl alcohol; water elimination from rhenium hydroxo and the proton of 3-octanol which likely resides on a μ-oxo in the ReO_x NPs upon coordination of the alcohol sets the stage for another cycle with glycerol coordination to rhenium(VII). As previously reported in DFT studies,[19,21] this breaking C-O bonds and releasing olefin step is slow and possibly contributing to the rate-determining

steps. The concurrent involvement of the reduction and the olefin extrusion in the rate-determining step results in the prevalence of both oxidation state Re^{V} and Re^{VII} during catalysis; this coexistence of two oxidation states is supported by the average oxidation state under the reaction conditions shown in the in-situ XANES. The observed rate constant is a combination of two steps and the binding of glycerol and 3-octanol in the preceding reversible steps. At the end of the reaction, some desoxo rhenium (V) might remain and be recovered without olefin extrusion. This notion is supported by the large amount of Re^{V} observed in XPS and the increased C-O-C peak around 1100 cm^{-1} in FT-IR spectra (Figure 2.10). Some side reactions such as allyl alcohol further dehydrogenation of acrolein and 3-octanol 'non-productive' dehydrogenation to 3-octanone take place but to a lesser extent than the main pathway illustrated in Scheme 2.1. The proposed DODH mechanism with a Re^{VII}/Re^{V} catalytic cycle is different from previous studies on heterogeneous DODH. Palkovits and coworkers showed increase in Re^{IV} content by pre-reduction of supported ammonium perrhenate led to higher catalytic activity than Re^{VII}, demonstrating Re^{IV} as active species.[25] Tomishige et al. prepared ReO_x-Au/CeO_2 for heterogeneous DODH driven by hydrogen and investigated change in oxidation states before and after reaction, proposing a mechanism with Re^{VI}/Re^{IV} redox cycle.[27] The differences in oxidation states of pre-catalysts and types of reductant might contribute to different mechanisms and redox pairs.

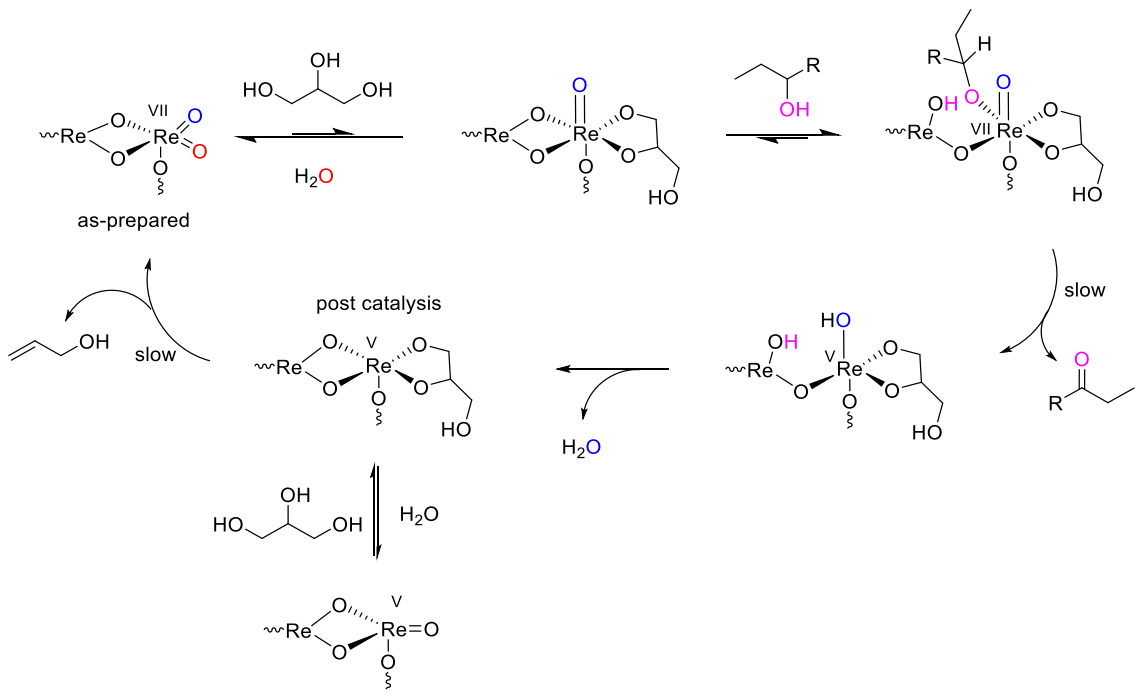

Scheme 2.1 Proposed mechanism for the heterogeneous DODH by ReO_x NPs in the presence of alcohol reductant.

D. Conclusion

Unsupported rhenium nanoparticles, efficient and reusable heterogeneous catalysts for DODH, were investigated to obtain insights for heterogeneous DODH reaction. In a reactive distillation system, the unsupported ReO_x NPs produced allyl alcohol from glycerol via DODH with yield of 76%. Hot filtration test demonstrated the heterogeneous nature of ReO_x NPs for DODH of polyols. This heterogeneous catalyst is recyclable up to seven consecutive cycles without significant loss of its efficiency. DODH of cis-but-2-ene-1,4-diol showed heterogeneous ReO_x catalyzes 1,4-diols as well as vicinal diols. XAS and XPS were used to characterize oxidation states and structures of ReO_x NPs in heterogeneous DODH. Combined with XRD analysis, three different scattering paths in EXAFS results indicated the structure of as-prepared ReO_x NPs is perrhenate like moieties with predominant

oxidation state of Re^{VII}. The Re species on ReO_x NPs undergo reduction during the DODH reaction. A decrease in amplitude of Re=O bond and increase in intensity of Re-O were observed after the catalytic cycle, consistent with reduced average oxidation state as observed in the XANES spectra. XPS spectra and fitting results of ReO_x NPs before and after DODH reaction corroborate reduction of Re species and involvement of high-oxidation state Re: Re^{V} and Re^{VII}. Under reaction conditions, the extent of reduction in oxidation states during DODH is roughly two units, observed by in-situ XANES analysis. The larger fraction of Re^{V} and Re^{VII} on ReO_x NPs showed higher activity for DODH, indicating the relevant active species for DODH is not metallic rhenium but oxo-rhenium species. The different KIE for reduction of ReO_x NPs by 3-octanol, 3-(OD)-octanol, and 3-d-3-octanol showed dissociation of C-H bond of 3-octanol during reduction as part of the rate-limiting step. Based on all experimental observations and knowledge from homogeneous DODH mechanism, a heterogeneous DODH reaction scheme is proposed, invoking the Re^{VII}/Re^{V} redox pair, dioxo rhenium(VII) as the active species, and desoxo rhenium(V) as alkene extrusion species.

E. References

(1) Dodds, D. R.; Gross, R. A. Chemicals from Biomass. *Science* **2007**, *318*, 1250–1251.

(2) Shiramizu, M.; Toste, F. D. Deoxygenation of Biomass-Derived Feedstocks: Oxorhenium-Catalyzed Deoxydehydration of Sugars and Sugar Alcohols. *Angew. Chem. Int. Ed.* **2012**, *51* (32), 8082–8086.

(3) Canale, V.; Tonucci, L.; Bressan, M.; D'Alessandro, N. Deoxydehydration of Glycerol to Allyl Alcohol Catalyzed by Rhenium Derivatives. *Catal. Sci. Technol.* **2014**, *4* (10), 3697–3704.

(4) Raju, S.; Moret, M.-E.; Klein Gebbink, R. J. M. Rhenium-Catalyzed Dehydration and Deoxydehydration of Alcohols and Polyols: Opportunities for the Formation of Olefins from Biomass. *ACS Catal.* **2015**, *5* (1), 281–300.

(5) Chapman, G.; Nicholas, K. M. Vanadium-Catalyzed Deoxydehydration of Glycols. *Chem. Comm.* **2013**, *49* (74), 8199–8201.

(6) Dethlefsen, J. R.; Lupp, D.; Teshome, A.; Nielsen, L. B.; Fristrup, P. Molybdenum-Catalyzed Conversion of Diols and Biomass-Derived Polyols to Alkenes Using Isopropyl Alcohol as Reductant and Solvent. *ACS Catal*. **2015**, 5, 3638-3647.

(7) Robinson, A. M.; Hensley, J. E.; Medlin, J. W. Bifunctional Catalysts for Upgrading of Biomass-Derived Oxygenates: A Review. *ACS Catal.* **2016**, *6* (8), 5026–5043.

(8) Cook, G. K.; Andrews, M. A. Toward Nonoxidative Routes to Oxygenated Organics: Stereospecific Deoxydehydration of Diols and Polyols to Alkenes and Allylic Alcohols Catalyzed by the Metal Oxo Complex $(C_5Me_5)ReO_3$. *J. Am. Chem. Soc.* **1996**, *118* (39), 9448–9449.

(9) Raju, S.; Jastrzebski, J. T. B. H.; Lutz, M.; Klein, R. J. M. Catalytic Deoxydehydration of Diols to Olefins by Using a Bulky Cyclopentadiene-Based Trioxorhenium Catalyst. *ChemSusChem* **2013**, 6, 1673–1680.

(10) Ziegler, J. E.; Zdilla, M. J.; Evans, A. J.; Abu-omar, M. M. H_2 -Driven Deoxygenation of Epoxides and Diols to Alkenes Catalyzed by Methyltrioxorhenium. *Inorg. chem.* **2009**, 48 (6), 9998–10000.

(11) Bi, S.; Wang, J.; Liu, L.; Li, P.; Lin, Z. Mechanism of the MeReO3-Catalyzed Deoxygenation of Epoxides. *Organometallics* **2012**, *31* (17), 6139–6147.

(12) Davis, J.; Srivastava, R. S. Oxorhenium-Catalyzed Deoxydehydration of Glycols and Epoxides. *Tetrahedron Lett.* **2014**, *55* (30), 4178–4180.

(13) Vkuturi, S.; Chapman, G.; Ahmad, I.; Nicholas, K. M. Rhenium-Catalyzed Deoxydehydration of Glycols by Sulfite. *Inorg. Chem.* **2010**, 49, 4744−4746.

(14) Ahmad, I.; Chapman, G.; Nicholas, K. M. Sulfite-Driven , Oxorhenium-Catalyzed Deoxydehydration of Glycols. *Organometallics* **2011**, 30, 2810−2818.

(15) Liu, P.; Nicholas, K. M. Mechanism of Sulfite-Driven, MeReO3-Catalyzed Deoxydehydration of Glycols. *Organometallics* **2013**, *32* (6), 1821–1831.

(16) Arceo, E.; Ellman, J. A.; Bergman, R. G. Rhenium-Catalyzed Didehydroxylation of Vicinal Diols to Alkenes Using a Simple Alcohol as a Reducing Agent. *J. Am. Chem. Soc.* **2010**, 132, 11408−11409.

(17) Yi, J.; Liu, S.; Abu-Omar, M. M. Rhenium-Catalyzed Transfer Hydrogenation and Deoxygenation of Biomass-Derived Polyols to Small and Useful Organics. *ChemSusChem* **2012**, *5* (8), 1401–1404.

(18) Liu, S.; Senocak, A.; Smeltz, J. L.; Yang, L.; Wegenhart, B.; Yi, J.; Kenttämaa, H. I.; Ison, E. A.; Abu-Omar, M. M. Mechanism of MTO-Catalyzed Deoxydehydration of Diols to Alkenes Using Sacrificial Alcohols. *Organometallics* **2013**, *32* (11), 3210–3219.

(19) Qu, S.; Dang, Y.; Wen, M.; Wang, Z. Mechanism of the Methyltrioxorhenium-Catalyzed Deoxydehydration of Polyols : A New Pathway Revealed. *Chem. - Eur. J.* **2013**, 19, 3827−3832

(20) Shiramizu, M.; Toste, F. D. Expanding the Scope of Biomass-Derived Chemicals through Tandem Reactions Based on Oxorhenium-Catalyzed Deoxydehydration. *Angew. Chem., Int. Ed.* **2013**, 52, 12905− 12909.

(21) Li, X.; Wu, D.; Lu, T.; Yi, G.; Su, H.; Zhang, Y. Angewandte Highly Efficient Chemical Process To Convert Mucic Acid into Adipic Acid and DFT Studies of the Mechanism of the Rhenium-Catalyzed Deoxydehydration *Angew. Chem. Int. Ed.* **2014**, *53* (16), 4200−4204.

(22) Dethlefsen, J. R.; Fristrup, P. Rhenium-Catalyzed Deoxydehydration of Diols and Polyols. *ChemSusChem* **2015**, 8, 767–775.

(23) Denning, A. L.; Dang, H.; Liu, Z.; Nicholas, K. M.; Jentoft, F. C. Deoxydehydration of Glycols Catalyzed by Carbon-Supported Perrhenate. *ChemCatChem* **2013**, *5* (12), 3567–3570.

(24) Li, X.; Zhang, Y. Highly Selective Deoxydehydration of Tartaric Acid over Supported and Unsupported Rhenium Catalysts with Modified Acidities. *ChemSusChem* **2016**, *9* (19), 2774–2778.

(25) Sandbrink, L.; Klindtworth, E.; Islam, H.-U.; Beale, A. M.; Palkovits, R. ReOx/TiO2: A Recyclable Solid Catalyst for Deoxydehydration. *ACS Catal.* **2016**, *6* (2), 677–680.

(26) Kon, Y.; Araque, M.; Nakashima, T.; Paul, S.; Dumeignil, F.; Katryniok, B. Direct Conversion of Glycerol to Allyl Alcohol Over Alumina-Supported Rhenium Oxide. *Chemistry Select* **2017**, *2* (30), 9864–9868.

(27) Tazawa, S.; Ota, N.; Tamura, M.; Nakagawa, Y.; Okumura, K.; Tomishige, K. Deoxydehydration with Molecular Hydrogen over Ceria-Supported Rhenium Catalyst with Gold Promoter. *ACS Catal.* **2016**, *6* (10), 6393–6397.

(28) Tomishige, K.; Tamura, M.; Nakagawa, Y. Role of Re Species and Acid Cocatalyst on Ir-ReOx/SiO2 in the C-O Hydrogenolysis of Biomass-Derived Substrates: Hydrogenolysis of Biomass-Derived Substrates. *Chem. Rec.* **2014**, *14* (6), 1041–1054.

(29) Nakagawa, Y.; Tazawa, S.; Wang, T.; Tamura, M.; Hiyoshi, N.; Okumura, K.; Tomishige, K. Mechanistic Study of Hydrogen-Driven Deoxydehydration over Ceria-Supported Rhenium Catalyst Promoted by Au Nanoparticles. *ACS Catal.* **2018**, *8* (1), 584–595.

(30) Yi, J.; Miller, J. T.; Zemlyanov, D. Y.; Zhang, R.; Dietrich, P. J.; Ribeiro, F. H.; Suslov, S.; Abu-Omar, M. M. A Reusable Unsupported Rhenium Nanocrystalline Catalyst for Acceptorless Dehydrogenation of Alcohols through γ-C-H Activation. *Angew. Chem.* **2014**, *126* (3), 852–855.

(31) Choe, J. K.; Boyanov, M. I.; Liu, J.; Kemner, K. M.; Werth, C. J.; Strathmann, T. J. X-Ray Spectroscopic Characterization of Immobilized Rhenium Species in Hydrated Rhenium–Palladium Bimetallic Catalysts Used for Perchlorate Water Treatment. *J. Phys. Chem. C* **2014**, *118* (22), 11666–11676.

(32) Greiner, M. T.; Rocha, T. C. R.; Johnson, B.; Klyushin, A.; Knop-Gericke, A.; Schlögl, R. The Oxidation of Rhenium and Identification of Rhenium Oxides During Catalytic Partial Oxidation of Ethylene: An In-Situ XPS Study. *Z. Phys. Chem.* **2014**, *228* (4–5), 521–541.

(33) Ravel, B.; Newville, M. ATHENA, ARTEMIS, HEPHAESTUS: Data Analysis for X-Ray Absorption Spectroscopy Using IFEFFIT. *J. Synchrotron Radiat* **2005**, *12* (4), 537–541.

(34) Petersen, A. R.; Fristrup, P. New Motifs in Deoxydehydration: Beyond the Realms of Rhenium. *Chem. - Eur. J* **2017**, *23* (43), 10235–10243.

(35) Kruger, G. J.; Reynhardt, E. C. Ammonium Perrhenate at 295 and 135 K. *Acta Crystallogr., Sect. B: Struct. Crystallogr. Cryst. Chem*.**1978**, *34* (1), 259–261.

(36) Michael McClain, J.; Nicholas, K. M. Elemental Reductants for the Deoxydehydration of Glycols. *ACS Catal.* **2014**, *4* (7), 2109–2112.

CHAPTER III. A Heterogeneous Pt-ReOx/C Catalyst for Making Renewable Adipates in One-Step from Sugar Acids

A. Introduction

Lignocellulosic biomass provides a renewable resource for sustainable routes to biofuels and biochemicals.[1,2] Adipic acid is a large volume, valuable chemical (1.8 €/kg) that can be obtained from biomass.[3] Its primary use is in the production of nylon-6,6 with a global market size of 3.7 million tons per annum.[4] The current manufacturing of adipic acid depends on petroleum-derived chemicals and emits nitrous oxide (N_2O).[5] One promising route to renewable adipic acid is from biomass-derived C6 carbohydrates. Glucose can be converted into *cis,cis*-muconic acid via biocatalysis, followed by direct hydrogenation over Pt/C to give adipic acid.[6,7] The conversion of glucose derivatives including glucaric acid[8] and 2,5-furandicarboxylic acid[9,10] through chemo-catalytic routes has also been studied. However, these pathways are either low yielding (< 30%) or employ undesirable reaction conditions such as requiring the use of corrosive halogens, high pressure of H_2 (> 50 bar), or acetic acid.

A combination of catalytic deoxydehydration (DODH) and hydrogenation offers an efficient and green route to adipates from mucic acid. Mucic acid (also known as galactaric acid) is an aldaric acid that can be produced by the oxidation of galactose.[11] Rhenium-catalyzed DODH reaction enables the selective conversion of vicinal diols to alkenes in the presence of reductants such as PPh_3, Na_2SO_4, H_2, and alcohols.[12,13] High oxidation state rhenium catalysts and alcohol reductants have been widely studied for DODH of various substrates including sugar alcohols and acids. Homogeneous oxorhenium (VII) catalysts with *n*-butanol as solvent and reductant convert mucic acid to muconate through DODH

(Scheme 3.1a). The following hydrogenation of muconate over Pd/C yields 62% adipates, reported by Toste's group.[14] Higher yield (99%) of adipates can be obtained by Zhang's group through two steps: 1) DODH by methyltrioxorhenium (MTO) and esterification over an acid co-catalyst and 2) catalytic transfer hydrogenation (CTH) over Pt/C.[11] In 2017, Toste's group reported that the mixture of $KReO_4$, Pd/C, and phosphoric acid in combination with H_2 as a reductant yielded 86% adipates.[5] Despite the high yield, the reaction system (homogeneous Re + heterogeneous Pt or Pd catalysts) presents challenging and likely costly separation and recycling problems. Due to the high cost of rhenium, employing a recyclable solid rhenium catalyst for DODH is desirable.[15] Recently, solid ReO_x/ZrO_2 catalyst with *n*-butanol as a reductant to convert D-glucaric acid-1,4-lactone to muconate with a yield of 41% and another DODH product with a five-membered ring.[16] When further processing the product stream via three different steps, including hydrogenation over Pd/C and ring-opening, adipates were produced at 82% yield. While the yield of adipate is promising, the multi-step process requires the isolation of intermediates and the use of different reaction conditions and catalysts.

In this chapter, a bifunctional heterogeneous catalyst is designed to effectively catalyze both DODH and CTH, converting mucic acid to adipates in one step. High oxidation state rhenium oxide on activated carbon (ReO_x/C) is chosen as a DODH catalyst. In order to catalyze CTH reaction of C-C unsaturated bonds produced by DODH reaction, metallic platinum is employed to the ReO_x/C, making Pt-ReO_x/C catalyst. In the Pt-ReO_x/C catalyst, ReO_x and Pt are active sites for DODH and CTH, respectively. The role of Re in previously reported Pt-Re bimetallic catalysts was explained as a promoter for Pt catalysts.[17] For example, in hydrocarbon reforming reactions over bimetallic Pt-Re catalysts, the addition of Re to Pt catalysts modified the electronic structure of Pt. This resulted in preventing carbon

fouling and extending the lifetime of the catalyst.[18–20] Furthermore, Pt-Re catalysts have shown increased activity for aqueous phase reforming of biomass-derived polyols compared to monometallic Pt catalysts. It is attributed that Re promotion of Pt catalysts decreased the binding energy of CO to the bimetallic surface and/or increased the number of acid sites.[21–23]

In addition to the separation and recycling problems, the aforementioned reaction systems (homogeneous + heterogeneous catalysts) require the use of acid additives and expensive alcohol reductants (C4 or higher) to achieve good yields of adipates. C4-C8 alcohols have been proven as effective reductants and solvents for DODH reaction.[13,24] Isopropanol is an attractive reductant for DODH because it is a cheap, green, and good solvent for reactants and products relative to the C4-C8 alcohols. For example, the ability of isopropanol as a reductant and solvent for DODH was demonstrated for 1,2-hexanediol with ammonium heptamolybdate (AMT) catalyst at high reaction temperature (240 - 250 ^{o}C).[25] However, MTO-catalyzed DODH didn't proceed in isopropanol at 170 ^{o}C.[26] Moreover, the higher polarity of isopropanol relative to 3-octanol reduced the leaching problem of ReO_x/support catalyst during DODH.[15] Re-diolate species, intermediate catalyst forms in DODH cycle, are less soluble in more polar solvents. In addition to the advantages in DODH, isopropanol is a good hydrogen donor for CTH reaction. CTH reactions using isopropanol as a hydrogen donor have garnered much attention as an alternative to direct hydrogenation because the hydrogen donor is easy to handle and environmentally friendly, minimizing possible hazards.[27–29] While CTH reactions have been mostly accomplished using noble metal complexes, several effective heterogeneous catalysts for CTH of ketone, imines, and polarized alkenes have been reported.[30–32]

Herein, the Pt-ReO_x/C catalyst is reported for one-step tandem catalysis of DODH and CTH (Scheme 3.1b). 85% yield of adipates from mucic acid is achieved without an acid

additive. Isopropanol is an effective solvent and hydrogen donor for both reactions DODH and CTH. Based on the reactivity, spectroscopic analysis, and isotope labeling experiments, a bifunctional mechanism of the tandem reaction is proposed. Catalyst recycling and regeneration are described.

A) Previous Work:

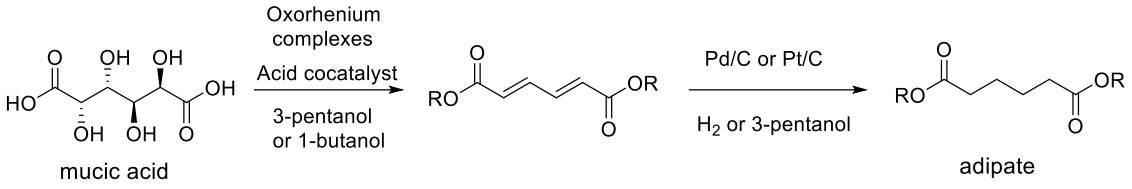

B) This Work:

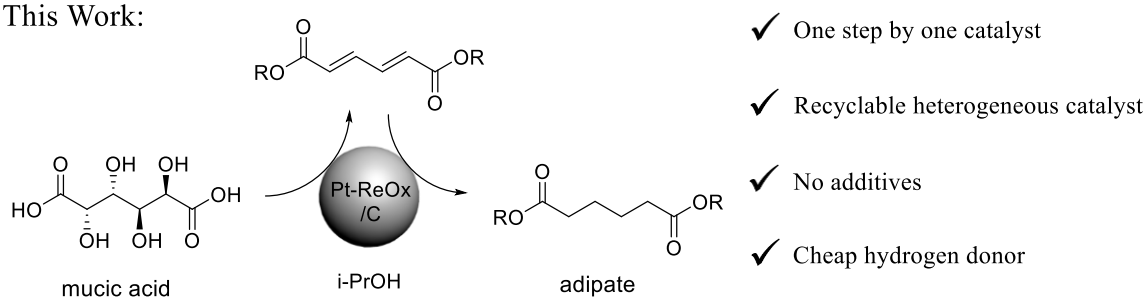

Scheme 3.1 DODH and hydrogenation of mucic acid by A) a combination of homogeneous Re and heterogeneous Pd or Pt catalysts in multiple steps; B) one-step and recyclable catalyst.

B. Experimental details

1. Synthesis

All commercial materials were used as received. Ammonium perrhenate(VII) (Strem Chemicals) was purchased from Strem Chemicals. Hexachloroplatinic(IV) acid solution, Nickel(II) nitrate, tetraamminepalladium(II) nitrate, Iridium(III) chloride, activated carbon (Darco 100 mesh), D-sorbitol, D-glucaric acid-1,4-lactone were purchased from Sigma-

Aldrich. Tris-(ethylenediamine)rhodium(III) chloride, methanol, ethanol, isopropanol, 1-butanol, 3-pentanol, glycerol, D-sorbitol, mucic acid, and L-(+)-tartaric acid were purchased from Alfa Aesar. Diisopropyl L-(+)-tartarate, diisopropyl fumarate, and diisopropyl succinate were purchased from TCI Chemicals. Isopropanol-2-d was purchased from Cambridge Isotope Laboratory.

ReO_x/C catalyst was prepared by wet impregnation of ammonium perrhenate aqueous solution. 72 mg of ammonium perrhenate was dissolved in 4 mL of distilled water. 1 g of activated carbon was mixed vigorously with the perrhenate solution overnight. After evaporating water in a preheated 80 ^oC oil bath for 1.5 h and drying in a 120 ^oC oven overnight, the catalyst was dehydrated at 480 ^oC for 4 h (heating rate of 8 ^oC/min) under flowing N_2. The bifunctional catalysts (M-ReO_x/C, M = Ni, Pd, Ru, Rh, Ir, Pt) were synthesized by impregnating metal precursor solution with the prepared ReO_x/C. The molar ratio of M/Re was fixed to 0.4. For Pt-ReO_x/C, 500 mg of the synthesized ReO_x/C was mixed with 263 mg of 8 wt% hexachloroplatinic(IV) acid solution and 2 mL of distilled water. The Pt-ReO_x/C catalyst was used after removing water in an oil bath at 80 ^oC, drying at 120 ^oC overnight, and dehydration (N_2/480^oC/2h) steps. The monometallic Pt/C catalyst was prepared by the same impregnation method with hexachloroplatinic acid. All catalysts were used and characterized without the treatment of reduction unless otherwise noted.

2. Characterization

High-angle annular dark-field scanning transmission electron microscope (HAADF-STEM) images were collected at 200 kV using a Thermo Scientific Talos equipped with a Super-X detector system. The samples were diluted in ethanol and deposited on a carbon film copper grid. In order to explore the distribution of ReO_x and Pt, energy-dispersive X-ray spectroscopy (EDX) mapping was performed on the distribution of Re, Pt, O elements.

The averaged particle size of Pt-ReO_x/C was calculated from the STEM images. Transmission electron microscope (TEM) images of ReO_x/C were obtained on FEI Tecnai G2Microscope.

X-ray photoelectron spectroscopy (XPS) analysis was acquired on a ThermoFisher Escalab Xi+ with a monochromatic Al Kα x-ray source. High-resolution spectra (20 eV) of the Re 4f, Pt 4f, C 1s, and O 1s and the survey spectra (100 eV) were recorded. All the spectra were calibrated by setting the binding energy of the peak of C 1s to 284.5 eV. CasaXPS software was utilized to deconvolute the spectra. The Pt-ReO_x/C catalyst prepared by the method described above was analyzed without further treatment. The samples after the reaction, reduction, and regeneration were transferred to a glovebox filled with N_2, avoiding exposure to air. The samples were mounted on a transfer vessel in the glovebox and transferred to the XPS chamber without air exposure.

X-ray diffraction (XRD) patterns were collected from 2θ range of 5^o to 80^o on a PANalytical Empyrean X-ray diffractometer using Cu Kα radiation. Inductively coupled plasma (ICP) analysis was carried out to quantify the amount of metal using a Thermo iCAP 6300. For the sample preparation, 20 mg of catalyst was digested with 2.5 mL of aqua regia by refluxing at 150 ^{o}C for 6 h. The solution was cooled down to room temperature, filtered, diluted, and used for ICP analysis. Because the catalysts after reaction contain organic deposits, they were regenerated under 5% H_2 in Ar at 230 ^{o}C for 4 h before the acid digestion.

The CO chemisorption studies were carried out using a Micromeritics AutoChem II 2920. The as-prepared catalysts were pretreated under Ar flow at 450 ^{o}C for 2 h, and CO adsorption was performed at 35 ^{o}C. The adsorption stoichiometry between CO and surface Pt sites was assumed to be 1:1. The catalysts after the reaction were pretreated under Ar or

H_2 flow and used for CO chemisorption. Temperature-programmed reduction (TPR) was carried out using a Micromeritics AutoChem II 2920. Before TPR, samples were pretreated under Ar flow at 400 ^oC for 4 h. A TPR run was carried out in a flow of 10% H_2/Ar mixture gas at a flow rate of 50 mL min^{-1} with a temperature ramp of 10 ^oC min^{-1}. The consumption of hydrogen was monitored as a function of temperature using the TCD.

Infrared spectra of catalysts were recorded with a Thermo Scientific Nicolet iS10 Fourier transform infrared spectroscopy (FTIR) spectrometer with a mercury cadmium telluride detector cooled by liquid nitrogen. Catalysts were diluted with KBr. Before characterization, catalysts were in-situ pretreated under Ar flow at 400 ^oC for 4 h. After pretreatment, the catalysts were cooled to room temperature under Ar, and then a baseline spectrum was taken before pyridine introduction. Pyridine was introduced to the catalyst by flowing Ar through a pyridine bubbler and then purged with 100 sccm Ar for 10 min to remove physisorbed pyridine. For all measurements, spectra were obtained by averaging 64 sequentially collected scans at a resolution of 4 cm^{-1}.

3. General catalytic procedure

The Pt-ReO_x/C catalyst (150 mg), mucic acid (1 mmol, 210 mg), and isopropanol (40 mL) were placed into a Parr vessel. The vessel was pressurized with nitrogen to 15 bar and heated to 170 ^oC. After 6 h reaction, the reactor was cooled down and the gases were collected in a gas sample bag. The used catalyst was filtered, washed with pure isopropanol (30 mL), and dried in the oven at 120 ^oC overnight for recycling test. The reaction solution was concentrated under the reduced pressure and the products were dissolved in d_6-DMSO and analyzed by NMR with benzaldehyde as an internal standard. ^1H NMR and ^{13}C NMR spectra were collected on an Agilent Technologies 400 MHz, 400-MR DD2 spectroscopy. The gas phase was analyzed by GC-TCD (Shimadzu GC-9AIT with a Shincarbon ST

column) and GC-MS (Shimadzu GC-2010 with a DB-1 capillary column coupled to a QP2010 MS). For acid hydrolysis, after removal of the solvent, the concentrated product mixture was refluxed at 110 ^{o}C overnight in 10 mL of 2N aqueous HCl. The reaction mixture was evaporated and the resulting solid was washed with 5mL of ice-cold water. The white solid was vacuum dried at 60 ^{o}C, yielding adipic acid. The recycling test of the Pt-ReO_x/C for the 6 h DODH-CTH reaction was conducted with or without regeneration under H_2. For regeneration, the used and recovered catalyst was treated at 230 ^{o}C for 4 h in a flow of H_2 (5%) in Ar and re-oxidized in a 120 ^{o}C oven for 1 h. During the recovery step, a slight loss less than 10 wt% was observed. Thus, the amount of mucic acid and isopropanol in each reuse experiment was determined based on the amount of the recycled catalyst.

4. Stability test

Diisopropyl L-(+)-tartarate and diisopropyl fumarate were used as substrates for the stability tests due to their good solubility in isopropanol. DODH of diisopropyl L-(+)-tartarate gave diisopropyl fumarate and CTH of diisopropyl fumarate produced diisopropyl succinate. These diester compounds in the product solution were analyzed with GC-FID (Agilent Technologies 6890N with a DB-5 capillary column) with mesitylene as an internal standard. 4 mmol of the substrate, 100 mg of Pt-ReO_x/C catalyst, 200 mg of activated carbon, and 40 mL of isopropanol were loaded into the reaction vessel and the vessel was pressurized with 15 bar of N_2. The reaction starts once the temperature reaches 170 ^{o}C. After 20 min, the reaction was stopped and quenched in an ice/water bath. The used catalysts were separated and washed with 30 mL of isopropanol and dried overnight in a 120 ^{o}C oven. The amount of mucic acid and isopropanol in each reuse experiment was determined based on the amount of the recycled catalyst. The regeneration step (5%H_2/230^{o}C/4h) including reoxidation was employed after deactivation was observed.

C. Results and discussion

1. DODH reaction

The heterogeneous oxorhenium catalyzed DODH reaction, as an alternative to homogeneous DODH, has attracted much attention due to process advantages.[15,33–37] Oxorhenium supported on activated carbon (ReO_x/C) is an active catalyst for DODH with 3-octanol as a reductant.[35] Recently, this catalyst also promoted the CTH reaction with isopropanol for C-O cleavage of lignin model compounds.[38] In this chapter, the ability of isopropanol to act as a reductant and solvent for both DODH and CTH catalyzed by a heterogeneous ReO_x/C catalyst was investigated. The ReO_x/C catalyst with 4.5 wt % of Re was prepared by wet impregnation method with ammonium perrhenate as a precursor. The ReO_x nanoparticle size ranges from 1 to 4 nm (Figure 3.1).

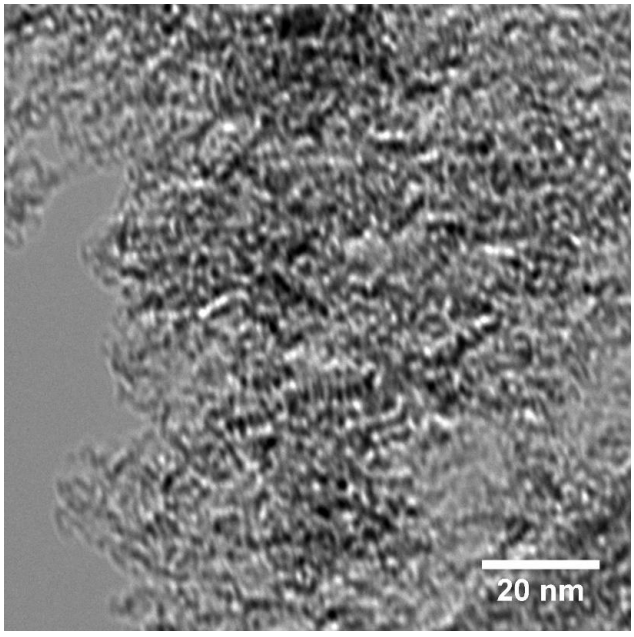

Figure 3.2 TEM image of ReO_x/C. The average particle size calculated from TEM images is 2.2 ± 0.4 nm.

In a batch reaction system, ReO_x/C with isopropanol converted 77% of mucic acid (**1**) to muconic acid and its esters (**2**) with high selectivity of 86% in 6 h (run 1 in Table 3.1), showing high DODH ability of ReO_x/C and isopropanol. After 12 h, conversion reached 94%, producing not only **2** but also hydrogenated products (**3**, **4**, and **5)**. CTH proceeded to some extent (14% selectivity of **3/4** and **5**), even with ReO_x/C alone (run 4). DODH in 3-pentanol also displayed high selectivity for **2**, but further hydrogenation was not observed (run 8). Lower selectivity for **2** was obtained in methanol and ethanol (run 6 and 7). Thus, among the tested C1-C5 secondary alcohols, isopropanol was found to be the most effective hydrogen donor for DODH and CTH over ReO_x/C.

The heterogeneous catalyst ReO_x/C with isopropanol did not require an acid additive and showed higher DODH turnover frequency per Re atom (3.1 h^{-1}) than MTO and para-toluene sulfonic acid with 3-pentanol (1.7 h^{-1}). It was previously reported that the addition of a Brønsted acid promotes the esterification of **1**, resulting in the enhanced solubility of mucic acid.[11] In the absence of para-toluene sulfonic acid, turnover frequency per Re atom in the homogeneously catalyzed system decreased to 0.9 h^{-1}. While the addition of a Brønsted acid to ReO_x/C increased the number of ester groups, it did not increase conversion or selectivity of **2** (run 2 in Table 3.1). This indicates that the reactant solubility has little impact on the rate of DODH with the solid ReO_x/C catalyst. Weak Lewis acid sites in ReO_x/C were detected by pyridine probe-molecule FT-IR (Figure 3.2). However, addition of exogenous Lewis acids such as $ZnCl_2$ had no effect on conversion or selectivity, indicating negligible involvement of the Lewis acid sites of ReO_x/C in the DODH reaction (run 3 in Table 3.1).

Table 3.1 DODH and CTH tandem reaction of **1** over ReO_x/C.[a]

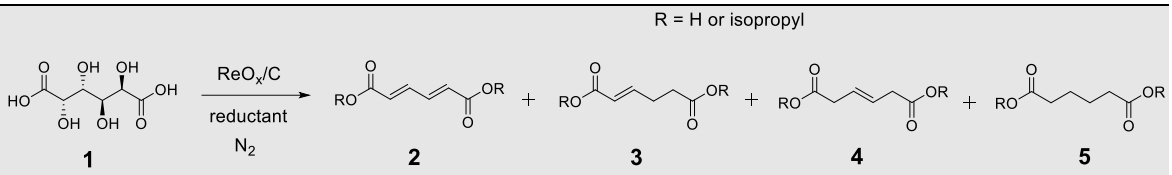

Run	Reductant	T (°C)	t (h)	Conv.[b] (%)	Product % Selectivity[b]			
					2	**3** & **4**	**5**	Others
1	isopropanol	170	6	77	86	2	0	12
2[c]	isopropanol	170	6	76	57	6	0	37
3[d]	isopropanol	170	6	70	82	3	0	15
4	isopropanol	170	12	94	75	13	1	11
5	isopropanol	230	24	100	0	19	35	46
6	methanol	170	12	88	60	13	0	27
7	ethanol	170	12	94	66	14	0	20
8	3-pentanol	170	12	83	87	0	0	13

[a]Reaction conditions: ReO_x/C (150 mg, 4.5 wt % Re), **1** (1 mmol), *i*-PrOH (40 mL), and N_2 (15 bar). [b]Calculated by ^1H NMR. [c]TsOH (5 mol%). [d]ZnCl2 (5 mol%)

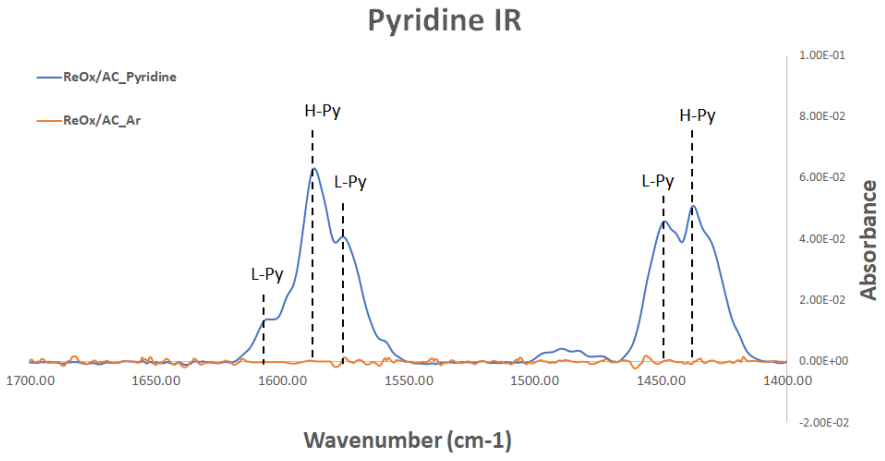

Figure 3.2 FT-IR spectra of pyridine adsorbed on ReO_x/C. The bands at 1436 and 1586 cm^{-1} were assigned to hydrogen-bonded pyridine (H-Py). The bands at 1446, 1574, and 1606 cm^{-1} represent Lewis bound pyridine (L-Py).

Despite the high rate and selectivity of DODH over ReO_x/C with isopropanol, CTH was quite slow at 170 °C (Table 3.1, run 4). Four different temperatures from 170 °C to 230 °C were investigated to convert *trans,trans*-muconic acid (**2-diacid**) to **5** through CTH (Figure 3.3). The highest yield of **5** (43%) was obtained at 230 °C. However, the elevated temperature also resulted in 35-50% byproducts including oxepane (**6**), alkylated adipates (**7**), and other unidentified products. As a result, the higher temperature conversion of **1** led to moderate yield of **5** (35%) and several other products (run 3 in Table 3.1).

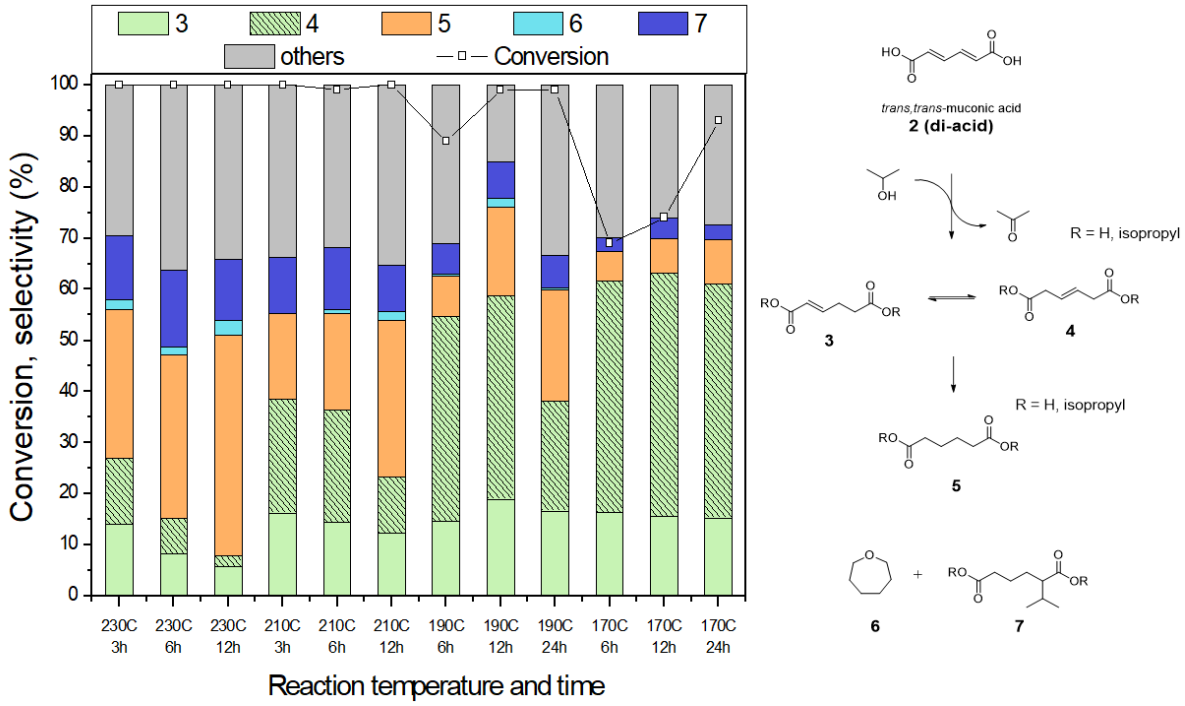

Figure 3.3 Transfer hydrogenation of trans,trans-muconic acid (**2-diacid**) by ReO_x/C at different reaction temperature and time. Reaction conditions: batch reaction, ReO_x/C (150 mg, 4.5 wt % Re), **2-diacid** (142 mg, 1 mmol), N_2 (15 bar), and *i*-PrOH (40 mL).

2. Bifunctional catalysis

A bifunctional catalyst provides two different catalytic sites for a consecutive reaction (A→B→C).[39,40] To realize high efficiency for both DODH and CTH, several bimetallic

catalysts (M-ReO_x/C) were prepared by sequential impregnation method and evaluated for mucic acid conversion (Figure 3.4). Among them, Pt-ReO_x/C showed the highest conversion (79%) and selectivity for adipates (82%, run 1 in Table 3.2). The bimetallic catalysts containing Ni and Pd did not promote the CTH reaction. Some hydrogenated products (**3**/**4** and **5**) were obtained by adding Ru, Ir, and Rh to ReO_x/C, but reactant conversion was low. The addition of Pt to ReO_x/C significantly enhanced the rate of CTH while maintaining the excellent DODH ability of ReO_x/C (Figure 3.4).

Monometallic Pt/C by itself was inactive for DODH (run 6 in Table 3.2), but with **2-diacid** as substrate, quantitative conversion to **5** was observed (99% yield). The rate of CTH was sensitive to Pt loading (run 7). Higher Pt loading (4.5 wt %) was detrimental because ReO_x active sites were blocked, lowering conversion of **1** (run 8). 1.8 wt % Pt loading along 4.5 wt % ReO_x was identified as an optimal composition for DODH and CTH. CTH over Pt-ReO_x/C in isopropanol was observed to be superior to that in 3-pentanol (run 9).

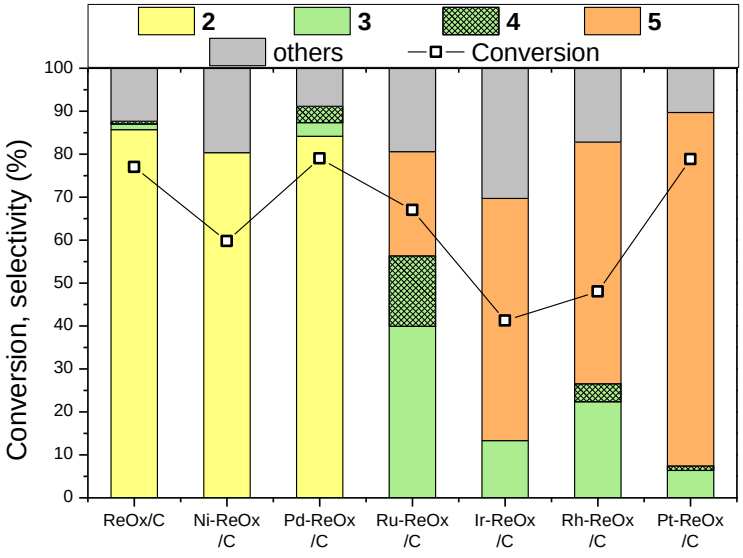

Figure 3.4 Conversion of **1** over several bimetallic catalysts. Reaction conditions: **1** (1 mmol), M-ReO_x/C (150 mg), isopropanol (40 mL), N_2 (15 bar), 170 ^oC, 6 h.

Table 3.2 DODH-CTH tandem reaction of **1** over Pt-ReO_x/C.[a]

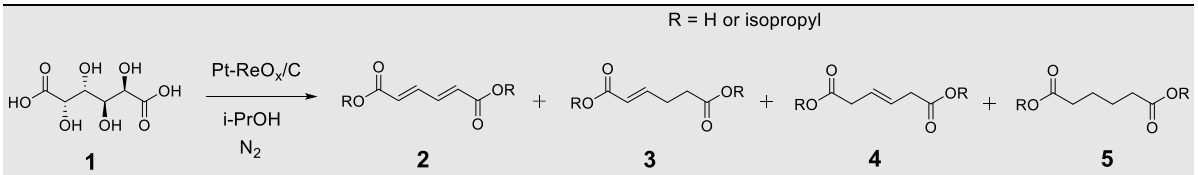

Run	Catalyst	Re/Pt amount (wt %)	Conversion[b] (%)	Products/ % Selectivity[b]			
				2	**3** & **4**	**5**	Others
1	Pt-ReO_x/C	4.5 / 1.8	79	0	7	82	11
2[c]	2nd cycle		64	1	50	40	9
3[d]	3rd cycle		77	0	10	82	8
4[d]	4th cycle		72	0	19	77	4
5[e]	5th cycle		81	0	6	83	11
6	Pt/C	0 / 1.8	No reaction				
7	Pt-ReO_x/C	4.5 / 0.9	78	42	44	5	9
8	Pt-ReO_x/C	4.5 / 4.5	44	0	9	71	20
9[f]	Pt-ReO_x/C	4.5 / 1.8	73	90	7	0	3
10[g]	ReO_x/C + Pt/C	4.5 / 1.8	78	0	3	83	14
11[e]	2nd cycle		48	0	4	85	11
12[e]	3rd cycle		53	0	18	68	14

[a]Reaction conditions: 170 °C, 6h, **1** (1 mmol), catalyst (150 mg), *i*-PrOH (40 mL), N_2 (15 bar). [b]Conversion and selectivity are calculated by ^{1}H NMR. [c]Without regeneration. [d]Regeneration conditions: H_2/230°C/2h. [e]Regeneration conditions: H_2/230°C/4h. [f]3-pentanol (40 mL). [g]1.8 wt % Pt/C (150 mg) + 4.5 wt % ReO_x/C (150 mg).

The carbon balance after 6 h DODH-CTH reaction over Pt-ReO_x/C catalyst is described in Table 3.3. The sum of C6 reactant and products (**1-5**) exhibited 92% carbon balance and the rest of 8% could be explained by organic deposits which are discussed in the later section. Isopropanol offered hydrogen for both DODH and CTH, producing acetone. The higher amount of acetone (5.1 mmol) was produced than the theoretically required amount of H_2 (2.8 mmol), indicating independent dehydrogenation of isopropanol by Pt-ReO_x/C. 1.2

mmol of molecular hydrogen was detected by GC-TCD analysis of the gas-phase. Dehydration of isopropanol also occurred, making some amount of propene and diisopropyl ether in the reaction solution (Table 3.3). Propene, propane, and isopropanol in the gas phase were detected by GC-MS. In addition to the conversion of isopropanol to the C3 compounds, solvent gasification during reaction and loss during separation and concentration steps could explain the 8% loss in the C3 carbon balance.

Table 3.3 DODH-CTH tandem reaction of **1** over Pt-ReO_x/C.[a]

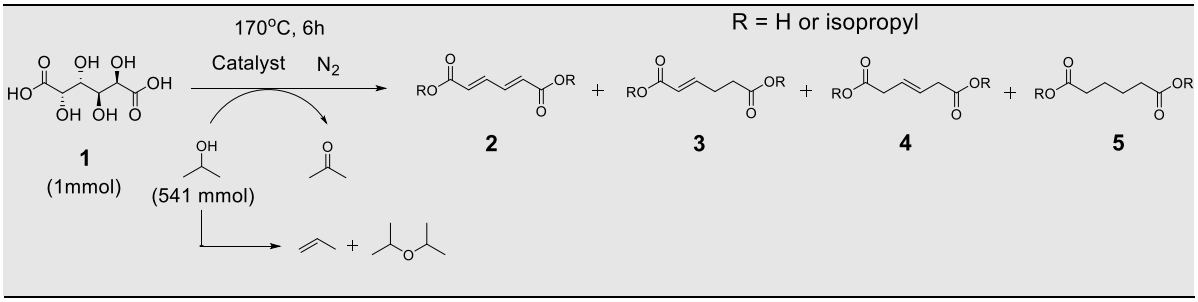

	C6 yield (mmol)					
	1	**2**	**3**	**4**	**5**	C6 carbon balance (%)[c]
Pt-ReO_x/C	0.21	0	0.05	0.01	0.65	92
	C3 yield (mmol)					
				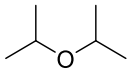		C3 carbon Balance (%)[d]
	494	5.1	0.22	0.12		92

[a]Reaction conditions: batch reaction, 170 °C, 6 h, catalyst (150mg, Re 3.6 mol %, Pt 1.4 mol %) **1** (210 mg), *i*-PrOH (40 mL), and N_2 (15 bar). [b]Yield is calculated by ^{1}H NMR. [c](yield of **1**+**2**+**3**+**4**+**5**)*100 [d](yield of 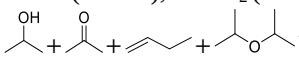)/541*100

The time profile of the DODH-CTH reaction over Pt-ReO_x/C is shown in Figure 3.5. It follows a sequential kinetic scheme of DODH followed by two steps of CTH: **1** → **2** → **3**/**4**

→ **5**. It is notable that both intermediates **2** and **3**/**4** were observed along the path of the reaction, indicating that CTH proceeded at similar rates as DODH. After 24 h, 85% overall yield of **5** was attained. **5** contains adipic acid (30%), isopropyl monoester (40%), and isopropyl diester (30%), quantified by ^{1}H and ^{13}C NMR (Figure 3.6). Acid hydrolysis of the products gave isolated adipic acid in 77% yield.

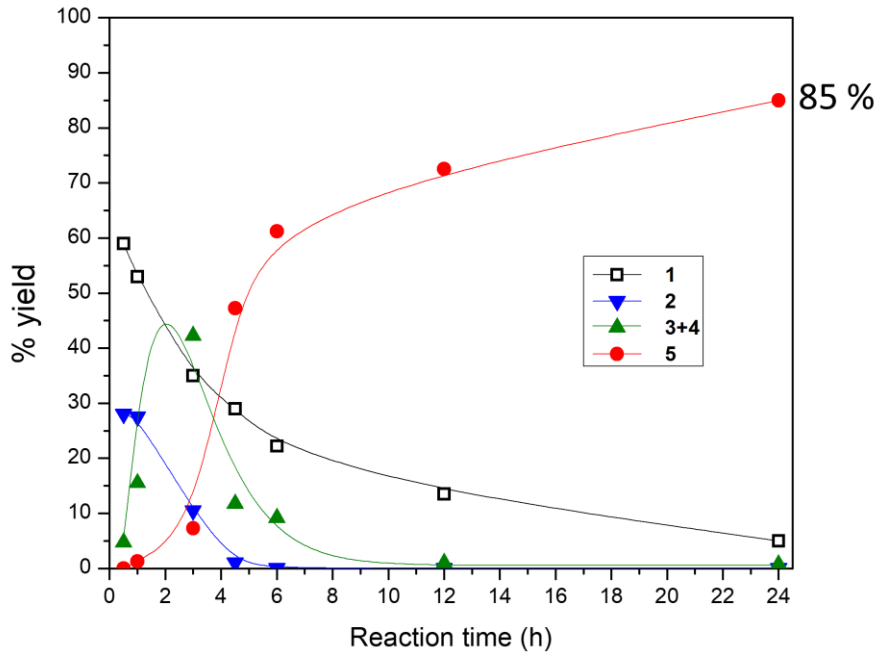

Figure 3.5 Reaction profile of DODH-CTH tandem reaction of **1** over Pt-ReO_x/C. Reaction conditions: **1** (1 mmol), Pt-ReO_x/C (150 mg), isopropanol (40 mL), N_2 (15 bar), 170 °C. The solid lines are to guide the eye.

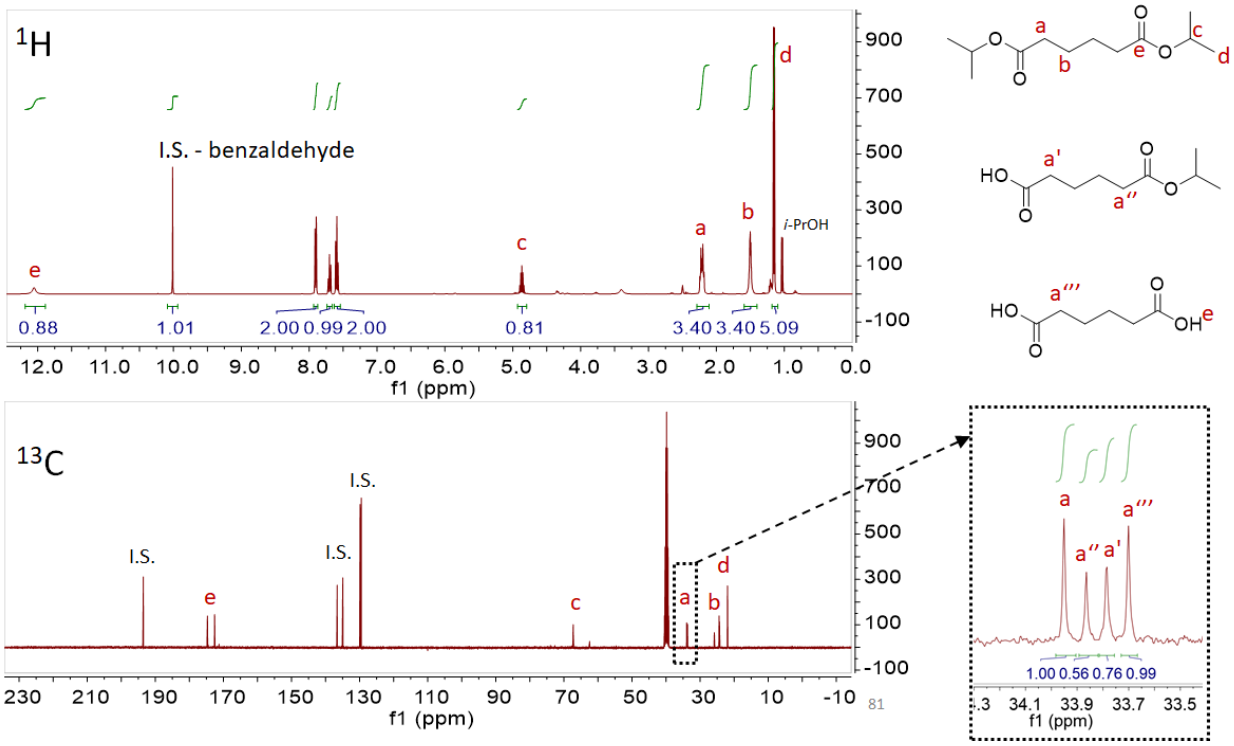

Figure 3.6 The composition of products was quantified based on β-C peaks in the quantitative ^{13}C NMR.

The reaction concentration increased from 0.025 to 0.1 to 0.25 M (run 1-3 in Table 3.4). In DODH-CTH with the higher concentration solution, the selectivity of **5** decreased mainly due to the side reactions and byproducts. The most probable side reaction was intramolecular dehydration of **1** to cyclic compounds and following DODH-CTH could make cyclic byproducts shown in Scheme 3.2. The side reactions could be suppressed by using diisopropyl mucate (**13**) as a substrate, showing high selectivity of **5** (83%) even in the higher concentration solution of 0.25 M (run 4 in Table 3.4).

Table 3.4 The effect of concentration of reaction solution [a]

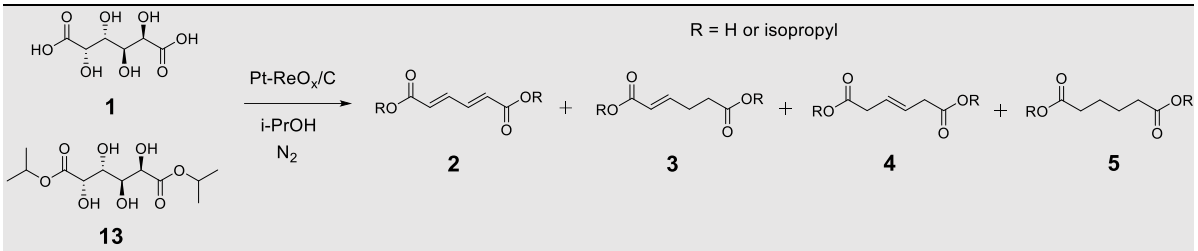

Run	Substrate	Conc.(M)	Conv.[b] (%)	Products/ % Selectivity[b]			
				2	**3** & **4**	**5**	Others
1[c]	**1**	0.025	95	0	0	89	11
2	**1**	0.1	100	0	2	77	21
3	**1**	0.25	100	0	5	65	30
4[d]	**13**	0.25	90	0	0	83	17

[a]Reaction conditions: 170 °C, 24 h, Pt-ReO_x/C (3.6 mol% Re and 1.4 mol% Pt relative to substrate), *i*-PrOH (10 mL), N_2 (15 bar). [b]Conversion and selectivity are calculated by ^{1}H NMR. [C]*i*-PrOH (40 mL). [d]12 h reaction

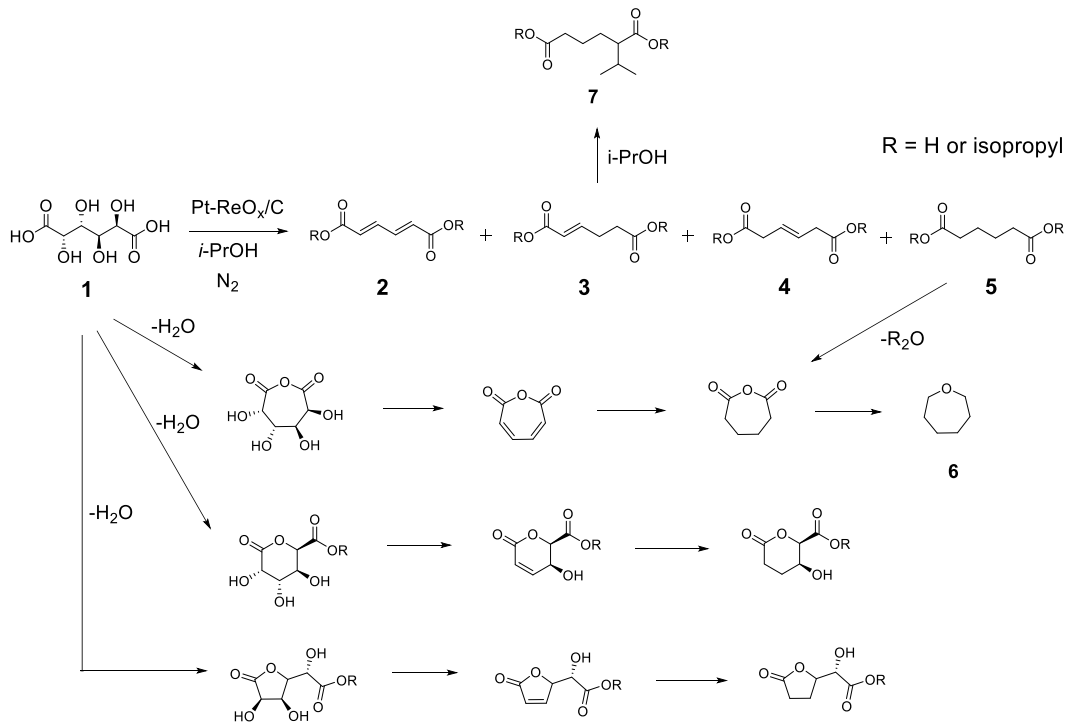

Scheme 3.2 Possible side reactions and byproducts

3. Catalyst characterization

Pt-ReO_x/C was characterized by microscopy and spectroscopy based methods. STEM combined with EDX analysis showed that Pt and Re existed on the same particles (Figure 3.7). The average particle size of Pt-ReO_x/C calculated from STEM images is 3.2 ± 1.5 nm, which is larger than that of ReO_x/C (2.2 ± 0.4 nm, Figure 3.1). This indicates the formation of larger particles when Pt is added to ReO_x/C.

H_2-TPR profiles of monometallic and bimetallic catalysts were analyzed to investigate the interaction between Re and Pt (Figure 3.7e). The peak at high temperature around 600 ^oC is due to methanation of carbon support with H_2.[41,42] The TPR result of Pt/C exhibits a uniform reduction peak at 303 ^oC, which is assigned to the reduction of Pt^{II} species shown in XPS results of Pt/C below. Two different peaks at 335 and 417 ^oC observed in the profile of ReO_x/C indicate the heterogeneous nature of Re on carbon support. The addition of Pt to ReO_x/C resulted in the shift of the first reduction peak to 275 ^oC in the profile of Pt-ReO_x/C. This shift can be attributed to the hydrogen spillover from metallic Pt to Re.[42,43] Moreover, the reduction behavior of Pt-ReO_x/C catalyst starts at a lower temperature (125 ^oC) compared to ReO_x/C (200 ^oC). Both shifts in the reduction peak and the reduction starting temperature exhibit the close interaction between Pt and Re in Pt-ReO_x/C catalyst, which is consistent with STEM and EDX analysis.

The as-prepared Pt-ReO_x/C has both high valent Re and metallic Pt as evident by XPS (Figure 3.8a,b). In the curve fitted results of Re 4f spectrum, the major oxidation states at binding energy of 44.7 and 47.1 represent Re^{VII} (72%), followed by Re^{IV} (27%) and a very small amount of metallic Re^0 (1%). Pt consists of 85% metallic Pt^0 with a $4f_{7/2}$ peak at 71.8 and 15% Pt^{II}. The reported binding energy for Pt $4f_{7/2}$ peak of bulk metallic Pt^0 ranged between 71.0-71.3 eV.[44] The shift towards higher binding energy indicates smaller size and

high dispersity of Pt particles.[44,45] The thermal treatment step under N_2 at 480 °C during synthesis results in Pt^{IV} precursor reduction to metallic Pt^0 due to the reductive properties of the carbon support.[46] Similar oxidation states of Pt and Re were observed in monometallic Pt/C and ReO_x/C samples.

XRD patterns of bare activated carbon, ReO_x/C, Pt/C, and Pt-ReO_x/C are shown in Figure 3.7f. Pt^0 and Re^{VII}, major species detected by XPS analysis, did not appear in the XRD patterns, suggesting high dispersion of particles in Pt/C and Pt-ReO_x/C. This is consistent with XPS analysis: the higher Pt^0 $4f_{7/2}$ peak position of the catalysts than that of bulk Pt. While the particles are small and well-dispersed, ReO_2 peaks in the pattern of ReO_x/C and Pt-ReO_x/C suggest the existence of larger particles containing ReO_2 phase.

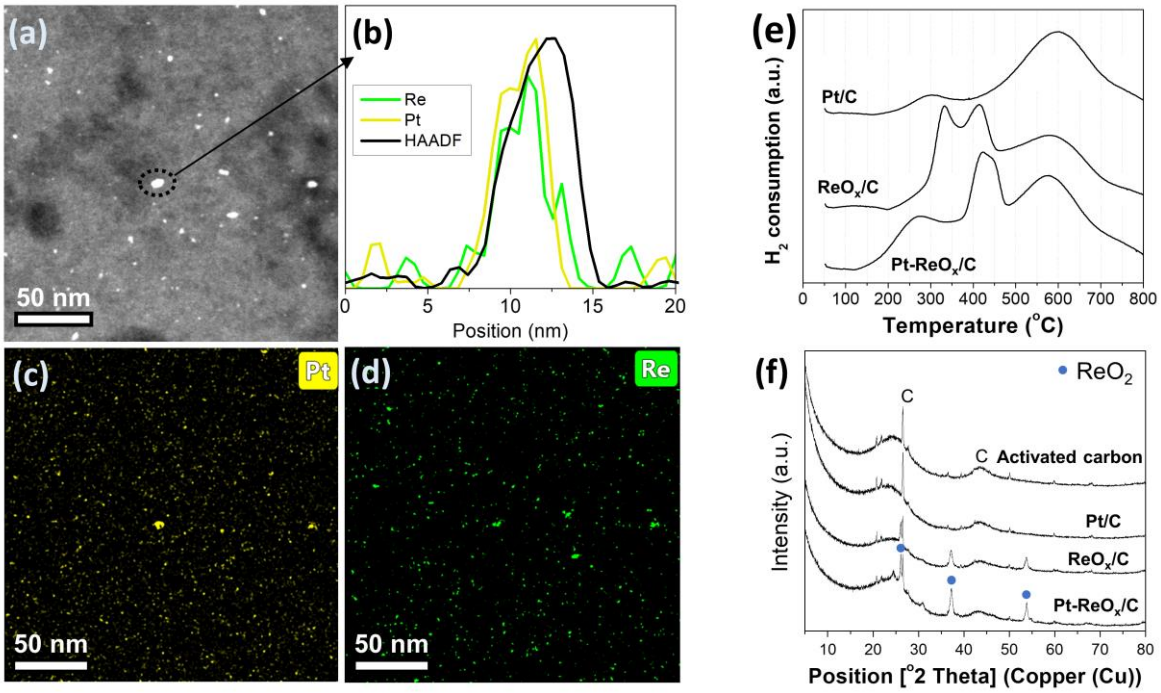

Figure 3.7 Characterization of as-prepared Pt-ReO_x/C catalyst (a) STEM high-angle annular dark-field (HAADF). (b) Line scan elemental analysis on a particle in (a). (c) EDX mapping of Pt. (d) EDX mapping of Re. (e) TPR profiles for Pt/C, ReO_x/C, and as-prepared Pt-ReO_x/C (f) XRD diffractograms of activated carbon, Pt/C, ReO_x/C, and as-prepared Pt-ReO_x/C. Peaks with blue circle at 26, 37, and 54° represent ReO_2.

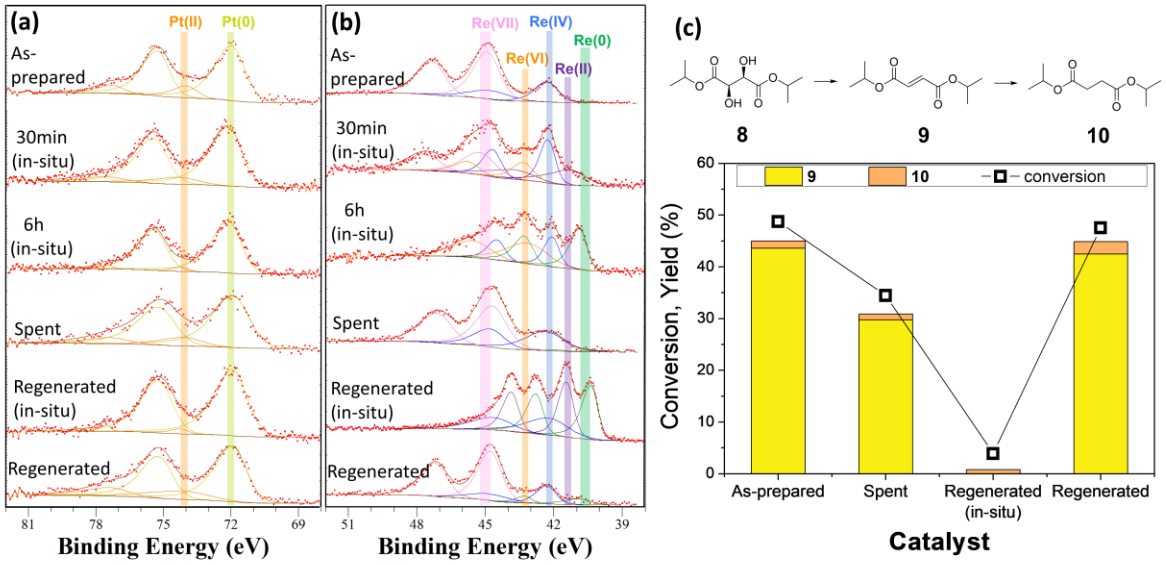

Figure 3.8 Changes in XPS spectra of (a) Pt 4f and (b) Re 4f in Pt-ReO_x/C over reaction and regeneration. In-situ 30 min and 6 h samples under the general reaction conditions for mucic acid (**1**) conversion were prepared without air exposure. After 6h reaction, the catalyst was separated and washed under atmospheric conditions, followed by drying overnight at 120 °C (spent sample). The spent sample was regenerated at 230 °C under H_2 and transferred to a glovebox without air exposure (in-situ regenerated sample). This in-situ sample was exposed to air and reoxidized at 120 °C (regenerated sample). (c) Activity test of as-prepared, spent, in-situ regenerated, and regenerated samples using diisopropyl L-(+)-tartarate (**8**) as a substrate. Reaction conditions: **8** (0.5 mmol), catalyst (20 mg), isopropanol (10 mL), N_2 (15 bar), 170 °C, 20 min. The reaction with the in-situ regenerated sample was carried out under inert conditions.

4. Proposed reaction mechanism

As discussed in bifunctional catalysis section, ReO_x/C was active for DODH but inactive for CTH at 170 °C. The addition of Pt to ReO_x/C showed significant increase in CTH. These, combined with no activity of Pt/C for DODH, suggest a bifunctional mechanism; DODH occurs on ReO_x and CTH on Pt in the Pt-ReO_x/C catalyst. The similar reactivity of a physical mixture of ReO_x/C and Pt/C for DODH-CTH reaction as Pt-ReO_x/C supports the bifunctional mechanism (run 10 in Table 3.2).

To identify active species of DODH and CTH, the changes in oxidation states of Re and Pt during the reaction were investigated. Under the general reaction conditions for mucic acid conversion, oxidation states of Re and Pt were gradually reduced over the course of the reaction in Figure 3.8. To avoid oxidation of Re during the preparation of samples for XPS, the catalyst after 30 min or 6 h reaction was separated and transferred to the XPS chamber without exposure to ambient atmosphere. In 30 min, a significant amount of Re^{VII} in the as-prepared sample was reduced with the appearance of Re^{VI} ($4f_{7/2}$ peak at 43.3) and Re^{II} ($4f_{7/2}$ peak at 41.2). Re in the in-situ 30 min sample consisted of Re^{VII} (31 %), Re^{VI} (16 %), Re^{IV} (28 %), and Re^{II} (25 %). Further reduction of Re proceeded during 6 h, making Re^{VI} (42 %), Re^{IV} (23 %), and metallic Re^{0} (35 %). The reaction profile in Figure 3.5 shows that the catalysts with the reduced Re oxidation states also converted mucic acid through DODH. It should be noted that DODH of the in-situ regenerated sample containing metallic Re^{0} and Re^{II} as dominant species is shown to be inactive later in this chapter (Figure 3.8c). These observations indicate that high oxidation states of ReO_x (Re^{VII}, Re^{IV}, and Re^{IV}) are involved species for DODH reaction. This is consistent with previously suggested DODH mechanisms including Re^{VII}/Re^{V} or Re^{VI}/Re^{IV} redox couples over heterogeneous ReO_x based catalysts.[33,35,36,47,48] Similarly, the reduction of Pt under the reaction conditions resulted in 96 % of metallic Pt^{0} and a small amount of Pt^{II} (4 %) after 6 h reaction, indicating metallic Pt^{0} as active species for CTH.

The reported DODH mechanism involves three steps: formation of Re-diolate, reduction of Re species, and extrusion of olefin.[14,11,26,33,36,49–51] In the literature on heterogeneous DODH catalysts, oxorhenium species in nanocluster can be active species for DODH,[33,35] while other authors demonstrated isolated ReO_x as active species.[47,48] Hot filtration experiments were performed to investigate the contribution of molecular species to the DODH reaction

(Figure 3.11a). After hot filtration at approximately 30% conversion at 170 °C, the additional reaction with the filtrate without solid catalyst showed a negligible increase in the conversion. This suggests that DODH proceeds mostly on the heterogeneous surface, precluding the involvement of the molecular species.[33,35] Re^{VII} and Re^{VI}, designated as the active species of DODH in the solid Pt-ReO_x/C catalyst, form Re-diolate by coordinating to **1** (Scheme 3.3). Isopropanol reduces the rhenium diolato complex, affording acetone as a byproduct. The reduced oxorhenium diolate releases an alkene (the reverse of a 3+2 dihydroxylation), closing the catalytic cycle on rhenium. After the DODH cycle, the reduced Re goes back to Re^{VII} or Re^{VI}. Two DODH cycles afford **2** from **1**.

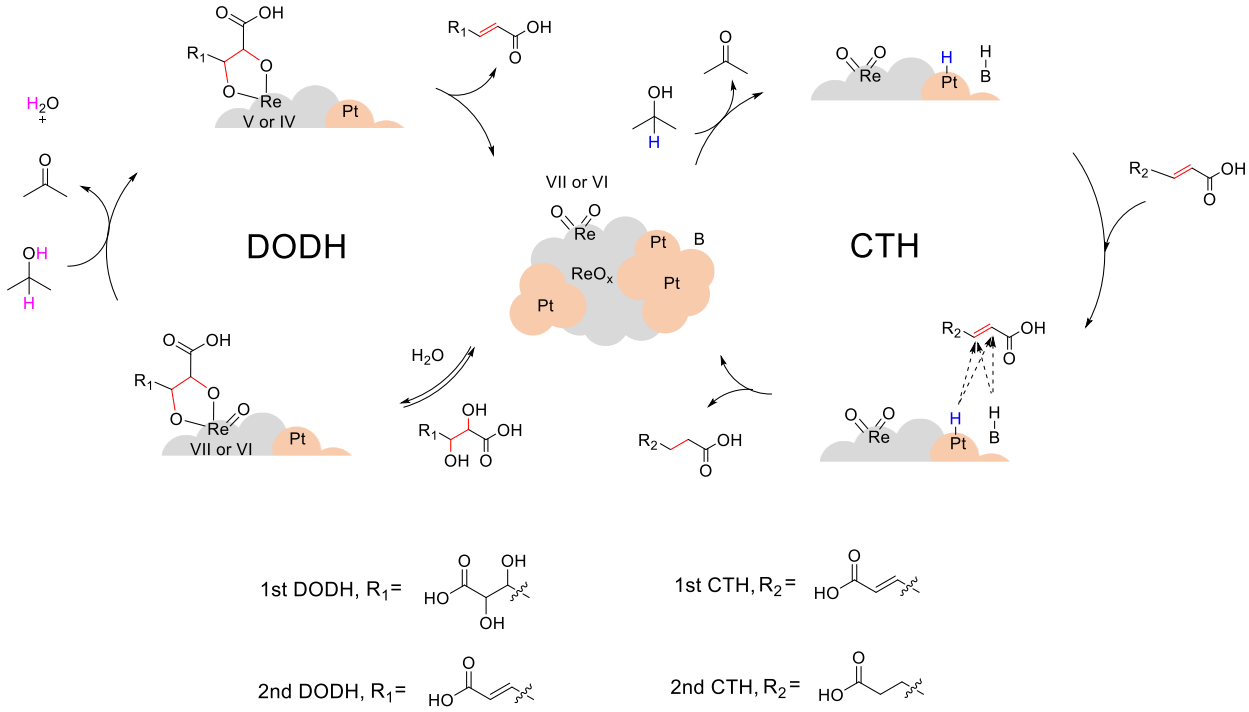

Scheme 3.3 Proposed bifunctional mechanism for DODH-CTH tandem reaction of **1**. B: basic site.

Concerning the mechanism of CTH over Pt, the isotope labeling experiments were conducted. Previously, both a "monohydride mechanism" and "dihydride mechanism" have been proposed for transition metal-catalyzed CTH.[52,53] Deuterium labeling experiment of acetophenone (**11**) using deuterated isopropanol is a widely used method to distinguish between the two possible CTH mechanisms.[54,55] Pt-ReO_x/C catalyzed-CTH of **11** with isopropanol-2-d_1 showed 80% incorporation of deuterium at the α-C (Scheme 3.4A and Figure 3.9). This is indicative of a monohydride mechanism. Only the α-H of the donor forms Pt-H and this hydride is transferred to the α-C of acetophenone exclusively while the O-H hydrogen ends up on the carbonyl oxygen.[56]

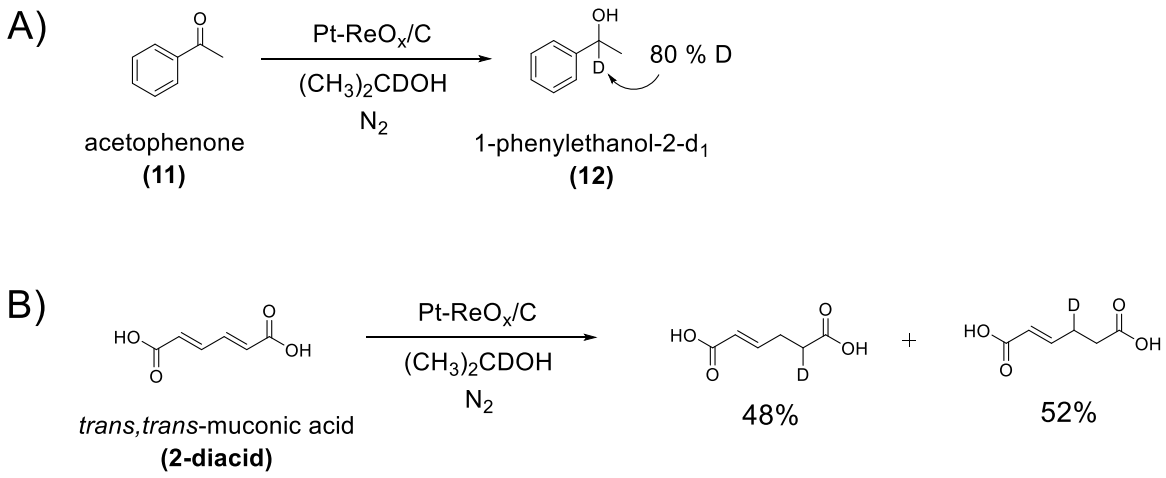

Scheme 3.4 The isotope labeling experiments for CTH of A) acetophenone (**11**) and B) *trans,trans*-muconic acid (**2-diacid**) with isopropanol-2-d_1. Reaction conditions: substrate (0.5 mmol), Pt-ReO_x/C (15mg, 4.5 wt% Re, 1.8wt% Pt), *i*-PrOH-2-d_1 (1 mL), N_2 (15 bar), 150 ^oC, 6h.

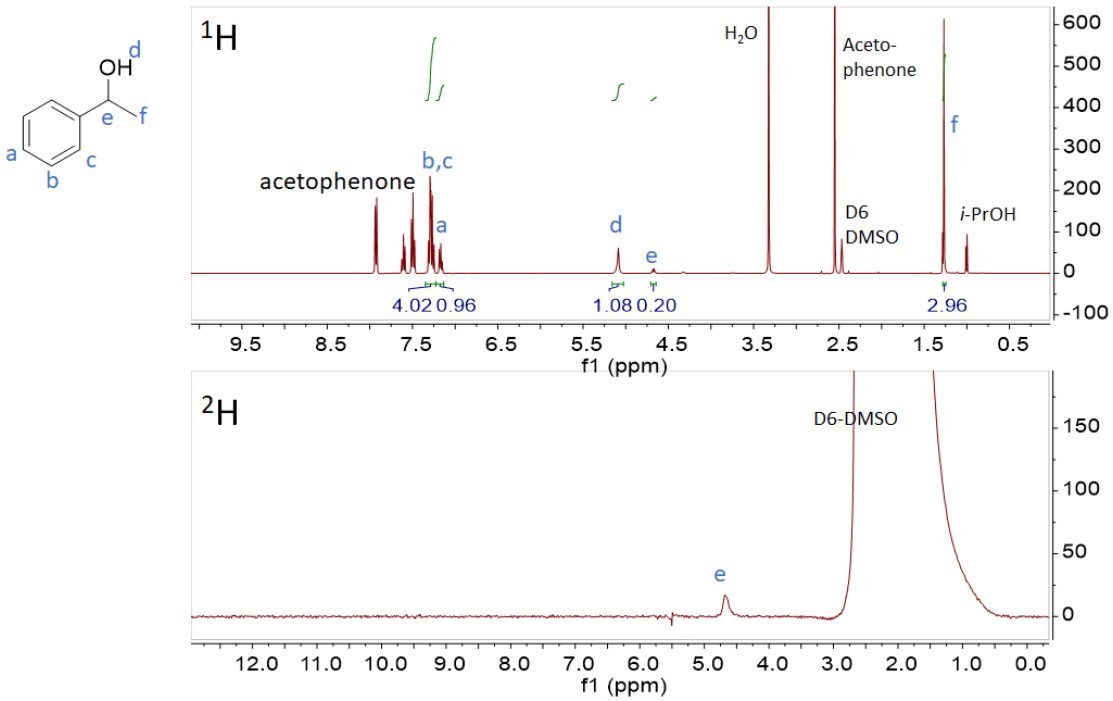

Figure 3.9 ^{1}H and ^{2}H NMR results of the deuteration test. Reaction conditions: **11** (0.5 mmol), Pt-ReO_x/C (15 mg, 4.5 wt % Re, 1.8 wt % Pt), *i*-PrOH-2-d_1 (1 mL), N_2 (15 bar), 150 ^{o}C, 6h.

However, CTH of **2-diacid** with isopropanol-2-d_1 resulted in the incorporation of deuterium both at α-C and at β-C of the molecule (Scheme 3.4B and Figure 3.10). This indicates that the hydride (Pt-H) generated by the monohydride mechanism can be transferred to both α-C and β-C of **2-diacid** (Scheme 3.3). Similarly, incorporation of metal monohydride to α-C and β-C without regioselectivity was observed in the literature on the hydrogenation of α,β-unsaturated carboxylic acid.[57,58] Moreover, it has been shown that noble metal heterogeneous catalysts with a base additive transfer hydrogen from isopropanol to ketone or olefin through a monohydride mechanism.[28,59] In Pt-ReO_x/C, base sites of the catalyst would act as the base additive, transferring O-H hydrogen in isopropanol to the olefin (Scheme 3.3). The possible basic sites include basic sites of activated carbon support and different Pt species.[60] It is reported that basic sites of support material play a similar role to base additives in CTH reaction.[61]

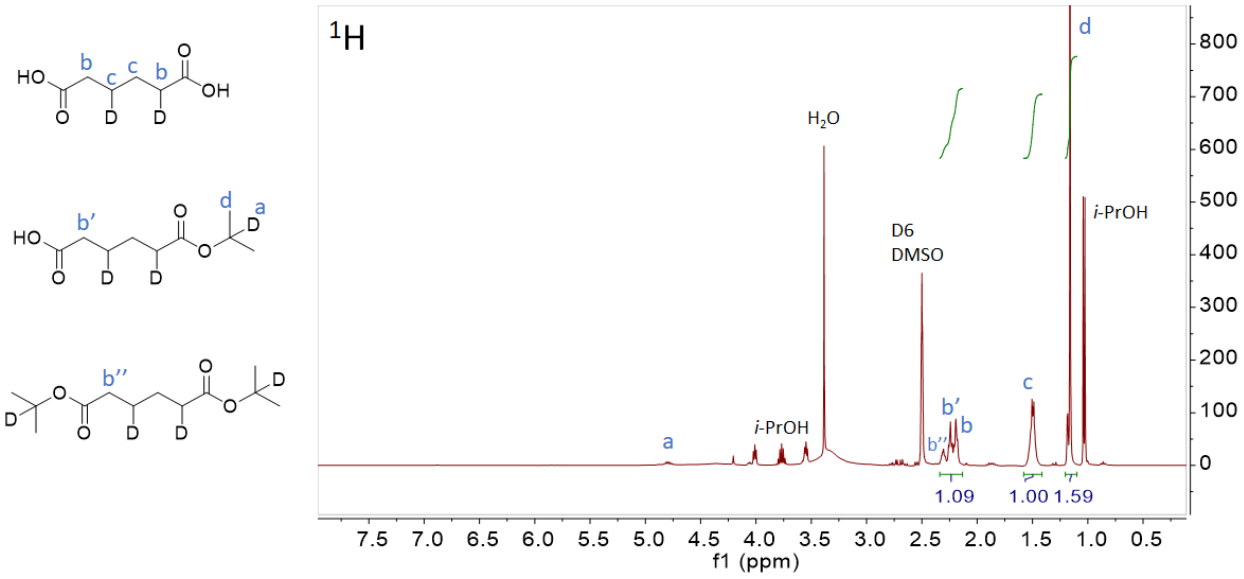

Figure 3.10 ^{1}H NMR results of the deuteration test. Reaction conditions: **2-diacid** (0.5 mmol), Pt-ReO_x/C (15 mg, 4.5 wt % Re, 1.8 wt % Pt), *i*-PrOH-2-d_1 (1 mL), N_2 (15 bar), 150 ^{o}C, 6h.

5. Catalyst recycling and regeneration

One of the main advantages of heterogeneous catalysts is the possibility of their reuse.[62] While supported ReO_x catalysts tend to deactivate due to leaching under DODH reaction conditions,[15,34] some stable and reusable solid ReO_x catalysts have been reported.[16,33,35] The reusability of the Pt-ReO_x/C catalyst was investigated. The recovered catalyst was tested with new substrate **1** and isopropanol. Lower conversion and selectivity of **5** were observed (run 2 in Table 3.2). However, ICP analysis of catalyst after 1 cycle showed small leaching of Re (4% of the original amount of Re added) and no leaching of Pt (Figure 3.11c). Thus, active site loss into solution during reaction did not make a major contribution to the loss of activity and selectivity of **5.** This, as well as hot filtration experiments, is a significant point in demonstrating that the active catalyst is indeed heterogeneous and not homogeneous from leaching. According to CO chemisorption data, strongly reduced CO adsorption on the spent sample (2% dispersion) was observed compared to the value of the as-prepared catalyst

(25% dispersion, Figure 3.11b). These observations suggest that organic deposits during the reaction result in deactivation and lower activity and selectivity. 5-15% of unidentified byproducts might be responsible for the organic deposits. It is not uncommon for heavy by-products to form a carbonaceous deposit on the surface of the catalysts in the reaction of organic compound.[63]

To recover reactivity, the spent catalyst was regenerated under H_2 atmosphere.[64] Regeneration temperature was chosen to remove the organic deposits on the catalysts and to minimize methanation of the support. With regeneration at 230 ^oC, the dispersion of Pt-ReO_x/C was restored to 20%, which is a clear indication of removal of organic deposits from the surfaces of the spent catalyst (Figure 3.11b). Lower temperature H_2 treatment (200 ^oC) did not remove organic deposits effectively. The changes in the oxidation states and the activity of Pt-ReO_x/C over the regeneration step were analyzed in Figure 3.8. Diisopropyl L-(+)-tartarate (**8)** was used as a substrate to study the activity of the catalysts for DODH. While the spent catalyst exhibited similar oxidation states to the as-prepared Pt-ReO_x/C catalyst, it showed the reduced conversion of **8** due to the organic deposits. During the regeneration step at 230 ^oC, high oxidation states of ReO_x in the spent sample were reduced to metallic Re^0 and Re^{II}, measured by in-situ sampling and analysis without exposure to air (in-situ regenerated sample). This is consistent with the low reduction starting temperature (125 ^oC) in TPR spectra of Pt-ReO_x/C (Figure 3.7e) and XPS results of the reduced Pt-Re bimetallic catalysts in previous reports.[22,23] The negligible activity of the in-situ regenerated sample indicates that the low oxidation states of Re are not active for DODH, agreeing with previous observations.[33,47] The in-situ regenerated sample was re-oxidized by exposure to air and drying at 120 ^oC for 1 h (regenerated sample). The regenerated sample showed similar oxidation states and activity for DODH to the as-prepared catalyst, confirming that the

regeneration at 230 ºC effectively removes the organic deposits. It should be also highlighted that the re-oxidation step is necessary after the regeneration to recover high oxidation states of Re and reactivity for DODH.

The regeneration and reoxidation were employed to the catalyst after the second run in Table 3.2. After regeneration at 230 ºC for 2 h and re-oxidation, the reactivity of Pt-ReO_x/C for the conversion of **1** was regained in subsequent third and fourth runs (run 3 and 4 in Table 3.2). Longer regeneration time (4 h) under H_2 at 230 °C resulted in a similar performance of the as-prepared catalyst (Table 3.2, run 5). Over the course of five sequential reactions with the same catalyst sample, some amount of Re and Pt was leached out, however, not affecting yield of **5** at high conversion (Figure 3.11c). It has been addressed that the recycling test with a single measurement at high conversion in a batch reaction system might not fully reflect the deactivation of the catalyst.[65,66] Thus, the catalyst stability should be tested at kinetically controlled conversion, which is shown later in this chapter. Based on XPS and XRD analysis, the Pt-ReO_x/C catalyst maintained its oxidation states and was still well-dispersed after multiple recycling tests (Figure 3.11d). After 5 consecutive cycles, ReO_2 peaks disappeared, possibly due to the phase change to amorphous over multiple reactions and regenerations.

Interestingly, in comparison to the bifunctional bimetallic Pt-ReO_x/C catalyst, the physical mixture of Pt/C and ReO_x/C could not be regenerated. Much lower conversions in the 2nd and 3rd cycles were observed (run 11 and 12 in Table 3.2). The recycled physical mixture after regeneration exhibited similar oxidation states and metal amount, but lower CO adsorption compared to as-prepared catalysts (Table 3.5). Thus, the lower conversion is attributed to organic deposits on ReO_x/C that were not removed during regeneration. In the physical mixture, ReO_x alone might not uptake enough hydrogen to eliminate organic

deposits. In contrast in Pt-ReO_x/C, hydrogen spillover from Pt enhances regeneration of ReO_x sites.[43,67–69] Thus, while the Pt-ReO_x interface was not critical for the bifunctional DODH/CTH reaction, it was critical for effective regeneration of the catalyst.

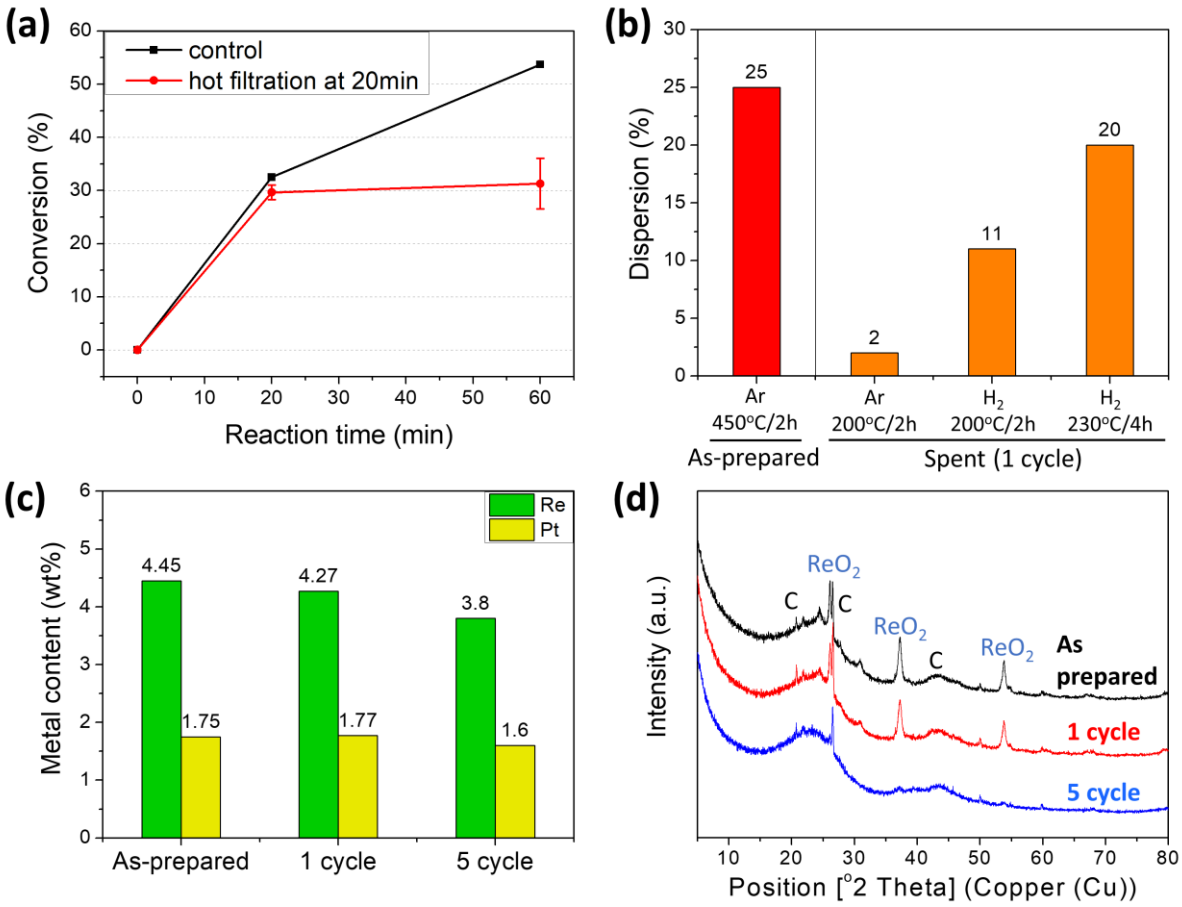

Figure 3.11 (a) Hot filtration test of Pt-ReO_x/C catalyst. For the control test, two samples were collected at 20 min and 60 min. For the hot filtration test, the reaction solution was extracted from a pressure reactor equipped with a ceramic filtration system at 170 °C after 20 min reaction. The filtrate was submitted to the same reaction conditions for an additional 40 min. Reaction conditions: **8** (4 mmol), Pt-ReO_x/C (100 mg), isopropanol (40 mL), N_2 (15 bar), 170 °C, 20 min. (b) Dispersion, calculated by CO chemisorption analysis, of as-prepared and spent (1 cycle) Pt-ReO_x/C with different pretreatment conditions. (c) ICP analysis and (d) XRD spectra of Pt-ReO_x/C over the recycling test.

Table 3.5 CO adsorption, ICP, and XPS analysis of as-prepared and recycled physical mixture.

Catalyst	Dispersion (%)	ICP (wt%)		XPS (%)				
		Re	Pt	Pt^0	Pt^{II}	Re^0	Re^{IV}	Re^{VII}
As-prepared physical mixture	37[b]	4.5	1.8	84	16	0	25	75
Recycled physical mixture[a]	17	4.3	1.7	84	16	9	21	70

[a]After regeneration (H_2/230°C/4h). [b]Pretreatment condition (Ar/450°C/2h).

6. Stability test

The stability of Pt-ReO_x/C was studied by observing changes in its activity for DODH and CTH at low conversion levels over multiple consecutive runs. The first run for the conversion of **8** with Pt-ReO_x/C showed 33% conversion after 20 min reaction at 170 °C, producing **9** as a major product through DODH (Figure 3.12a). The conversion gradually decreased until the 6th cycle where the conversion was 12%. This deactivation was attributed to both organic deposits on ReO_x and active sites leaching. The regeneration including re-oxidation increased the conversion up to 28% in the 7th cycle, indicating organic deposits as a major contribution of the observed deactivation in the first 6 cycles. The 4% difference between the 1st and 7th cycle can be explained by the leaching of Re over the multiple runs. ICP analysis of the catalyst after 8 cycles showed some leaching of Re, attributing to the slightly reduced conversion of the regenerated catalyst compared to the as-prepared catalyst (Figure 3.12c). While ReO_x in Pt-ReO_x/C catalyst can be deactivated by both fouling and leaching during DODH-CTH reaction, the amount of Re leached out from the catalyst is small (Figure 3.11c and 3.12c). As result, the catalyst could be reusable several times after regeneration without significantly reduced reactivity.

Interestingly, the activity of Pt sites for CTH did not change much (Figure 3.12b). Over 12 consecutive runs, the conversion of **9** was slightly reduced from 40% to 30% and maintained around 30% even with regeneration. The results indicate that deactivation by organic deposits on Pt sites is negligible and small leaching of Pt sites could be a reason for the reduced conversion (Figure 3.12c). Loss of Re over the 12 runs in Figure 3.12b is more pronounced than that over 8 runs in Figure 3.12a. This is probably because the organic deposits on ReO_x in Figure 3.12a inhibit the leaching of Re.

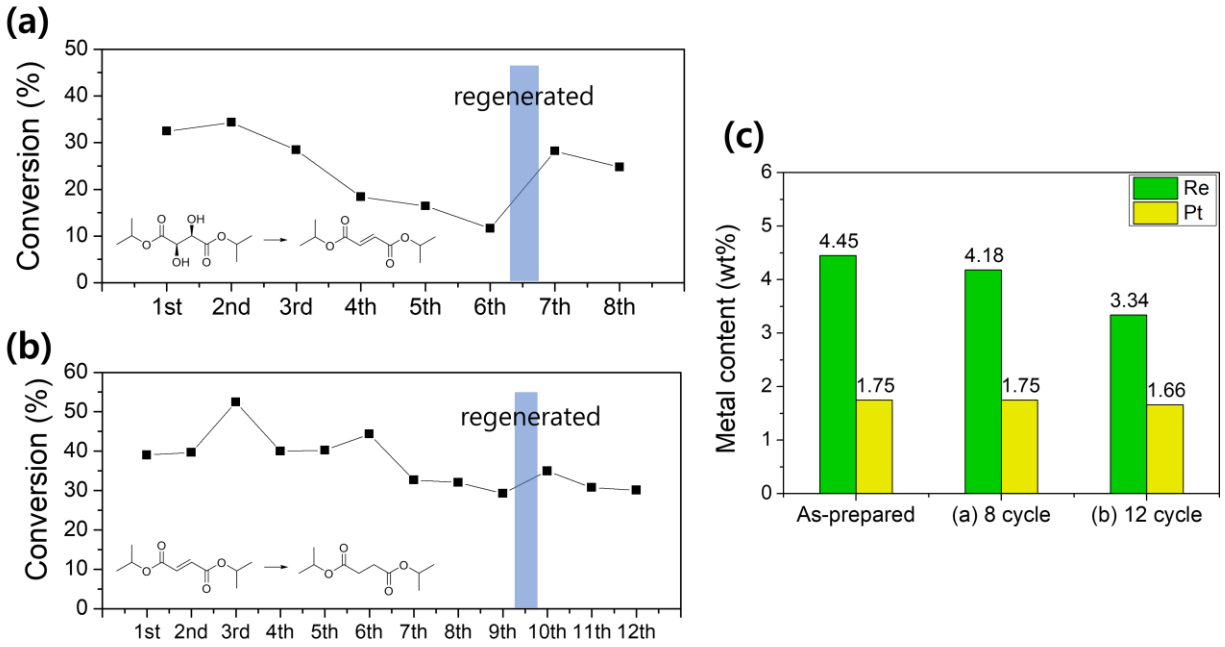

Figure 3.12 Stability of Pt-ReO_x/C for (a) DODH (**8** to **9**) and (b) CTH (**9** to **10**). Reaction conditions: substrate (4 mmol), Pt-ReO_x/C (100 mg), activated carbon (200 mg), isopropanol (40 mL), N_2 (15 bar), 170 °C, 20 min. (c) ICP analysis of as-prepared Pt-ReO_e/C, spent sample after 8 cycles in (a), and 12 cycles in (b). Regeneration conditions: 5% H_2 in Ar, 230 °C, and 4 h.

7. Substrate scope

To explore the substrate scope for Pt-ReO_x/C, various diols were studied (Table 3.6). Diisopropyl mucate (**13**) was converted to **5-diester** in high yield (90%). This indicates that the rate of conversion of **1** is hampered by competition between DODH and esterification. D-glucaric acid lactone can be used as a substrate to produce **5**.[5,16] Conversion of D-glucaric-1,4-lactone (**14**) through DODH-CTH over Pt-ReO_x/C gave 41% of **15** and 15% of **5**. Ring-opening of **15** is required to increase yields of **5**. In addition to C6 sugar acids, the bifunctional catalyst successfully converted L-(+)- tartaric acid (**16**), a C4 sugar acid to 98% yield of succinic acid and its esters (**17**). The same reaction was also applied to sugar alcohols. Glycerol (**18**) was converted to 1-propanol (**19**) in 87% yield. D-sorbitol (**20**) contains six OH groups, thus three DODH-CTH cycles produced n-hexane (**22**).

Table 3.6 Substrate scope of DODH-CTH tandem reaction of sugar acids and alcohols over Pt-ReO_x/C.[a]

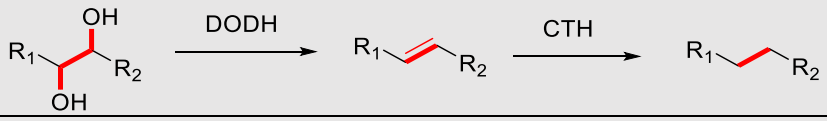

Run	Substrate	Reaction condition	Product (% yield)[b]
1	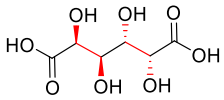 **1**	170 °C 24 h	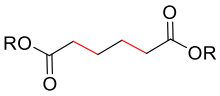 **5** (85%)
2	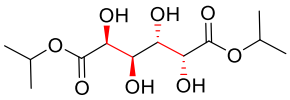 **13**	170 °C 6 h	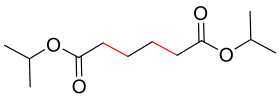 **5-diester** (90%)
3[c]	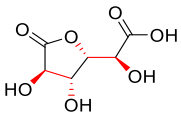 **14**	170 °C 24 h	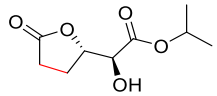 **15** (41%) 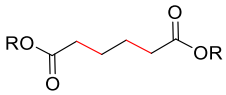 **5** (15%)
4	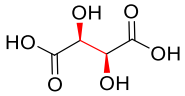 **16**	170 °C 6 h	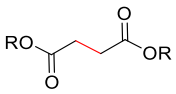 **17** (98%)
5	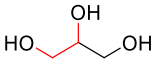 **18**	170 °C 6 h	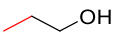 **19** (87%)
6	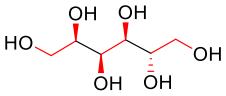 **20**	200 °C 24 h	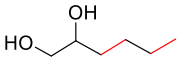 **21** (18%)[d] 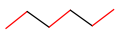 **22** (19%)[d]

[a]Reaction conditions: Pt-ReO_x/C (150 mg, 4.5 wt % Re, 1.8 wt % Pt), substrate (1.0 mmol), *i*-PrOH (40 mL), and N_2 (15 bar). [b]Calculated by ^{1}H NMR. [c]substrate (0.5 mmol). [d]Calculated by GC-FID.

D. Conclusion

Bifunctional Pt-ReO_x/C catalysts were prepared and shown to produce adipate **5** from the sugar diacid **1** through tandem DODH-CTH reactions in high yield (77% isolated adipic acid). Evidence was provided that the oxorhenium(VI and VII) sites are responsible for DODH. The metallic Pt^0 sites in Pt-ReO_x/C enhanced significantly the rate of CTH without impacting DODH, as long as the Pt loading was maintained at or below 1.8 wt %. Isopropanol is an effective and cheap hydrogen donor as well as solvent for both DODH and CTH relative to previously used C4-C8 alcohols. Reusability and stability tests of the Pt-ReO_x/C catalyst indicate catalyst deactivation mostly due to organic material deposition that can be removed by regeneration with H_2. Because metal leaching during DODH-CTH reaction is not remarkable (2-4% of the original amount of metal added per cycle of 6 h reaction), the Pt-ReO_x/C catalyst can be regenerated and reusable multiple times without significantly reduced performance. Furthermore, the bimetallic catalyst is effective for various sugar acids and alcohols. A bifunctional mechanism was proposed on the basis of the reactivity with various substrates, spectroscopic analysis, and isotope labeling experiments.

E. References

(1) Rinaldi, R.; Jastrzebski, R.; Clough, M. T.; Ralph, J.; Kennema, M.; Bruijnincx, P. C. A.; Weckhuysen, B. M. Paving the Way for Lignin Valorisation: Recent Advances in Bioengineering, Biorefining and Catalysis. *Angew. Chem. Int. Ed.* **2016**, *55* (29), 8164–8215.

(2) Lin, Y.-C.; Huber, G. W. The Critical Role of Heterogeneous Catalysis in Lignocellulosic Biomass Conversion. *Energy Environ. Sci.* **2009**, *2* (1), 68–80.

(3) Straathof, A. J. J.; Bampouli, A. Potential of Commodity Chemicals to Become Bio-based According to Maximum Yields and Petrochemical Prices. *Biofuels, Bioprod. Bioref.* **2017**, *11* (5), 798–810.

(4) Veski, R.; Veski, S. Aliphatic Dicarboxylic Acids from Oil Shale Organic Matter – Historic Review. *Oil Shale* **2019**, *36* (1), 76.

(5) Larson, R. T.; Samant, A.; Chen, J.; Lee, W.; Bohn, M. A.; Ohlmann, D. M.; Zuend, S. J.; Toste, F. D. Hydrogen Gas-Mediated Deoxydehydration/Hydrogenation of Sugar Acids: Catalytic Conversion of Glucarates to Adipates. *J. Am. Chem. Soc.* **2017**, *139* (40), 14001–14004.

(6) Draths, K. M.; Frost, J. W. Environmentally Compatible Synthesis of Adipic Acid from D-Glucose. *J. Am. Chem. Soc.* **1994**, *116* (1), 399–400.

(7) Niu, W.; Draths, K. M.; Frost, J. W. Benzene-Free Synthesis of Adipic Acid. *Biotechnol. Prog.* **2002**, *18* (2), 201–211.

(8) Boussie, T. R.; Dias, E. L.; Fresco, Z. M.; Murphy, V. J.; Shoemaker, J.; Archer, R.; Jiang, H. Production of Adipic Acid and Derivatives from Carbohydrate-Containing Materials. US8669397B2, March 11, **2014**.

(9) Gilkey, M. J.; Mironenko, A. V.; Vlachos, D. G.; Xu, B. Adipic Acid Production via Metal-Free Selective Hydrogenolysis of Biomass-Derived Tetrahydrofuran-2,5-Dicarboxylic Acid. *ACS Catal.* **2017**, *7* (10), 6619–6634.

(10) Wei, L.; Zhang, J.; Deng, W.; Xie, S.; Zhang, Q.; Wang, Y. Catalytic Transformation of 2,5-Furandicarboxylic Acid to Adipic Acid over Niobic Acid-Supported Pt Nanoparticles. *Chem. Commun.* **2019**, *55* (55), 8013–8016.

(11) Li, X.; Wu, D.; Lu, T.; Yi, G.; Su, H.; Zhang, Y. Highly Efficient Chemical Process to Convert Mucic Acid into Adipic Acid and DFT Studies of the Mechanism of the Rhenium-Catalyzed Deoxydehydration. *Angew. Chem. Int. Ed.* **2014**, *53* (16), 4200–4204.

(12) Tshibalonza, N. N.; Monbaliu, J.-C. M. The Deoxydehydration (DODH) Reaction: A Versatile Technology for Accessing Olefins from Bio-Based Polyols. *Green Chem.* **2020**, *22* (15), 4801-4848

(13) Dethlefsen, J. R.; Fristrup, P. Rhenium-Catalyzed Deoxydehydration of Diols and Polyols. *ChemSusChem* **2015**, *8* (5), 767–775.

(14) Shiramizu, M.; Toste, F. D. Expanding the Scope of Biomass-Derived Chemicals through Tandem Reactions Based on Oxorhenium-Catalyzed Deoxydehydration. *Angew. Chem. Int. Ed.* **2013**, *52* (49), 12905–12909.

(15) Sharkey, B. E.; Jentoft, F. C. Fundamental Insights into Deactivation by Leaching during Rhenium-Catalyzed Deoxydehydration. *ACS Catal.* **2019**, *9* (12), 11317–11328.

(16) Lin, J.; Song, H.; Shen, X.; Wang, B.; Xie, S.; Deng, W.; Wu, D.; Zhang, Q.; Wang, Y. Zirconia-Supported Rhenium Oxide as an Efficient Catalyst for the Synthesis of Biomass-Based Adipic Acid Ester. *Chem. Commun.* **2019**, *55* (74), 11017–11020.

(17) Wei, Z.; Sun, J.; Li, Y.; Datye, A. K.; Wang, Y. Bimetallic Catalysts for Hydrogen Generation. *Chem. Soc. Rev.* **2012**, *41* (24), 7994-8008.

(18) Carter, J. L.; McVinker, G. B.; Weissman, W.; Kmak, M. S.; Sinfelt, J. H. Bimetallic Catalysts; Application in Catalytic Reforming. *Appl. Catal.* **1982**, *3* (4), 327–346.

(19) Barbier, J. Deactivation of Reforming Catalysts by Coking - a Review. *Appl. Catal.* **1986**, *23* (2), 225–243.

(20) Parera, J. Stability of Bimetallic Reforming Catalysts. *J. Catal.* **1988**, *112* (2), 357–365.

(21) Kunkes, E. L.; Simonetti, D. A.; Dumesic, J. A.; Pyrz, W. D.; Murillo, L. E.; Chen, J. G.; Buttrey, D. J. The Role of Rhenium in the Conversion of Glycerol to Synthesis Gas over Carbon Supported Platinum–Rhenium Catalysts. *J. Catal.* **2008**, *260* (1), 164–177.

(22) Zhang, L.; Karim, A. M.; Engelhard, M. H.; Wei, Z.; King, D. L.; Wang, Y. Correlation of Pt–Re Surface Properties with Reaction Pathways for the Aqueous-Phase Reforming of Glycerol. *J. Catal.* **2012**, *287*, 37–43.

(23) Falcone, D. D.; Hack, J. H.; Klyushin, A. Yu.; Knop-Gericke, A.; Schlögl, R.; Davis, R. J. Evidence for the Bifunctional Nature of Pt–Re Catalysts for Selective Glycerol Hydrogenolysis. *ACS Catal.* **2015**, *5* (10), 5679–5695.

(24) Raju, S.; Moret, M.-E.; Klein Gebbink, R. J. M. Rhenium-Catalyzed Dehydration and Deoxydehydration of Alcohols and Polyols: Opportunities for the Formation of Olefins from Biomass. *ACS Catal.* **2015**, *5* (1), 281–300.

(25) Dethlefsen, J. R.; Lupp, D.; Teshome, A.; Nielsen, L. B.; Fristrup, P. Molybdenum-Catalyzed Conversion of Diols and Biomass-Derived Polyols to Alkenes Using Isopropyl Alcohol as Reductant and Solvent. *ACS Catal.* **2015**, *5* (6), 3638–3647.

(26) Shiramizu, M.; Toste, F. D. Deoxygenation of Biomass-Derived Feedstocks: Oxorhenium-Catalyzed Deoxydehydration of Sugars and Sugar Alcohols. *Angew. Chem. Int. Ed.* **2012**, *51* (32), 8082–8086.

(27) Wang, Y.; Huang, Z.; Leng, X.; Zhu, H.; Liu, G.; Huang, Z. Transfer Hydrogenation of Alkenes Using Ethanol Catalyzed by a NCP Pincer Iridium Complex: Scope and Mechanism. *J. Am. Chem. Soc.* **2018**, *140* (12), 4417–4429.

(28) Alonso, F.; Riente, P.; Rodríguez-Reinoso, F.; Ruiz-Martínez, J.; Sepúlveda-Escribano, A.; Yus, M. Platinum Nanoparticles Supported on Titania as an Efficient Hydrogen-Transfer Catalyst. *J. Catal.* **2008**, *260* (1), 113–118.

(29) Johnstone, R. A. W.; Wilby, A. H.; Entwistle, I. D. Heterogeneous Catalytic Transfer Hydrogenation and Its Relation to Other Methods for Reduction of Organic Compounds. *Chem. Rev.* **1985**, *85* (2), 129–170.

(30) Wang, D.; Astruc, D. The Golden Age of Transfer Hydrogenation. *Chem. Rev.* **2015**, *115* (13), 6621–6686.

(31) Alonso, F.; Riente, P.; Yus, M. Nickel Nanoparticles in Hydrogen Transfer Reactions. *Acc. Chem. Res.* **2011**, *44* (5), 379–391.

(32) Yang, G.; Bauer, T. J.; Haller, G. L.; Baráth, E. H-Transfer Reactions of Internal Alkenes with Tertiary Amines as H-Donors on Carbon Supported Noble Metals. *Org. Biomol. Chem.* **2018**, *16* (7), 1172–1177.

(33) Jang, J. H.; Sohn, H.; Camacho-Bunquin, J.; Yang, D.; Park, C. Y.; Delferro, M.; Abu-Omar, M. M. Deoxydehydration of Biomass-Derived Polyols with a Reusable Unsupported Rhenium Nanoparticles Catalyst. *ACS Sustain. Chem. Eng.* **2019**, *7* (13), 11438–11447.

(34) Denning, A. L.; Dang, H.; Liu, Z.; Nicholas, K. M.; Jentoft, F. C. Deoxydehydration of Glycols Catalyzed by Carbon-Supported Perrhenate. *ChemCatChem* **2013**, *5* (12), 3567–3570.

(35) Sandbrink, L.; Klindtworth, E.; Islam, H.-U.; Beale, A. M.; Palkovits, R. ReO_x/TiO_2: A Recyclable Solid Catalyst for Deoxydehydration. *ACS Catal.* **2016**, *6* (2), 677–680.

(36) Tazawa, S.; Ota, N.; Tamura, M.; Nakagawa, Y.; Okumura, K.; Tomishige, K. Deoxydehydration with Molecular Hydrogen over Ceria-Supported Rhenium Catalyst with Gold Promoter. *ACS Catal.* **2016**, *6* (10), 6393–6397.

(37) Ota, N.; Tamura, M.; Nakagawa, Y.; Okumura, K.; Tomishige, K. Hydrodeoxygenation of Vicinal OH Groups over Heterogeneous Rhenium Catalyst Promoted by Palladium and Ceria Support. *Angew. Chem. Int. Ed.* **2015**, *54* (6), 1897–1900.

(38) Zhang, B.; Qi, Z.; Li, X.; Ji, J.; Zhang, L.; Wang, H.; Liu, X.; Li, C. Cleavage of Lignin C–O Bonds over a Heterogeneous Rhenium Catalyst through Hydrogen Transfer Reactions. *Green Chem.* **2019**, *21* (20), 5556–5564.

(39) Robinson, A. M.; Hensley, J. E.; Medlin, J. W. Bifunctional Catalysts for Upgrading of Biomass-Derived Oxygenates: A Review. *ACS Catal.* **2016**, *6* (8), 5026–5043.

(40) Bao, J.; He, J.; Zhang, Y.; Yoneyama, Y.; Tsubaki, N. A Core/Shell Catalyst Produces a Spatially Confined Effect and Shape Selectivity in a Consecutive Reaction. *Angew. Chem. Int. Ed.* **2008**, *47* (2), 353–356.

(41) Simonetti, D.; Kunkes, E.; Dumesic, J. Gas-Phase Conversion of Glycerol to Synthesis Gas over Carbon-Supported Platinum and Platinum–Rhenium Catalysts. *J. Catal.* **2007**, *247* (2), 298–306.

(42) Di, X. Influence of Re–M Interactions in Re–M/C Bimetallic Catalysts Prepared by a Microwave-Assisted Thermolytic Method on Aqueous-Phase Hydrogenation of Succinic Acid. *Catal. Sci. Technol.* **2017**, *7* (22), 5212-5223.

(43) Mieville, R. Platinum-Rhenium Interaction: A Temperature-Programmed Reduction Study. *J. Catal.* **1984**, *87* (2), 437–442.

(44) Torres, G. C.; Jablonski, E. L.; Baronetti, G. T.; Castro, A. A.; de Miguel, S. R.; Scelza, O. A.; Blanco, M. D.; Pen˜a Jiménez, M. A.; Fierro, J. L. G. Effect of the Carbon Pre-Treatment on the Properties and Performance for Nitrobenzene Hydrogenation of Pt/C Catalysts. *Appl. Catal., A* **1997**, *161* (1–2), 213–226.

(45) Kuo, C.-T.; Lu, Y.; Kovarik, L.; Engelhard, M.; Karim, A. M. Structure Sensitivity of Acetylene Semi-Hydrogenation on Pt Single Atoms and Subnanometer Clusters. *ACS Catal.* **2019**, *9* (12), 11030–11041.

(46) de Miguel, S. R.; Scelza, O. A.; Román-Martínez, M. C.; Salinas-Martínez de Lecea, C.; Cazorla-Amorós, D.; Linares-Solano, A. States of Pt in Pt/C Catalyst Precursors after Impregnation, Drying and Reduction Steps. *Appl. Catal., A* **1998**, *170* (1), 93–103.

(47) Ota, N.; Tamura, M.; Nakagawa, Y.; Okumura, K.; Tomishige, K. Performance, Structure, and Mechanism of ReO_x–Pd/CeO_2 Catalyst for Simultaneous Removal of Vicinal OH Groups with H_2. *ACS Catal.* **2016**, *6* (5), 3213–3226.

(48) Xi, Y.; Yang, W.; Ammal, S. C.; Lauterbach, J.; Pagan-Torres, Y.; Heyden, A. Mechanistic Study of the Ceria Supported, Re-Catalyzed Deoxydehydration of Vicinal OH Groups. *Catal. Sci. Technol.* **2018**, *8* (22), 5750–5762.

(49) Yi, J.; Liu, S.; Abu-Omar, M. M. Rhenium-Catalyzed Transfer Hydrogenation and Deoxygenation of Biomass-Derived Polyols to Small and Useful Organics. *ChemSusChem* **2012**, *5* (8), 1401–1404.

(50) Liu, S.; Senocak, A.; Smeltz, J. L.; Yang, L.; Wegenhart, B.; Yi, J.; Kenttämaa, H. I.; Ison, E. A.; Abu-Omar, M. M. Mechanism of MTO-Catalyzed Deoxydehydration of Diols to Alkenes Using Sacrificial Alcohols. *Organometallics* **2013**, *32* (11), 3210–3219.

(51) Arceo, E.; Ellman, J. A.; Bergman, R. G. Rhenium-Catalyzed Didehydroxylation of Vicinal Diols to Alkenes Using a Simple Alcohol as a Reducing Agent. *J. Am. Chem. Soc.* **2010**, *132* (33), 11408–11409.

(52) Bäckvall, J.-E. Transition Metal Hydrides as Active Intermediates in Hydrogen Transfer Reactions. *J. Organomet. Chem.* **2002**, *652* (1–2), 105–111.

(53) Samec, J. S. M.; Bäckvall, J.-E.; Andersson, P. G.; Brandt, P. Mechanistic Aspects of Transition Metal-Catalyzed Hydrogen Transfer Reactions. *Chem. Soc. Rev.* **2006**, *35* (3), 237-248.

(54) Zhang, G.; Hanson, S. K. Cobalt-Catalyzed Transfer Hydrogenation of C=O and C=N Bonds. *Chem. Commun.* **2013**, *49* (86), 10151-10153.

(55) Alonso, F.; Riente, P.; Yus, M. Hydrogen-Transfer Reduction of Carbonyl Compounds Promoted by Nickel Nanoparticles. *Tetrahedron* **2008**, *64* (8), 1847–1852.

(56) Gilkey, M. J.; Xu, B. Heterogeneous Catalytic Transfer Hydrogenation as an Effective Pathway in Biomass Upgrading. *ACS Catal.* **2016**, *6* (3), 1420–1436.

(57) Brown, J. M.; Parker, D. Mechanism of Asymmetric Homogeneous Hydrogenation. Rhodium-Catalyzed Reductions with Deuterium and Hydrogen Deuteride. *Organometallics* **1982**, *1* (7), 950–956.

(58) Landis, C. R.; Brauch, T. W. Probing the Nature of H_2 Activation in Catalytic Asymmetric Hydrogenation. *Inorg. Chim. Acta* **1998**, *270* (1–2), 285–297.

(59) Abarca, B.; Adam, R.; Ballesteros, R. An Efficient One Pot Transfer Hydrogenation and N-Alkylation of Quinolines with Alcohols Mediated by Pd/C/Zn. *Org. Biomol. Chem.* **2012**, *10* (9), 1826-1833.

(60) Shafeeyan, M. S.; Daud, W. M. A. W.; Houshmand, A.; Shamiri, A. A Review on Surface Modification of Activated Carbon for Carbon Dioxide Adsorption. *J. Anal. Appl. Pyrol.* **2010**, *89* (2), 143–151.

(61) Long, J.; Zhou, Y.; Li, Y. Transfer Hydrogenation of Unsaturated Bonds in the Absence of Base Additives Catalyzed by a Cobalt-Based Heterogeneous Catalyst. *Chem. Commun.* **2015**, *51* (12), 2331–2334.

(62) Dhakshinamoorthy, A.; Asiri, A. M.; Garcia, H. Metal Organic Frameworks as Versatile Hosts of Au Nanoparticles in Heterogeneous Catalysis. *ACS Catal.* **2017**, *7* (4), 2896–2919.

(63) Goula, M. A.; Lemonidou, A. A.; Efstathiou, A. M. Characterization of Carbonaceous Species Formed during Reforming of CH_4 with CO_2 over Ni/CaO–Al_2O_3 Catalysts Studied by Various Transient Techniques. *J. Catal.* **1996**, *161* (2), 626–640.

(64) Jae, J.; Zheng, W.; Lobo, R. F.; Vlachos, D. G. Production of Dimethylfuran from Hydroxymethylfurfural through Catalytic Transfer Hydrogenation with Ruthenium Supported on Carbon. *ChemSusChem* **2013**, *6* (7), 1158–1162.

(65) Sádaba, I.; López Granados, M.; Riisager, A.; Taarning, E. Deactivation of Solid Catalysts in Liquid Media: The Case of Leaching of Active Sites in Biomass Conversion Reactions. *Green Chem.* **2015**, *17* (8), 4133–4145.

(66) Scott, S. L. A Matter of Life(Time) and Death. *ACS Catal.* **2018**, *8* (9), 8597–8599.

(67) Conner, W. Curtis.; Falconer, J. L. Spillover in Heterogeneous Catalysis. *Chem. Rev.* **1995**, *95* (3), 759–788.

(68) Ro, I.; Resasco, J.; Christopher, P. Approaches for Understanding and Controlling Interfacial Effects in Oxide-Supported Metal Catalysts. *ACS Catal.* **2018**, *8* (8), 7368–7387.

(69) Ro, I.; Xu, M.; Graham, G. W.; Pan, X.; Christopher, P. Synthesis of Heteroatom Rh–ReO_x Atomically Dispersed Species on Al_2O_3 and Their Tunable Catalytic Reactivity in Ethylene Hydroformylation. *ACS Catal.* **2019**, *9* (12), 10899–10912.

CHAPTER IV. Preparation of Bimetallic Catalyst with Reduced Metal Contents for Deoxydehydration and Catalytic Transfer Hydrogenation Tandem Reaction

A. Introduction

In Chapter 3, heterogeneous bifunctional Pt-ReO_x/C catalyst is introduced to prepare adipates from mucic acid through a one-step DODH-CTH reaction. Although the tandem catalysis over Pt-ReO_x/C produced a high yield of adipates, the high cost of both rhenium and platinum remains a challenge to be practical in industry. To solve this challenge, molybdenum and vanadium based catalysts have been developed for DODH reaction as alternatives of rhenium-based catalysts as described in Chapter 1.[1–4] However, the yield of olefins was much lower than the yield of rhenium-catalyzed DODH.[5,6] In the literature of a combination of DODH and hydrogenation including the studies in Chapter 3, the amount of hydrogenation or CTH metal is between 0.8 – 2 mol% of the substrate.[7–9] In this chapter, Ir-ReO_x catalyst is studied for DODH-CTH reaction of mucic acid, reducing the amount of CTH metal to 0.04 mol% of the substrate.

B. Experimental details

1. Synthesis

Monometallic 5 wt% ReO_x/C catalyst was prepared by wet impregnation of activated carbon (Sigma-Aldrich) with ammonium perrhenate (NH_4ReO_4) (Strem Chemicals) aqueous solution. 1 g of activated carbon (Darco, 100 mesh) was added to 4 ml of ammonium perrhenate aqueous solution (50 mg of Re) and stirred for 3 h. Water was evaporated in a

preheated 80 ^{o}C oil for 1.5 h, followed by further dehydration in 120 ^{o}C oven overnight. The catalyst was pretreated at 480 or 530 ^{o}C with N_2 flow (40 ccm) for 4h. 0.05 wt% Ir/C catalyst was prepared by the same procedure with an aqueous solution of iridium chloride ($IrCl_3$). Bimetallic M–ReO_x/C (0.05 wt% M and 5 wt% of Re, M = Ni, Pd, Pt, and Ir) catalysts were synthesized by coimpregnating activated carbon with an appropriate amount of aqueous solution of both ammonium perrhenate and M precursor. Hexachloroplatinic(IV) acid, Nickel(II) nitrate, tetraaminepalladium(II) nitrate, and Iridium(III) chloride (Sigma-Aldrich) were used as metal precursors. After evaporating water in the oil bath and the oven, dehydration of the catalysts was conducted at the same condition above (N_2/480^{o}C or 530^{o}C/4h).

2. General catalytic procedure

Deoxydehydration and catalytic transfer hydrogenation of mucic acid were conducted in a batch Parr reactor. The Ir-ReO_x/C (150mg, 4.5 wt% Re and 0.05 wt% Ir) was mixed with mucic acid (1 mmol, 210 mg) and isopropanol (40 mL) in the Parr vessel. The vessel was pressurized with 15 bar of N_2 and heated to the reaction temperature. After the reaction, the spent catalyst was filtered, washed with isopropanol, and dried in the 120 ^{o}C oven overnight. The solvent in the reaction solution was removed under the reduced pressure. The concentrated products were dissolved in D_6-DMSO and analyzed by NMR with benzaldehyde as an internal standard. ^{1}H NMR and ^{13}C NMR spectra were acquired on an Agilent Technologies 400 MHz, 400-MR DD2 spectroscopy.

C. Results and discussion

1. DODH-CTH reaction by M-ReO_x/C

In chapter3, the Pt-ReO_x/C, a bimetallic bifunctional catalyst, converted **1** to **5** through a one-step DODH-CTH tandem reaction (run 2 in Table 4.1). CTH reaction proceeds slowly with ReO_x/C alone (run 1 in Table 4.1), but the addition of Pt significantly increased the rate of CTH reaction. The Pt-ReO_x/C catalyst contains 4.5 wt% of Re and 1.8 wt% Pt. With aiming for the preparation of a cheaper catalyst, the amount of Pt was reduced. Under the same reaction conditions, the half amount of Pt in the catalyst (4.5 wt% Re and 0.9 wt% Pt) resulted in a lower yield of **5** and a higher yield of unsaturated products (run 3). Further decrease in the Pt metal content (4.5 wt% Re and 0.05 wt% Pt) produced a negligible amount of hydrogenated products (**3**/**4** and **5**) in run 4. This is indicative of the high dependence of CTH reaction on the amount of Pt. It should be noted that the changes in Pt amount did not affect conversion, proving DODH reaction over ReO_x instead of Pt as described in the previous chapter. A decrease in the Pt content reduced CTH ability and yield of **5**, which are not desirable.

In order to achieve higher selectivity of **5** even with a small amount of CTH metal, several different metals were employed. The bimetallic catalysts containing Ni and Pd did not promote the CTH reaction, yielding **2** as a major product (run 5 and 6 in Table 4.1). Pd-ReO_x/C catalyst exhibited less conversion, indicating the negative impact of Pd on ReO_x-catalyzed DODH. Interestingly, Ir-ReO_x/C (4.5 wt% Re and 0.05 wt% Ir) made some partially hydrogenated and fully hydrogenated products under the same conditions (run 7). This catalyst showed much better CTH ability with isopropanol as a hydrogen donor than other tested bimetallic catalysts. Iridium-based complexes have attracted much attention for the CTH reaction due to their high activity. Various types of iridium complexes have been

used for CTH.[10] However, few heterogeneous iridium catalysts for CTH were studied. Hermans et al. synthesized CeO_2 supported iridium oxide catalyst for CTH of cyclohexanol with Ir_2O_3 as active species.[11] Crabtree and Hintermair et al. synthesized metallic Ir^0 nanoparticles and showed its high activity in the CTH of acetophenone to with KOH additive.[12]

Table 4.3 DODH-CTH tandem reaction of **1** by M-ReO_x/C.

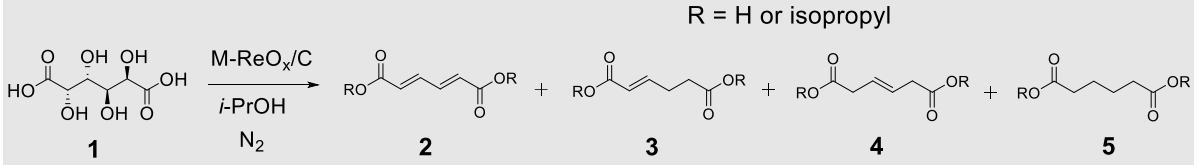

Run	Catalyst	Metal amount (wt%)	Conv.[b] (%)	Products/ % yield[b]		
				2	**3** & **4**	**5**
1	ReO_x/C	Re(4.5)	78	66	2	1
2	Pt-ReO_x/C	Re(4.5) Pt(1.8)	83	-	4	70
3	Pt-ReO_x/C	Re(4.5) Pt(0.9)	79	33	34	4
4	Pt-ReO_x/C	Re(4.5) Pt(0.05)	85	71	2	-
5	Ni-ReO_x/C	Re(4.5) Ni(0.05)	73	65	2	-
6	Pd-ReO_x/C	Re(4.5) Pd(0.05)	38	28	-	-
7	Ir-ReO_x/C	Re(4.5) Ir(0.05)	83	24	40	3

[a]Reaction conditions: batch reaction, 180 °C, 6h, M-ReO_x/C (150mg), **1** (210 mg), *i*-PrOH (40 mL), and N_2 (15 bar). [b]Conversion and yield are calculated by ^{1}H NMR.

2. DODH-CTH by Ir-ReO_x/C: reaction temperature

The DODH-CTH of **1** by the 0.05Ir-ReO_x/C (0.05 wt% Ir and 4.5 wt% Re) was investigated at different temperatures (180 – 220 °C) shown in Figure 4.1. At 180 °C, **1** was

selectively converted to **2** in 1 h with 60% completion. After 12 h, 96% of **1** was converted and partial hydrogenation of **2** gave **3**/**4**. Additional 12 h reaction rarely converted **3**/**4** to **5**, indicating the slow rate of the second hydrogenation step (**3**/**4** to **5**) than that of the first hydrogenation (**2** to **3**/**4**). This might be due to competition between the second hydrogenation and isomerization (**3** to **4** or cis-**3**). A small amount of cis-**3** was observed in NMR. In addition to the isomerization, deactivation of the catalyst led to the slow rate of the second hydrogenation. To investigate if the catalyst was deactivated during the reaction, the used catalyst after 12 h reaction was replaced with new catalyst, followed by 12 h further reaction (12h+12h in Figure 4.1a). Compared to 24 h reaction without interruption, replacement with new catalyst at 12 h produced more **5**, showing catalytic deactivation which will be discussed below. The rate of transfer hydrogenation was facilitated at the higher temperature, yielding higher selectivity of **5**. The highest yield of **5** (63 %) was obtained at 200 ^{o}C after 48 h. At 220 ^{o}C, all hydrogenation steps were completed within 24h, giving **5** with a yield of 59 %. The reaction pathway is DODH of **1** to **2**, followed by two sequential hydrogenation steps to **5** over the course of the reaction for 24 h at 220 ^{o}C. In addition to DODH and CTH, several side reactions gave some byproducts. Cyclization of **5**, followed by hydrogenation, produces oxepane-2-one and oxepane. Terminal CH_3 peaks in Figure 4.5 (δ = 0.7-0.9 ppm) are assigned to byproducts including isopropyl hexanoate and 2-propyl malonate. In the reaction, there are 10-15 wt% carbon loss. Based on the TGA results of activated carbon, as-prepared, and spent 0.05Ir-ReO_x/C catalysts show about 6 wt% of mass loss that is attributed to the organic deposits generated during catalysis (Figure 4.2).

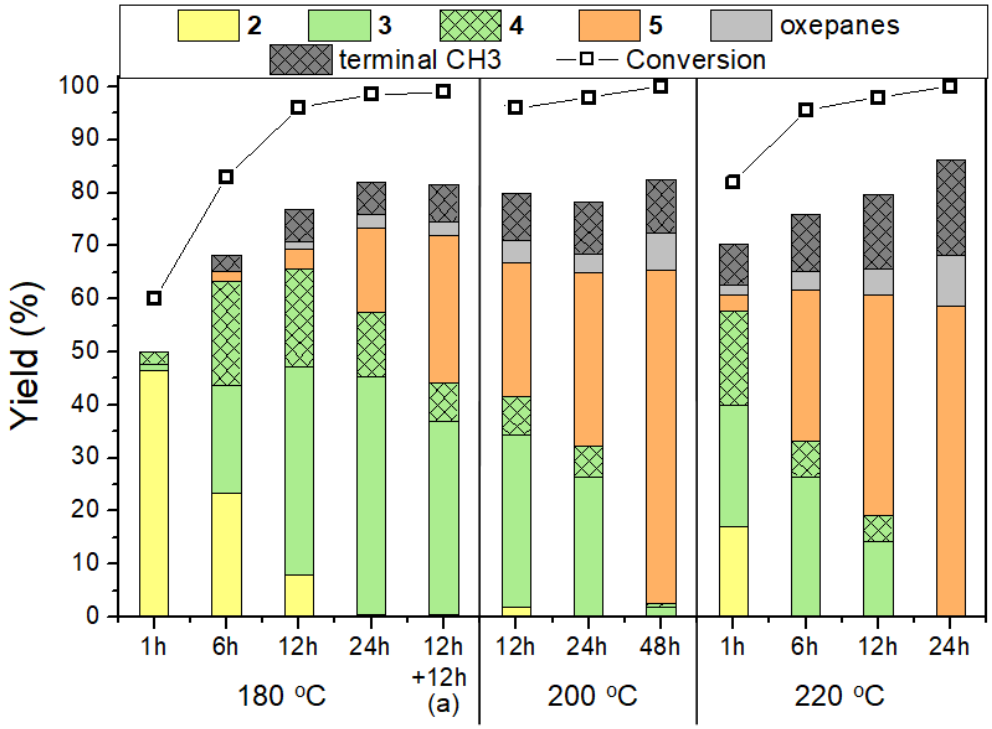

Figure 4.1 DODH-CTH by Ir-ReO_x/C at different temperatures. Reaction conditions: batch reaction, Ir-ReO_x/C (150 mg, 4.5 wt% Re and 0.045 wt% Ir), **1** (210 mg, 1 mmol), N_2 (15 bar), isopropanol (40 mL), (a) After 12h reaction, the catalyst was filtered and new catalyst was added. Another 12 h reaction was conducted with the fresh catalyst.

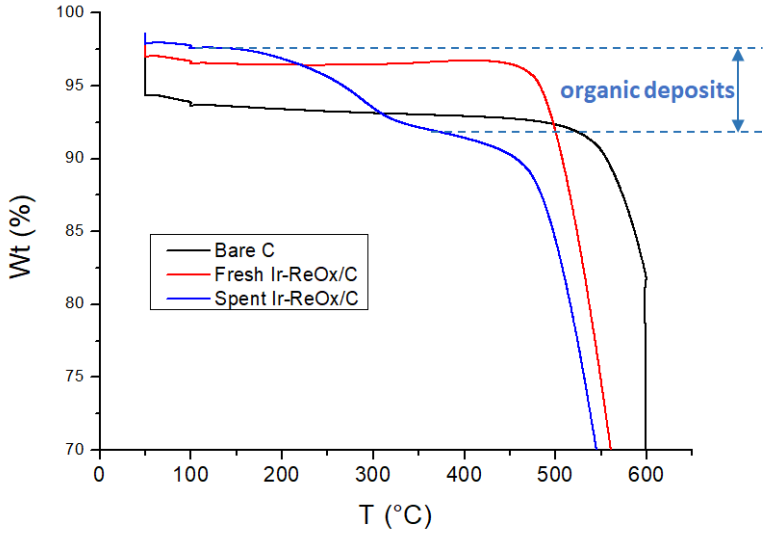

Figure 4.2 TGA results of activated carbon, fresh 0.05Ir-ReO_x/C, and spent 0.05Ir-ReO_x/C. Spent sample was prepared from 220°C/6h reaction of **1**.

3. DODH-CTH by Ir-ReO_x/C: pretreatment temperature

In order to reuse catalysts, stability of the catalyst is an important issue. The stability of Ir-ReO_x/C catalyst was tested by measuring metal content before and after reaction. Based on ICP analysis, the catalyst consists of 4.5 wt% of Re and 0.046 wt% Ir. After 6 h reaction at 220 ^oC, both the amount of Re and Ir decreased to 3.75 wt% and 0.038 wt%, respectively (Figure 4.3b). This shows the leaching of both Re and Ir at high temperature (< 200 ^oC). To alleviate the leaching problem, the pretreatment temperature during the catalyst synthesis increased, resulting in the stronger affinity between metal and support. The catalysts dehydrated at 530 ^oC and 580 ^oC showed a negligible decrease in the amount of Re and Ir between fresh and spent catalyst (Figure 4.3). Thus, higher pretreatment temperature shows stronger affinity, avoiding the leaching problem. Despite the higher stability of the catalysts dehydrated at the higher temperature, the conversion of **1** was reduced (Figure 4.3a). This might be because higher pretreatment temperature led to a larger particle size of ReO_x, reducing DODH ability. Otherwise, the selectivity of **5** increased with the catalyst prepared at the higher temperature.

Figure 4.4 shows the time profile of the conversion of **1** with 0.05Ir-ReO_x/C-530 catalyst. In 6 h at 220 ^oC, 34% yield of **5** and 21% of partially hydrogenated products (**3**/**4**) were gained. The second hydrogenation proceeded and is completed within 24h, producing 50% yield of **5**. To be industrially practical, the concentration of the substrate increased from 0.025M to 0.1M (Figure 4.4 (a)). In the higher concentration solution, the yield of **5** remained (52%).

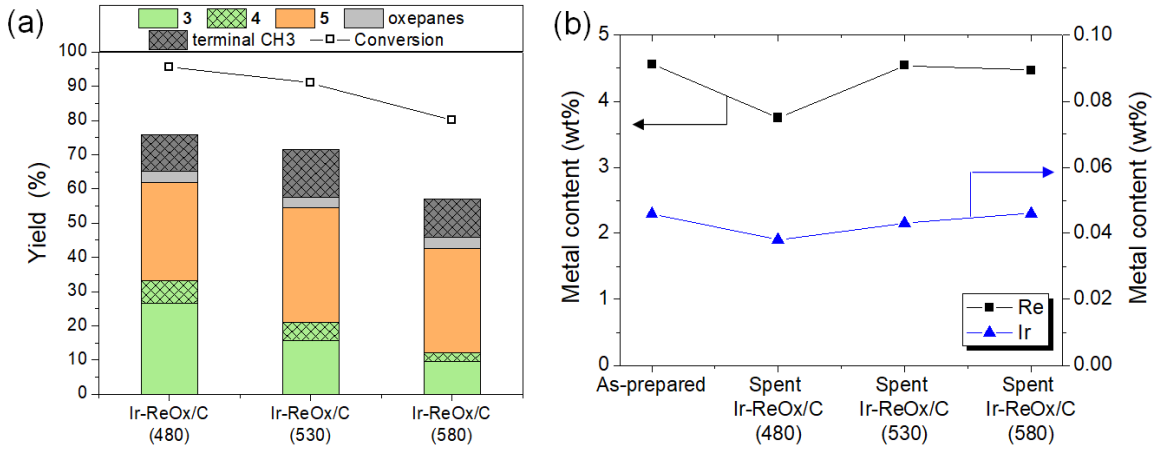

Figure 4.3 (a) The conversion of **1** with catalysts prepared at different pretreatment temperature. Reaction conditions: catalyst (150 mg), **1** (210 mg, 1 mmol), N_2 (15 bar), isopropanol (40 mL) 220 °C, and 6 h. (b) ICP results of the as-prepared catalyst and spent catalysts from (a).

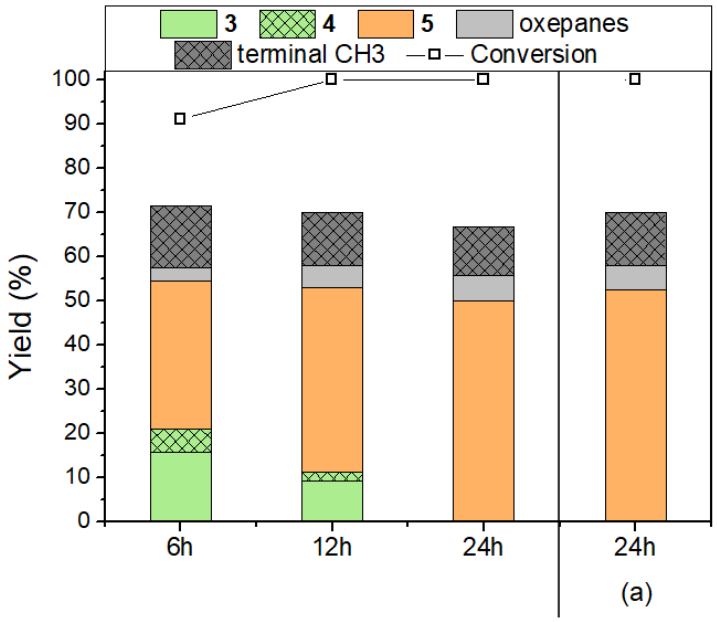

Figure 4.4 DODH-CTH reaction of **1** with 0.05Ir-ReO_x/C prepared at 530 °C. Reaction conditions: catalyst (150 mg), **1** (210 mg, 1 mmol), N_2 (15 bar), isopropanol (40 mL), 220 °C. (a) High concentration of substrate. Reaction conditions: catalyst (750 mg), **1** (1050 mg, 5 mmol), isopropanol (40 mL), N_2 (15 bar), isopropanol (40 mL), 220 °C.

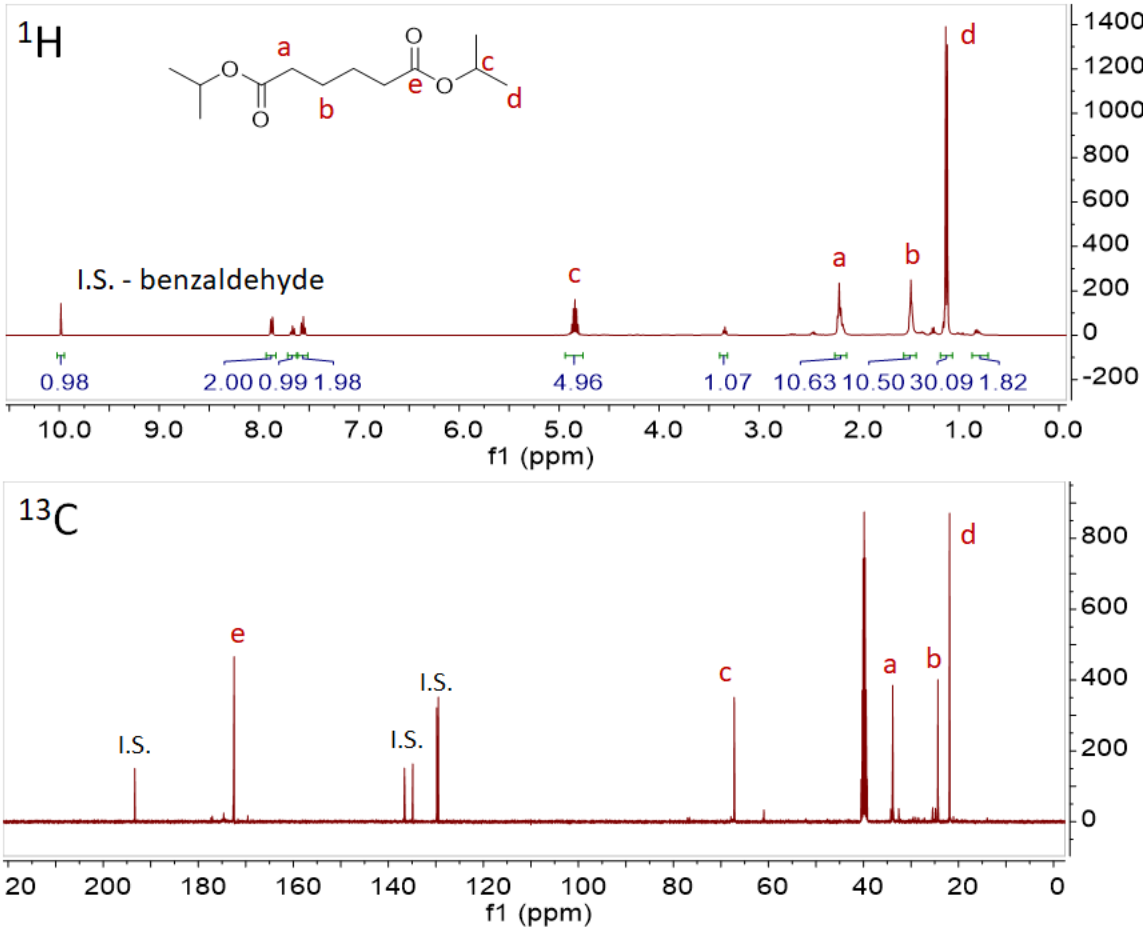

Figure 4.5 ^{1}H and ^{13}C NMR spectra of reaction solution. Reaction conditions: 0.05Ir-ReO_x/C-530 (750 mg), **1** (1050 mg, 5 mmol), isopropanol (40 mL), N_2 (15 bar), isopropanol (40 mL), 220 °C, and 24 h.

D. Conclusion

In this chapter, one step DODH-CTH reaction of mucic acid to adipates by using a reduced amount of metal is studied. Bimetallic Ir-ReO_x/C catalyst with 0.05 wt% Ir content could catalyze both DODH and CTH reaction with isopropanol as a hydrogen donor. Under the optimized conditions, 63% yield of adipates was produced from mucic acid. An increase in the pretreatment temperature during catalyst synthesis reduced metal leaching of rhenium and iridium, probably due to the higher affinity between carbon support and metals.

E. References

(1) Dethlefsen, J. R.; Lupp, D.; Teshome, A.; Nielsen, L. B.; Fristrup, P. Molybdenum-Catalyzed Conversion of Diols and Biomass-Derived Polyols to Alkenes Using Isopropyl Alcohol as Reductant and Solvent. *ACS Catal.* **2015**, *5* (6), 3638–3647.

(2) Sandbrink, L.; Beckerle, K.; Meiners, I.; Liffmann, R.; Rahimi, K.; Okuda, J.; Palkovits, R. Supported Molybdenum Catalysts for the Deoxydehydration of 1,4-Anhydroerythritol into 2,5-Dihydrofuran. *ChemSusChem* **2017**, *10* (7), 1375–1379.

(3) Chapman, G.; Nicholas, K. M. Vanadium-Catalyzed Deoxydehydration of Glycols. *Chem. Comm.* **2013**, *49* (74), 8199–8201.

(4) Petersen, A. R.; Nielsen, L. B.; Dethlefsen, J. R.; Fristrup, P. Vanadium-Catalyzed Deoxydehydration of Glycerol Without an External Reductant. *ChemCatChem* **2018**, 10, 769-778.

(5) Tshibalonza, N. N.; Monbaliu, J.-C. M. The Deoxydehydration (DODH) Reaction: A Versatile Technology for Accessing Olefins from Bio-Based Polyols. *Green Chem.* **2020**, 22, 4801-4848.

(6) Petersen, A. R.; Fristrup, P. New Motifs in Deoxydehydration: Beyond the Realms of Rhenium. *Chem. Eur. J.* **2017**, *23*, 10235–10243.

(7) Larson, R. T.; Samant, A.; Chen, J.; Lee, W.; Bohn, M. A.; Ohlmann, D. M.; Zuend, S. J.; Toste, F. D. Hydrogen Gas-Mediated Deoxydehydration/Hydrogenation of Sugar Acids: Catalytic Conversion of Glucarates to Adipates. *J. Am. Chem. Soc.* **2017**, *139* (40), 14001–14004.

(8) Shiramizu, M.; Toste, F. D. Expanding the Scope of Biomass-Derived Chemicals through Tandem Reactions Based on Oxorhenium-Catalyzed Deoxydehydration. *Angew. Chem. Int. Ed.* **2013**, *52* (49), 12905–12909.

(9) Li, X.; Wu, D.; Lu, T.; Yi, G.; Su, H.; Zhang, Y. Highly Efficient Chemical Process To Convert Mucic Acid into Adipic Acid and DFT Studies of the Mechanism of the Rhenium-Catalyzed Deoxydehydration. *Angew. Chem. Int. Ed.* **2014**, *53* (16), 4200–4204.

(10) Wang, D.; Astruc, D. The Golden Age of Transfer Hydrogenation. *Chem. Rev.* **2015**, *115* (13), 6621–6686.

(11) Hammond, C.; Schümperli, M. T.; Conrad, S.; Hermans, I. Hydrogen Transfer Processes Mediated by Supported Iridium Oxide Nanoparticles. *ChemCatChem* **2013**, *5* (10), 2983–2990.

(12) Hintermair, U.; Campos, J.; Brewster, T. P.; Pratt, L. M.; Schley, N. D.; Crabtree, R. H. Hydrogen-Transfer Catalysis with Cp*Ir ^{III} Complexes: The Influence of the Ancillary Ligands. *ACS Catal.* **2014**, *4* (1), 99–108.

CHAPTER V. Deoxydehydration and Catalytic Transfer Hydrogenation: New Strategy to Valorize Tartaric Acid and Succinic Acid to γ-Butyrolactone and Tetrahydrofuran

A. Introduction

Biomass is one of the promising renewable energy resources to provide sustainable routes to biofuels and chemicals.[1] High valued fine chemicals can be produced from biomass-derived building-block chemicals.[2] In 2004, the U.S. Department of Energy selected succinic acid (SA), a C4-dicarboxylic acid, as one of the bio-based key platform chemicals.[3] The renewable SA can replace maleic anhydride to synthesize many valuable chemicals including γ-butyrolactone (GBL), tetrahydrofuran (THF), and 1,4-butanediol (BDO).[4–7] GBL has been used as a starting material for the production of N-methyl-2-pyrrolidone and other pyrrolidone derivatives. THF is a monomer of poly(tetramethylene ether) glycol (PTMEG). Both GBL and THF are also utilized as a reaction solvent. The demand for GBL and THF is increasing annually and the global market size of GBL and THF in 2018 was approximately 0.6 and 3.2 billion USD, respectively.[8,9] Thus, the preparation of renewable SA and its transformation into GBL and THF are getting much attention.

Several methods to synthesize SA from biomass-derived materials have been studied. Renewable SA has been typically prepared through the bio-fermentation of glucose.[10,11] While recent breakthroughs in the biological process, costly separation and large quantity of wastes make it difficult to realize industrial production of renewable SA.[12] SA was synthesized from furfural through thermochemical processes.[13–15] However, the C5 starting material forms C1 byproducts such as CO_2 and formic acid. Tartaric acid (TA), a C4 sugar acid, has been proposed as an alternative resource to prepare SA without carbon loss.

Tartaric acid is a naturally occurred organic acid and is generated in large quantities as a byproduct of wine-making.[16,17] MoO_x-catalyzed hydrodeoxygenation converted TA to SA, but it required the harsh conditions such as corrosive halogen, high pressure of H_2, and acetic acid.[18] Moreover, the transformation of TA to SA was achieved through a combination of deoxydehydration (DODH) and hydrogenation in two steps.[19] DODH is an attractive deoxygenation reaction to prepare alkenes from vicinal diols.[20,21] DODH with oxorhenium complexes converts TA to maleic acid (MA) and the resulting MA is hydrogenated over Pt/C catalyst, yielding SA.[19]

In Chapter 2, unsupported ReO_x nanoparticles (ReO_x NPs) were used as an active and reusable heterogeneous catalyst for DODH of polyols with a secondary alcohol reductant. High oxidation states of Re (Re^{5+} and Re^{7+}) in the nanoparticles are involved in DODH reaction.[22] It has been found that the ReO_x NPs are not only active for DODH but also for CTH at high reaction temperature (> 200 ^oC) with isopropanol as a hydrogen donor. The sequential reaction of DODH-CTH over the ReO_x NPs can transform TA into SA and its esters in one step without the harsh conditions. In addition, the ReO_x NPs further convert the prepared SA and its esters to GBL and THF through cyclization and CTH. The formation of GBL or THF from SA has been achieved using direct hydrogenation over various monometallic or bimetallic catalysts including palladium, ruthenium, and rhenium based catalysts.[2,5–7,23] CTH reactions using isopropanol as a hydrogen donor is a promising alternative to direct hydrogenation because the hydrogen donor is easy to handle and environmentally friendly, preventing possible hazards.[24–26] However, CTH has not been employed to prepare GBL or THF from SA. Herein, new reaction pathways to prepare GBL and THF from renewable substrates over the ReO_x NPs are reported. First, the conversion of

SA to GBL or THF through cyclization and CTH with ReO_x NPs is tested. Furthermore, a combination of DODH, CTH, and cyclization produces GBL or THF from TA in one step.

B. Experimental details

1. Synthesis

Unsupported ReO_x NPs were prepared from ammonium perrhenate (NH_4ReO_4, Strem Chemicals) in the presence of 3-octanol (Sigma-Aldrich), as described in Chapter 2 and elsewhere.[22] A mixture of ammonium perrhenate (268 mg, 1 mmol) and 3-octanol (20 mL, 126 mmol) was placed in a 100 mL round bottom flask and heated at 180 ^oC in a pre-heated oil bath. Black ReO_x nanoparticles were synthesized after 12 h reflux in air and isolated by centrifugation (11 000 rpm for 1.5 h). Unreacted ammonium perrhenate was removed by washing repeatedly with ethanol and hexane solution (1:1 wt %) and further centrifugation. The ReO_x NPs were dried in 120 ^oC oven overnight and kept in powder form for future use.

2. General catalytic procedure

All activity tests were performed in a Parr batch vessel. The prepared unsupported ReO_x nanoparticles (10 mg) was mixed with TA (1 mmol, 150 mg) and isopropanol (10 mL) in the vessel. The vessel was pressurized with 15 bar of N_2 and heated to the reaction temperature for a certain amount of time. The spent catalyst was separated from reaction solution. The product solution was analyzed by NMR and GC with mesitylene as an internal standard. The yield of TA, MA, SA, and their esters was calculated by ^1H NMR measured on an Agilent Technologies 400 MHz, 400-MR DD2 spectroscopy. The yield of GBL and THF were quantified by gas chromatography with a flame ionized detector (Agilent Technologies

6890N with a DB-5 capillary column). The conversion of different substrates including MA and SA (Alfa Aesar) was conducted under the same conditions.

$$\text{Conversion of TA (\%)} = \frac{\text{mole of TA reacted}}{\text{mole of TA supplied}} \times 100, \quad (1)$$

$$\text{Yield for product (\%)} = \frac{\text{mole of product formed}}{\text{mole of TA supplied}} \times 100, \quad (2)$$

3. Characterization

The physical and chemical properties of ReO_x NPs were characterized using various characterization methods, which are presented in Chapter 2.[22] In order to identify the acid type of catalyst samples, infrared spectra of catalysts were obtained with a Thermo Scientific Nicolet iS10 Fourier transform infrared spectroscopy (FT-IR) spectrometer. The catalysts were diluted with KBr, and then a baseline spectrum was obtained before pyridine introduction. Pyridine was introduced to the sample by flowing Ar through a pyridine bubbler for 10 min. To remove physisorbed pyridine, 100 sccm Ar was purged for 30 min.

C. Results and discussion

1. Conversion of succinic acid (SA)

CTH reaction of succinic acid over ReO_x NPs with isopropanol as a hydrogen donor was investigated at different reaction temperatures (170 – 250 ^oC). At lower temperatures (< 200 ^oC), esterification of SA gave succinic acid monoisopropyl ester (SA-ME) as a major product and a small quantity of succinic acid diisopropyl ester (SA-DE) in 1 h (Figure 5.1a). The CH_2 peak in ^1H NMR spectra of SA (δ = 2.43 ppm) in DMSO-d_6 were shifted to the downfield by 0.02 ppm (SA-ME) and 0.05 ppm (SA-DE) after esterification (Figure 5.2a).

At 210 °C, SA conversion over ReO_x produced not only ester compounds (SA-ME and SA-DE) but also GBL. Higher GBL yields of 16% and 43% were obtained in 1 h at 230 °C and 250 °C, respectively (Figure 5.1a). Previously, GBL was synthesized from SA aqueous solution with molecular H_2. The proposed mechanisms include dehydration of SA to succinic anhydride (SAN) over acid sites of the catalysts, followed by hydrogenation to GBL over metal sites.[7,23] ReO_x NPs converted SAN to 47% yield of GBL and 40% of SA-ME/DE at 250 °C and 1 h (Figure 5.1d). This indicates SAN as a possible intermediate in the conversion of SA to GBL while it was not detected. At 250 °C, SAN in isopropanol is susceptible to be alcoholized to SA-ME which is further esterified to SA-DE (Scheme 5.1). The alcoholization and further esterification also occurred without catalyst, but no GBL was synthesized (Figure 5.1d). This indicates that CTH of SAN to GBL was catalyzed by ReO_x NPs. SAN can be formed by dehydration of SA or dealcoholization of SA-ME and the resulting SAN is hydrogenated through CTH with isopropanol over ReO_x NPs (Scheme 5.1). Pyridine probe FT-IR shows that ReO_x NPs have both Brønsted and Lewis acid sites that can catalyze dehydration and dealcoholization (Figure 5.3). The bands at 1450, 1487, and 1608 cm^{-1} represent Lewis bond pyridine. The bands at 1487, 1538, and 1631 cm^{-1} were assigned to Brønsted bond pyridine. The control test without catalyst under the same conditions (250 °C, 1 h) yielded ester compounds (Figure 5.1a). Even though esterification occurs at 250 °C without catalyst, ReO_x NPs facilitate esterification, yielding the higher SA-DE/SA-ME ratio.

The time profile of the conversion of SA over ReO_x/C is shown in Figure 5.1b. In half-hour at 250 °C, all SA were converted to SA-ME/DE or GBL. Over the course of the first 6 h reaction, SA-ME disappeared, yielding more SA-DE, GBL, and THF. THF can be made by the further CTH of the synthesized GBL, evident by the observation of THF from GBL as a

starting material (Figure 5.1e). The reaction between 6 and 12 h indicates that SA-DE was also transformed into GBL while the CTH rate of SA-DE is slower compared to the rate of transformation of SA. This is in agreement with Figure 5.1c that shows GBL is slowly produced from SA-DE as a starting material. To investigate if the slow conversion of SA-DE is not due to catalyst deactivation, the used catalyst after 6 h reaction was replaced with new catalyst, followed by 6 h further reaction (6h+6h in Figure 5.1b). The composition of 6h+6h reaction is similar to 12 h reaction without interruption, excluding the possibility of the catalyst deactivation. A higher temperature was required to facilitate the conversion of SA-DE to GBL. At the elevated temperature of 270 ^{o}C, more GBL (50% yield) was produced from SA in 1 h. The 3 h reaction yielded 60% GBL and 9% THF with 22% of remaining SA-DE. Most of the SA-DE were converted in 6 h and CTH of GBL also proceeded, making more THF (28% yield). Unsupported ReO_x NPs successfully catalyzed simultaneous CTH and dehydration of SA, preparing GBL and THF.

Isopropanol offered hydrogen for CTH, producing acetone. The amount of the produced acetone after 250^{o}C/1h reaction (5.5 mmol) is much higher than the theoretically required amount of H_2 (0.9 mmol) to produce 0.43 mmol of GBL and 0.02 mmol of THF. This indicates independent dehydrogenation of isopropanol over ReO_x NPs and the possibility of the conversion of SA to GBL by direct hydrogenation with the produced H_2 from isopropanol. To test this possibility, direct hydrogenation of SA was tested in dioxane with 15 bar of H_2 which is approximately 39 mmol H_2 calculated using the ideal gas law (Figure 5.1f). After 1 h at 250 ^{o}C, the amount of the synthesized GBL (16% yield) was much lower than that in the reaction with isopropanol as a reductant (43% yield). This demonstrates that the major pathway of the formation of GBL from SA is CTH reaction. In the presence of

both isopropanol and molecular H_2, higher amount GBL (55% yield) was gained through both CTH and direct hydrogenation.

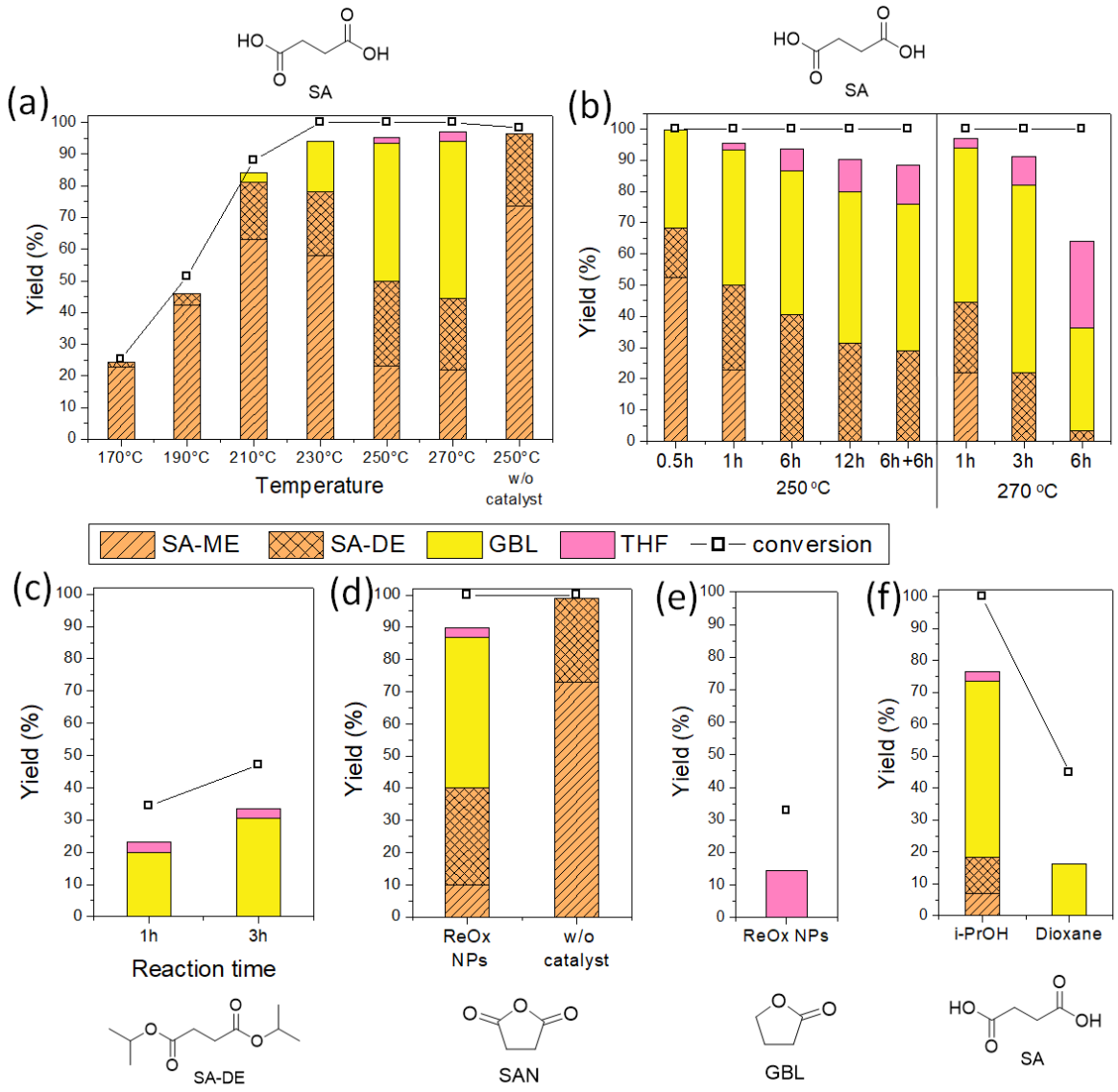

Figure 5.1 Conversion of SA, SAN, and SA-DE over ReO_x/C in isopropanol. (a)-(e) Reaction conditions: batch reaction, ReO_x NPs (10 mg, 4 mol% Re relative to substrate), substrate (1 mmol), *i*-PrOH (10 mL), and N_2 (15 bar). (f) H_2 (15 bar) and solvent (10 mL). Conversion and yield are calculated by ^{1}H NMR and GC-FID.

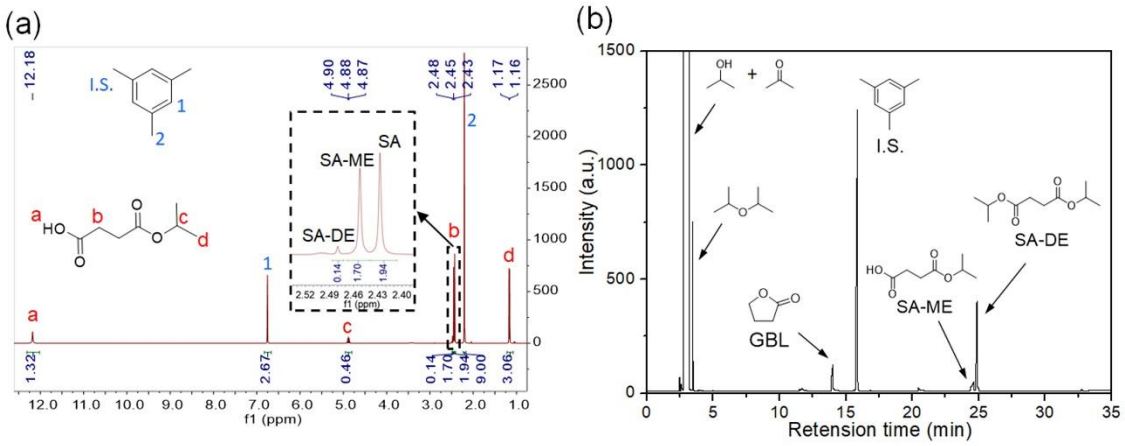

Figure 5.2 (a) NMR spectra of the reaction mixture of 190 °C and 1h in Figure 5.1a. (b) GC spectra of the reaction mixture of 250 °C and 1h in Figure 5.1a.

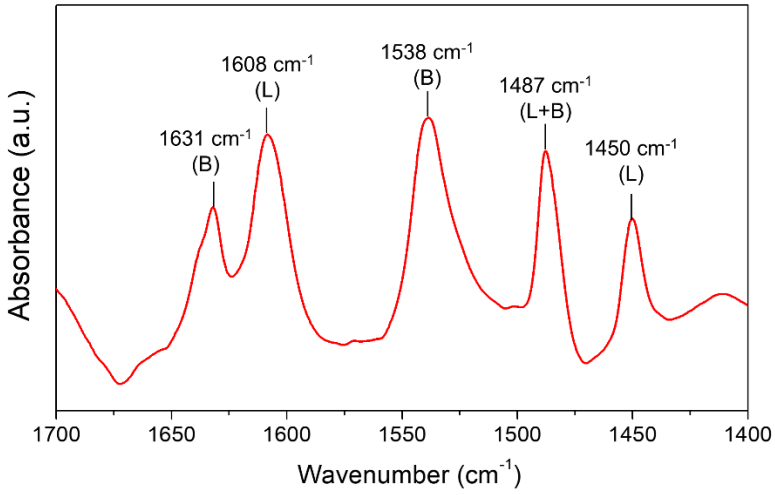

Figure 5.3 FT-IR spectra of pyridine adsorbed on ReO_x NPs after pyridine adsorption and desorption of physisorbed pyridine. L: Lewis bond pyridine. B: Brønsted bond pyridine.

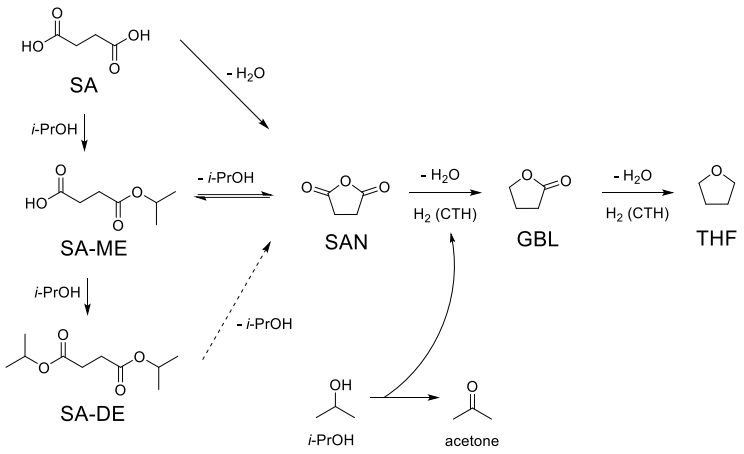

Scheme 5.1 Possible reaction pathway for the conversion of SA.

2. Conversion of maleic acid (MA)

MA is another versatile 1,4-dicarboxylic acid because it includes an unsaturated bond. Figure 5.4 shows the conversion of MA with ReO_x NPs in isopropanol at different reaction temperatures. At all tested temperatures from 170 to 270 ^oC, esterification on ReO_x NPs converts MA to maleic acid monoisopropyl ester (MA-ME) or maleic acid diisopropyl ester (MA-DE). Under the reaction conditions, MA and its esters were partially isomerized to fumaric acid (FA) and its esters (FA-ME and FA-DE). The resulting double bond compounds including MA, FA, and their esters were hydrogenated to SA, SA-ME, or SA-DE through CTH reaction with isopropanol as a hydrogen donor. At 170 ^oC, 13% yield of SA and its esters was obtained after 3 h reaction. At the elevated temperature of 250 ^oC, SA, SA-ME, and SA-DE are major products with a yield of 69% in 3 h. Similarly, it was recently reported that CTH of MA to SA with noble metal catalysts and formic acid as a reductant.[27] While CTH of C-C double bonds occurred without catalyst, ReO_x NPs facilitated CTH reaction and yielded a higher yield of C-C single bond compounds. Further

conversion of SA and SA-ME/DE to GBL, as discussed in the previous section, produced some amount of GBL with yields of 15% and 29% at 250 °C and 270 °C, respectively.

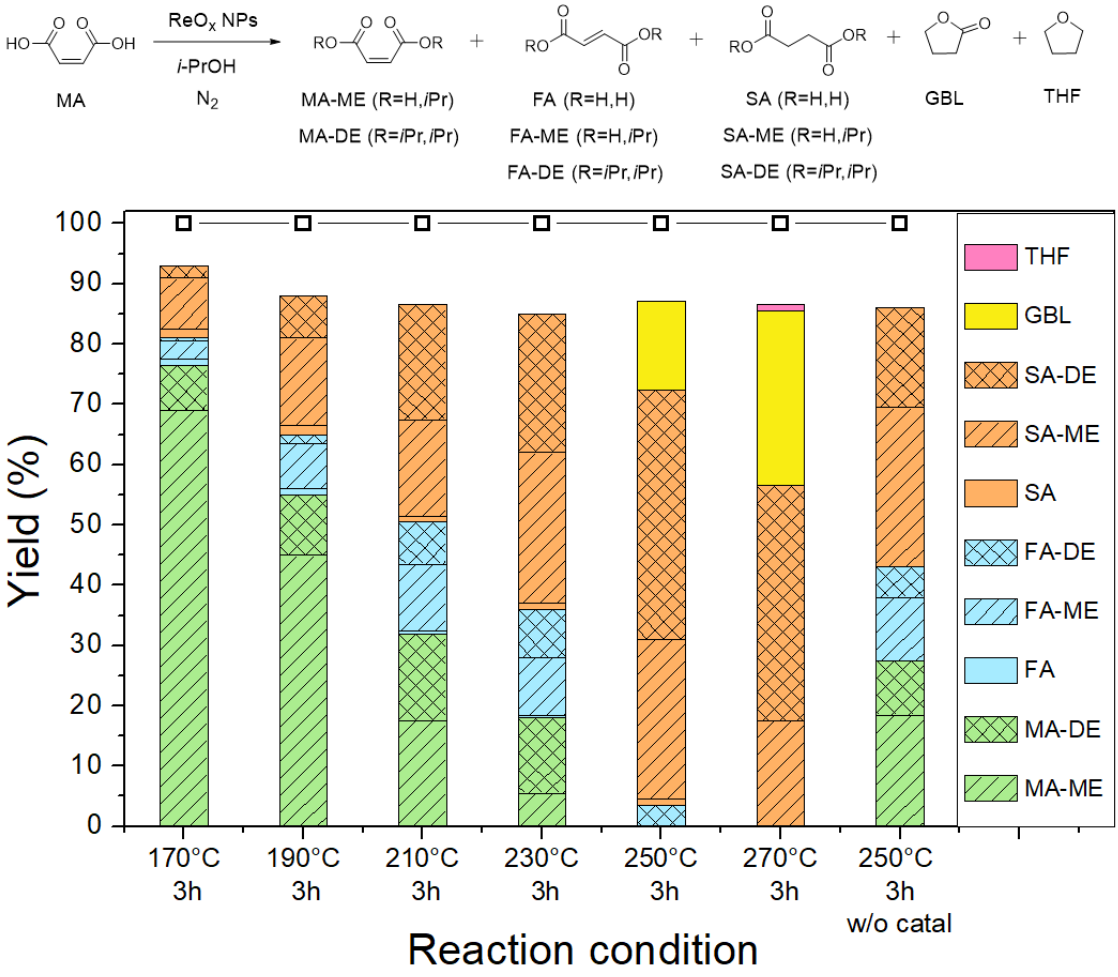

Figure 5.4 Conversion of MA over ReO_x/C in isopropanol. Reaction conditions: batch reaction, ReO_x NPs (10 mg, 4 mol% Re relative to substrate), MA (1 mmol), *i*-PrOH (10 mL), and N_2 (15 bar). Conversion and yield are calculated by ^{1}H NMR and GC-FID.

3. Conversion of tartaric acid (TA)

Unsupported ReO_x NPs and isopropanol directly convert SA and MA, affording GBL and THF. We previously proved that the ReO_x NPs efficiently catalyzed DODH reaction of glycerol with secondary alcohol as a reductant at 170 ^oC.[22] The possibility that DODH, combined with CTH and dehydration/dealcoholization, converts TA to GBL or THF in one-step was investigated. First, the transformation of TA to FA and its esters occurs on ReO_x through DODH and esterification at 170 and 210 ^oC (run 1 and 2 in Table 5.1). MA and its esters were not detected, indicating that *trans*-alkene is the more favored DODH product from (2R,3R)-tartric acid. It was reported that MTO-catalyzed DODH converts (R,R)-1,2-diphenyl-1,2-ethandiol to *trans*-stilbene while *cis*-stilbene was formed from (R,S)-1,2-diphenyl-1,2-ethandiol.[28] At the reaction temperature above 250 ^oC, CTH reaction also proceeded as well as DODH, making SA and its esters (run 3 and 4). In addition to the saturated products, GBL was also formed by further simultaneous CTH and dehydration/dealcoholization with a yield of 20% at 270 ^oC. In order to get a higher yield of GBL, the reaction was performed at 290 ^oC. After 12 h reaction, 34% yield of GBL was produced from tartaric acid and 18 h reaction gave more GBL with a yield of 43%. Over the course of the reaction from tartaric acid, only a small amount of THF was formed (< 2% yield) in run 5 and 6. A control experiment without catalyst showed small conversion, proving that the conversion of TA was catalyzed by ReO_x NPs (run 7).

Table 5.1 Conversion of tartaric acid over ReO_x NPs.[a]

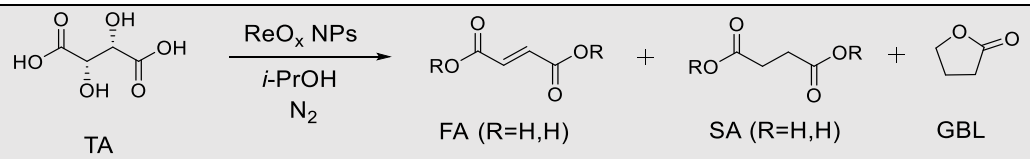

Run	Catalyst	T (°C)	t (h)	Conv.[b] (%)	Product % yield[b]			
					FA and FA-ME,DE	SA and SA-ME	SA-DE	GBL
1	ReO_x NPs	170	12	72	65	0	0	0
2	ReO_x NPs	210	12	87	75	1	2	0
3	ReO_x NPs	250	12	88	0	30	17	18
4	ReO_x NPs	270	12	91	0	18	20	20
5	ReO_x NPs	290	12	95	0	10	6	34
6	ReO_x NPs	290	18	100	0	0	1.5	43
7	-	250	12	8	4	0	2	0

[a]Reaction conditions: batch reaction, ReO_x NPs (10 mg, 4 mol% Re relative to substrate), TA (150 mg, 1 mmol), *i*-PrOH (10 mL), N_2 (15 bar). [2]Conversion and yield are calculated by ^{1}H NMR and GC-FID.

4. Reaction pathway

Based on the results of the conversion of SA, MA, and TA with unsupported ReO_x NPs, the possible reaction scheme is illustrated in scheme 5.2. TA is converted to FA through DODH, removing hydroxyl groups and making a *trans*-double bond. Hydrogen is provided from isopropanol and is transferred for DODH reaction. This step produces acetone as a by-product. In isopropanol, the carboxylic acid group in FA is esterified, making FA-ME or FA-DE. CTH reaction over ReO_x in isopropanol saturates the resulting double bond in FA,

FA-ME, and FA-DE to SA, SA-ME, and SA-DE, respectively. SA undergoes intramolecular dehydration and CTH, affording GBL. Dealcoholization and CTH also form GBL from SA-ME/DE. Further CTH of GBL yields THF. MA, another starting material, is isomerized to FA. Both MA and FA can be hydrogenated to SA via CTH with isopropanol as a hydrogen donor. The resulting SA and SA-ME/DE follow the same pathway, resulting in GBL and THF.

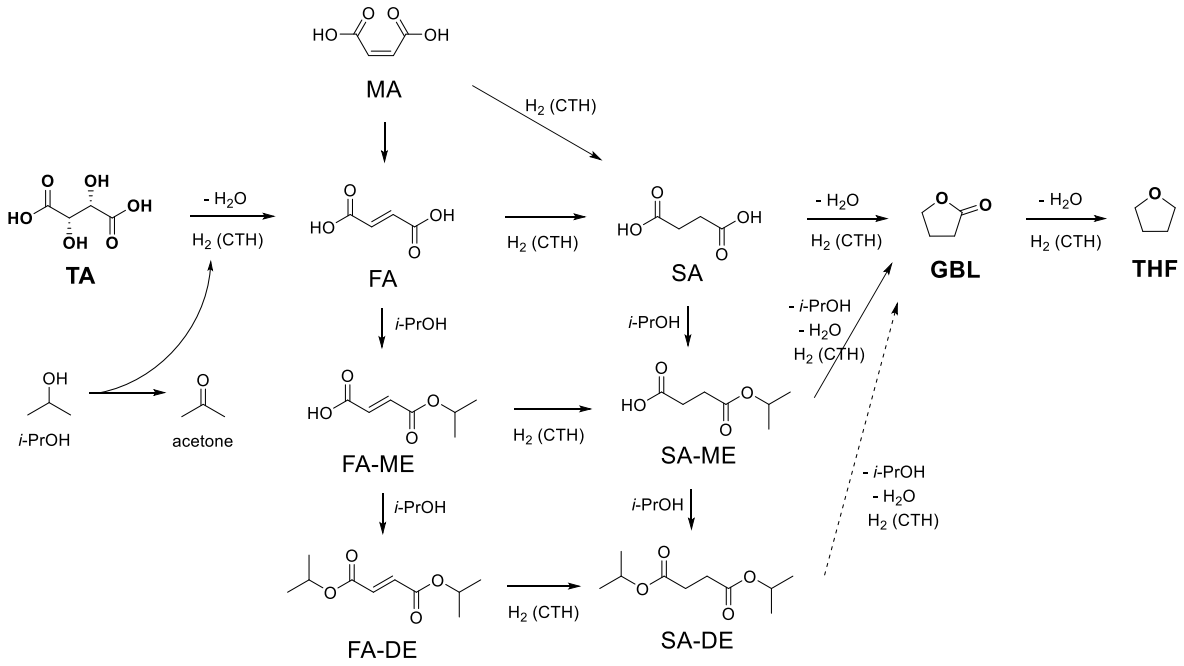

Scheme 5.2 Possible reaction pathway for the conversion of TA.

D. Conclusion

In this chapter, valuable C4 chemicals including GBL and THF were synthesized from SA, MA, and TA through ReO_x-catalyzed DODH, CTH, and cyclization reactions. Isopropanol offered hydrogen for both DODH and CTH reactions without using H_2 gas. GBL was produced from SA at a temperature above 200 ^oC with a possible intermediate of SAN.

Intramolecular dehydration or dealcoholization was catalyzed by acidic sites on ReO_x. Further CTH of GBL yielded THF. The highest yield of GBL from SA was 60% with 9% yield of THF at 270 ^oC. SA and its esters can be prepared from MA by CTH of C-C double bond and from TA by DODH-CTH of a diol. Under the optimized conditions, ReO_x NPs afforded 43% GBL from TA with isopropanol as a hydrogen donor in a one-step reaction.

E. References

(1) Petrus, L.; Noordermeer, M. A. Biomass to Biofuels, a Chemical Perspective. *Green Chem.* **2006**, *8* (10), 861-867.

(2) Le, S. D.; Nishimura, S. Highly Selective Synthesis of 1,4-Butanediol via Hydrogenation of Succinic Acid with Supported Cu–Pd Alloy Nanoparticles. *ACS Sustainable Chem. Eng.* **2019**, *7* (22), 18483–18492.

(3) Werpy, T.; Petersen, G. *Top Value Added Chemicals from Biomass: Volume I -- Results of Screening for Potential Candidates from Sugars and Synthesis Gas*; **2004** DOE/GO-102004-1992, 15008859.

(4) Delhomme, C.; Weuster-Botz, D.; Kühn, F. E. Succinic Acid from Renewable Resources as a C $_4$ Building-Block Chemical—a Review of the Catalytic Possibilities in Aqueous Media. *Green Chem.* **2009**, *11* (1), 13–26.

(5) Di, X.; Shao, Z.; Li, C.; Li, W.; Liang, C. Hydrogenation of Succinic Acid over Supported Rhenium Catalysts Prepared by the Microwave-Assisted Thermolytic Method. *Catal. Sci. Technol.* **2015**, *5* (4), 2441–2448.

(6) Shao, Z.; Li, C.; Di, X.; Xiao, Z.; Liang, C. Aqueous-Phase Hydrogenation of Succinic Acid to γ-Butyrolactone and Tetrahydrofuran over Pd/C, Re/C, and Pd–Re/C Catalysts. *Ind. Eng. Chem. Res.* **2014**, *53* (23), 9638–9645.

(7) Patankar, S. C.; Sharma, A. G.; Yadav, G. D. Biobased Process Intensification in Selective Synthesis of γ-Butyrolactone from Succinic Acid via Synergistic Palladium–Copper Bimetallic Catalyst Supported on Alumina Xerogel. *Clean Tech. Environ. Policy* **2018**, *20* (4), 683–693.

(8) Garner Insights. Global Gamma-Butyrolactone Market Report 2019. **2019**.

(9) Verified Market Research. Global Tetrahydrofuran Market By Technology, By Application, By Geographic Scope And Forecast To 2026. **2019**.

(10) Nghiem, N.; Kleff, S.; Schwegmann, S. Succinic Acid: Technology Development and Commercialization. *Fermentation* **2017**, *3* (2), 26-39.

(11) Song, H.; Lee, S. Y. Production of Succinic Acid by Bacterial Fermentation. *Enzyme and Microb. Technol.* **2006**, *39* (3), 352–361.

(12) Cao, D.; Cai, W.; Tao, W.; Zhang, S.; Wang, D.; Huang, D. Lactic Acid Production from Glucose Over a Novel Nb2O5 Nanorod Catalyst. *Catal. Lett.* **2017**, *147* (4), 926–933.

(13) Tachibana, Y.; Masuda, T.; Funabashi, M.; Kunioka, M. Chemical Synthesis of Fully Biomass-Based Poly(Butylene Succinate) from Inedible-Biomass-Based Furfural and Evaluation of Its Biomass Carbon Ratio. *Biomacromolecules* **2010**, *11* (10), 2760–2765.

(14) Choudhary, H.; Nishimura, S.; Ebitani, K. Metal-Free Oxidative Synthesis of Succinic Acid from Biomass-Derived Furan Compounds Using a Solid Acid Catalyst with Hydrogen Peroxide. *Appl. Catal. A* **2013**, *458*, 55–62.

(15) Zhu, W.; Tao, F.; Chen, S.; Li, M.; Yang, Y.; Lv, G. Efficient Oxidative Transformation of Furfural into Succinic Acid over Acidic Metal-Free Graphene Oxide. *ACS Sustainable Chem. Eng.* **2019**, *7* (1), 296–305.

(16) Howell, B. A.; Sun, W. Biobased Plasticizers from Tartaric Acid, an Abundantly Available, Renewable Material. *Ind. Eng. Chem. Res.* **2018**, *57*, 15234-15242.

(17) Howell, B. A.; Sun, W. Biobased Flame Retardants from Tartaric Acid and Derivatives. *Polym. Degrad. Stab.* **2018**, *157*, 199–211.

(18) Fu, J.; Vasiliadou, E. S.; Goulas, K. A.; Saha, B.; Vlachos, D. G. Selective Hydrodeoxygenation of Tartaric Acid to Succinic Acid. *Catal. Sci. Technol.* **2017**, *7* (21), 4944–4954.

(19) Li, X.; Zhang, Y. Highly Selective Deoxydehydration of Tartaric Acid over Supported and Unsupported Rhenium Catalysts with Modified Acidities. *ChemSusChem* **2016**, *9* (19), 2774–2778.

(20) Tshibalonza, N. N.; Monbaliu, J.-C. M. The Deoxydehydration (DODH) Reaction: A Versatile Technology for Accessing Olefins from Bio-Based Polyols. *Green Chem.* **2020**, *22*, 4801-4848.

(21) Yi, J.; Liu, S.; Abu-Omar, M. M. Rhenium-Catalyzed Transfer Hydrogenation and Deoxygenation of Biomass-Derived Polyols to Small and Useful Organics. *ChemSusChem* **2012**, *5* (8), 1401–1404.

(22) Jang, J. H.; Sohn, H.; Camacho-Bunquin, J.; Yang, D.; Park, C. Y.; Delferro, M.; Abu-Omar, M. M. Deoxydehydration of Biomass-Derived Polyols with a Reusable Unsupported Rhenium Nanoparticles Catalyst. *ACS Sustainable Chem. Eng.* **2019**, *7* (13), 11438–11447.

(23) Hong, U. G.; Hwang, S.; Seo, J. G.; Lee, J.; Song, I. K. Hydrogenation of Succinic Acid to γ-Butyrolactone (GBL) over Palladium Catalyst Supported on Alumina Xerogel: Effect of Acid Density of the Catalyst. *J. Ind. Eng. Chem.* **2011**, *17* (2), 316–320.

(24) Wang, Y.; Huang, Z.; Leng, X.; Zhu, H.; Liu, G.; Huang, Z. Transfer Hydrogenation of Alkenes Using Ethanol Catalyzed by a NCP Pincer Iridium Complex: Scope and Mechanism. *J. Am. Chem. Soc.* **2018**, *140* (12), 4417–4429.

(25) Alonso, F.; Riente, P.; Rodríguez-Reinoso, F.; Ruiz-Martínez, J.; Sepúlveda-Escribano, A.; Yus, M. Platinum Nanoparticles Supported on Titania as an Efficient Hydrogen-Transfer Catalyst. *J. Catal.* **2008**, *260* (1), 113–118.

(26) Johnstone, R. A. W.; Wilby, A. H.; Entwistle, I. D. Heterogeneous Catalytic Transfer Hydrogenation and Its Relation to Other Methods for Reduction of Organic Compounds. *Chem. Rev.* **1985**, *85* (2), 129–170.

(27) López Granados, M.; Moreno, J.; Alba-Rubio, A. C.; Iglesias, J.; Martín Alonso, D.; Mariscal, R. Catalytic Transfer Hydrogenation of Maleic Acid with Stoichiometric Amounts of Formic Acid in Aqueous Phase: Paving the Way for More Sustainable Succinic Acid Production. *Green Chem.* **2020**, *22* (6), 1859–1872.

(28) Liu, S.; Senocak, A.; Smeltz, J. L.; Yang, L.; Wegenhart, B.; Yi, J.; Kenttämaa, H. I.; Ison, E. A.; Abu-Omar, M. M. Mechanism of MTO-Catalyzed Deoxydehydration of Diols to Alkenes Using Sacrificial Alcohols. *Organometallics* **2013**, *32* (11), 3210–3219.